Statistical modelling of games

by

Yu Gao, MSci.

Thesis submitted to the University of Nottingham
for the degree of Doctor of Philosophy

July 2016

Abstract

This thesis mainly focuses on the statistical modelling of a selection of games, namely, the minority game, the urn model and the Hawk-Dove game. Chapters 1 and 2 give a brief introduction and survey of the field. In Chapter 3, the key characteristics of the minority game are reproduced. In addition, the minority game is extended to include wealth distribution and leverage effect. By assuming that each player has initial wealth which rises and falls according to profit and loss, with the potential of borrowing and bankruptcy, we find that modelled wealth distribution may be power law distributed and leverage increases the instability of the system. In Chapter 4, to explore the effects of memory, we construct a model where agents with memories of different lengths compete for finite resources. Using analytical and numerical approaches, our research demonstrates that an instability exists at a critical memory length; and players with different memory lengths are able to compete with each other and achieve a state of co-existence. The analytical solution is found to be connected to the well-known urn model. Additionally, our findings reveal that the temperature is related to the agent's memory. Due to its general nature, this memory model could potentially be relevant for a variety of other game models. In Chapter 5, our main finding is extended to the Hawk-Dove game, by introducing the memory parameter to each agent playing the game. An assumption is made that agents try to maximise their profits by learning from past experiences, stored in their finite memories. We show that the analytical results obtained from these two games are in agreement with the results from our simulations. It is concluded that the instability occurs when agents' memory lengths reach the critical value. Finally, Chapter 6 provides some concluding remarks and outlines some potential future work.

List of publications

Some of the results presented in this thesis are also published in the following manuscripts:

Chapter 4:

1. James Burridge, **Yu Gao**, Yong Mao, *Forgetfulness Can Help You Win Games*, Physical Review E **92**, 032119 (2015).

Chapter 5:

2. James Burridge, **Yu Gao**, Yong Mao, *Memory and Limit Cycles in the Hawk-Dove Game*, in preparation for European Physics Letters.

Acknowledgements

I acknowledge my studentship funding from the School of Physics and Astronomy.

I am grateful to my supervisor, Dr Yong Mao, from the School of Physics and Astronomy and co-supervisor Dr James Burridge from the University of Portsmouth. I am extremely thankful and indebted to them for their expertise, guidance and encouragement. I have also benefited from valuable discussions with Dr John Fry from the University of Sheffield.

I would like to take this opportunity to express gratitude to all faculty members for their help and support. In particular, I am thankful for the IT support from Philip Hawker, and LaTeX help from Siyuan Ji.

I want to offer my special thanks to my parents, grand-parents, and cousins for their unceasing encouragement, support and attention. I am also grateful to my wife Shuangqi who supported me throughout this journey. Her love is most precious to me.

I also place on record, my sense of gratitude to one and all, who directly or indirectly, have let their hands in this venture.

Contents

List of Figures

List of Tables

Chapter 1

Introduction

1.1 Econophysics

The term 'econophysics' was first coined by Mantegna and Stanley [1] in 1996, to describe the application of statistical physics to study economic and financial systems. Specifically, concepts such as stochastic modelling and probability theory have been fruitfully applied to economics, finance and social science [1, 2, 3, 4]. The subject of econophysics has received much attention [5, 6, 7, 8], and subsequently developed to such an extent that some has argued that it can be classified into two broad categories, namely, the statistical and the phenomenological econophysics [9]. Today, econophysics is often regarded as a subject in its own right, and in recognition of its significance, many universities/institutions offer courses and training programmes on econophysics [10].

A key strength of econophysics is that it offers a rigorous and quantitative approach to understanding and analysing economic issues [11, 12]. Historically, its most established contribution is in the area of complex correlations and financial time series analyses [13, 14]. For example, the fluctuations and volatilities of individual stocks are shown to be correlated, which can in turn help explain the financial behaviour of the overall market [15]. As an example, Stanley et al. [16] used a detrended fluctuation analysis (DFA) to quantify the correlations in their

analysis of S&P 500 data.

In econophysics, probabilistic method is a common approach to economics and finance [17]. For example, Silva et al. [18] applied the Lévy distribution to investigate the multi-scale properties in foreign exchange rates. From the Lévy sections theorem, the relationship between the local volatility in foreign exchange rates and fat tails in distribution can be explained [19].

The ubiquitous power law distribution in statistical physics also makes frequent appearance in finance, e.g. in the time series of stock prices and exchange rates [20, 21]. Econophysics attempts to relate pricing to equilibrium thermodynamics [22, 23]. The economic system is extremely complex, but the statistics of the market is often characterised by a power-law distribution [22]. Interestingly, the two-power law function has been successfully applied to analyses of the distribution of personal income as well as gross domestic production by using two different exponents to fit high and low-to-middle regions respectively [24].

In recent years, it has become popular to regard econophysics as an interdisciplinary research. According to the research by Fan et al. [25], econophysics is interconnected with other fields as part of a network: this approach can explain the rapid development of the subject of econophysics, and it is believed that the network will continue to enhance its research and development. For example, econophysics can be studied in connection with subjects like psychology, probability theory and the theory of preference [26], and of course, econophysics can play a vital role in society through economics and finance. For instance, Fry [27, 28, 29] developed mathematical models to understand dramatic financial bubbles which affect us all.

The past few decades saw a meteoric rise in the volumes traded in the financial derivatives market, involving instruments such as the options. An option provides its holder(s) with the right to buy or sell an underlying asset in the future, but it is not compulsory to implement this agreed contract [30]. The Black-Scholes formula, essentially a diffusion equation, has been hugely successful in pricing

options [31], though discrepancies exists, e.g. the option smile [32].

It is well known that the derivatives can lead to a significantly leveraged and risky market. This leverage effect has been studied in order to explain the financial crisis of 2008 [33, 34]. Although there is a huge trading volume in existing derivatives, investors sometimes are unlikely to consider the worst possible scenario [35]. When traders employ new financial derivatives, they seem to pay less attention to risks. The improvement of financial markets regulation is likely to keep the risks at an acceptable range [36]. Academics and market participants need to analyse potential risks with suitable methods [37]. Till now, research has largely focussed on analysing those risks in the financial markets, especially for highly-leveraged derivatives [38].

A well-constructed option game theory can offer an understanding of the uncertainty in a competitive environment [39]. Option game theory can provide insights into the financial markets, for example, levered firm's equity can be regarded as an option on the firm and priced by option pricing techniques [40, 41].

1.2 Models of games

Econophysics can become more productive and relevant when combined with statistical models of games, an example of which is the minority game. Whilst simple in construction, the game captures the complex collective behaviour of a group of agents competing for finite resources. The minority game has been studied extensively with tools of statistical physics, and it has been suggested that the game provides a basis for understanding broader financial markets [42, 43]. For example, agents may cooperate to create a more resilient market, and develop a particular wealth distribution [44, 45, 46]. In this thesis, we extend the minority game by allowing agents to accumulate wealth through play, and borrowing and bankruptcy are introduced. A key feature of the game model is the propagation

of information through time: the game memorises the past via wealth distribution and strategy choice, but resets via bankruptcy.

The theme of memory is formally explored through two classes of models, namely the statistical urn model and the Hawk-Dove model. We find that, when competing in a game for finite resources, a long memory can help players to make 'wiser' choices by weeding out irrelevant noises, but too long a memory could lead to large collective fluctuations resulting in limit cycles and instability. In those situations, players with shorter memory could gain an advantage by adapting faster to the changing environment, and thus players of different memories could coexist in a dynamical equilibrium, characterised by a Hopf bifurcation [47]. Our main findings with memory are general, and should be applicable to other game models such as the rock-paper-scissors game [48, 49].

The rest of this thesis is structured as follows: Chapter 2 provides a focussed review of the three models considered in this thesis: the minority game, the urn model and the Hawk-Dove game. In Chapter 3, we present the minority game with extension to the wealth distribution and the leverage effect. Chapter 4 offers our variation of the urn model to explore the effectiveness of memory. In Chapter 5, we demonstrate how our findings from Chapter 4 are applied to the Hawk-Dove game. In the final chapter, a conclusion is drawn, along with a description of the limitations of the study and what further developments could be undertaken.

Chapter 2

Review of models

2.1 The minority game

Game theory models offer an alternative approach to finance, especially in areas such as asset pricing and corporate finance [50, 51, 52]. For instance, models can be used to understand the arrangement of dividend payments, firms capital structure, market microstructure, etc [53]. More recently, game theory models have been employed to study multifractality and turbulence found in financial markets' dynamics, e.g. logarithm stock price, absolute returns and transaction volume [54, 55, 56]. Furthermore, the game theory model has been extended to seek methods for stabilising the financial markets including the futures market [57]. Interestingly, some researchers have also attempted to predict the stock markets using game theory models [58, 59]. For example, the minority game is one of the most popular game models for market behaviour [60]. In contrast, the majority game is dominated by the majority group. The mixed majority-minority game can be used to model the market dynamics and traders strategies [61, 62, 63].

The minority game (MG) formulates the El Farol bar problem, in which a group of people have to decide whether to go to the El Farol bar each night [64]. The capacity of the bar is limited, so that if the number of visitors exceeds its capacity on a given night, these people will not enjoy their night out, in which

case, it would be better for them to stay at home. However, if the capacity is not reached, all attendees share a positive experience. The minority rule governs this problem. Everybody attending the bar expects that it will not be overcrowded, but in reality, they will face one of two outcomes. Based on the knowledge of previous attendance records and their individual strategies, people try to optimise their next decision.

The El Farol bar problem was formulated and solved, providing insight into some complex scenarios [65, 66, 67, 68]. Marsili, Challet and Zecchina's work [69] provided significant results in the attendance (price) dependence of each player. Franke [70] also found a long-run equilibrium frequency distribution in addition to the Nash equilibrium solutions. Furthermore, the El Farol bar problem with externally 'imposed comfort levels' was explored [71]. In Lustosa and Cajueiro's study [72], previous work in this area was extended by offering players unparalleled information to analyse arbitrage opportunities. The MG has also been utilised in various fields, such as the financial markets. Therefore, it is instructive to investigate the relation between the minority game and financial games [68].

In the MG, each of N agents has to make a choice between two strategies, and the overall minority category wins. However, the agents are free to specialise in a line of strategies, S [67]. Players can utilise the history of their previous strategy performances to determine their future outcome. The following conditions govern the game: firstly, the resources are scarce, and participating agents cannot all win. Secondly, the behaviour of participants is determined by others' behaviour. Thirdly, there is no classification of bad or good behaviour in the game. Fourthly, prediction is possible but only through players' experiences and choices (strategies).

Traditionally, market and economics models utilise equilibrium ideology, the assumption being that the players' decisions in the financial market revolve around two factors [73, 74, 75]. One factor is that markets are subject to external influences, such as incoming information relating to regulation change, business,

technological advances and political dealings. The quest for equilibrium in the financial markets must cope with the fact that balance is often disturbed by external factors. These models typically assume that markets would remain inherently stable even after large external shocks. The second factor is that the large number of market participants (pursuing their individual interests) necessarily create a fluctuating market, where decisions by key players may result in market prices moving out of equilibrium. However, market activities such as arbitrage will ensure that fundamental values are more or less sustained in the long run. Challet et al. [76, 77] used the MG to model the real market mechanisms by accounting for roles of different agents.

The minority game can be interpreted in terms of buying and selling preferences. In the case of the buyer/seller, it is not possible to determine the day that most clients would be buying or selling, and, therefore, the day chosen by a client might turn out to be one when the market is over- or under- sold. In particular, consider a new product in the market where N players are expected to participate in either buying or selling of a specific commodity at time t. If the minority decides to buy, then buyers gain an advantage [78]. Similarly, if the minority decides to sell, they gain by obtaining a better price due to the excess demand.

The market scenario resembles the minority game to a degree. Interaction in the market is not controlled by one factor or one strategy. The profitable strategy is not independent of other strategies. After all, the winner is determined by the other strategies in play. In particular, the minority game engages interrelated strategies [79]. Although buyer and seller strategies may move the price in ways that will be an advantage to one or the other (minority or majority), the market dynamics are also controlled by time t. Players who fall into the majority category, say selling, may opt to change their strategies with time and join the minority buyers [69]. Evidently, the market would fluctuate without any external influence affecting it. The agents' evolving strategies ultimately control the market dynamics.

The strategy for optimising two choices can arise from trial-and-error learning. It may require a player to have played the game for a considerable period to successfully come up with a personal definitive strategy. If we use 1 and -1 to represent the two choices available to a player, then a strategy is a particular way of mapping from a sequence of M outcomes, represented by a string of 1's and -1's, to a single number of 1 or -1 [67]. Each player may have a number of available strategies to choose from, according to their historical performance. In theory, each player will have to consider 2^M of possible scenarios. We defer the detailed formulation to Chapter 3.

2.2 Urn models

The statistical urn model consists of a number of urns containing different coloured balls [80, 81]. Players pick up and add ball(s) from urn(s) each round according to certain rules of play. The rules vary, leading to different types of urn models. Following play, the distributions of different coloured balls and other statistics can be analysed. The distributions can range from the discrete to the continuous, and ultimately, urns and/or balls represent some real objects of interest, such as atoms or people.

The basic Pólya urn model has been heavily studied [82], and it consists of only one urn, containing balls of two different colours, say white and black. Each round, a player randomly selects a ball from the urn and returns it with an extra ball of the same colour. As play continues, the number of balls increases, and the number of white or black draws can be shown to settle into the beta-binomial distribution. More recently, Chen and Kuba's [83] derived the exact equations to demonstrate the expected value and variance for the Pólya model, together with a new two-urn generalisation [84]. Mahmoud [85] investigated the relationship between Pólya urn models and random trees.

The Ehrenfest model is another popular type of urn model, first introduced to

the second law of thermodynamics. There are only two urns and N balls, which are labelled from 1 to N. A ball is randomly selected and moved into the other urn. It can be shown that when the system stabilises, the entropy reaches a maximum [86]. Metzler et al. [87] studied this class of urn models with deterministic, time-reversible conditions using different types of distributions, including hierarchical and power-law ones. Prestipino [88] generalised the Ehrenfest model enabling it to be used for energy considerations.

Many variations of the urn model exist [89]. For instance, we may insist that different coloured balls are picked in the two consecutive rounds; it is also possible to temporarily neglect one or more urns [90, 91]. We can add balls of the opposite colour to the urn if there are only two coloured balls. Or we do not have to add back any balls at all. Another example is where the number of replacement balls is a random variable generated by a specific distribution. We can also increase the number of coloured balls in the urn to more than two. Godrèche and Luck [92] investigated the non-equilibrium dynamics of urn models, especially the backgammon model and the zeta urn model. Prestipino [88] generalised the Ehrenfest model to study an ideal gas, reproducing the Boltzmann entropy formula ($S = k_B \ln W$). In ideal gas, S is the entropy, W is number microstates of system of gas particles, and k_B is Boltzmann constant. In urn model, S is corresponding entropy and W arises from the number of urns. The system can lead to a stable state by using a stochastic urn model to analyse the probable evolution of the system. In the paper by Buhot et al. [93], a generalised form of urn model yielding non-constant number of particles was obtained and both equilibrium and non-equilibrium dynamics were analysed using mean-field theory which has the form of a diffusion-annihilation process and is accurate in describing out-of-equilibrium dynamics in the low temperature regime. Randomness is a key issue connected with urn models. Laruelle and Pagè [94] demonstrated its efficiency when applying stochastic approximation to randomised urn models. The combination of the urn model and the random partitioning model has been used

to explore the multiplicities of box occupancies [95].

The urn model, which can be classified into the Ehrenfest class and the Monkey class, has been applied not only to physics, but also to economics. Different from Ehrenfest class, which randomly chooses the ball initially, the Monkey class will randomly choose the urn first. The equilibrium statistical properties of a disordered urn model, including both classes, were studied by Jun-ichi Inoue and Jun Ohkubo [96]. Interestingly, they found heavy-tailed power-law behaviour in the occupation probability distribution. The arbitrary energy function was added to the formula and a possible linkage to the macro economy was constructed [96].

The application of urn models extends to the social sciences [97, 98, 99, 100, 101, 102]. For example, a one-dimensional urn model can be applied to traffic models and driven-diffusive systems. A generalised form for one class of zero-range processes was achieved by Levine, Mukamel and Ziv [98]. As another example, the relationship between Italian cities' economical structure and population distribution has been analysed in association with economic, historical, demographic and political considerations at national and regional levels [99]. In Tong and Mahmoud's paper [100], an Ehrenfest urn model was generalised to develop an understanding of migration issues. Lambersona and Page [101] used an urn model to model feedback from the markets. The urn model can be applied to inventory distribution, products reproduction, frequency of seeing films, etc [101]. They built new theorem showing the relationship between second-order stochastic dominance and expected market share [101]. In addition, a new model named 'immigrated urn' was proposed by Zhang et al. [102], which can be employed to analyse the immigration process.

Urn models have also been applied to medical studies. A clinical trial using an urn model with modification of the reinforcement scheme was constructed by Aletti et al [103]. Their work presented the convergence theorem numerically. Their goal was to help patients receive treatments more efficiently and effectively [103].

2.2.1 Pólya-Eggenberger model

To illustrate the mathematics involved, we choose the Pólya-Eggenberger urn model [104], which differs from the basic Pólya model only in the exact criteria for adding extra balls. We start with the basic Pólya model of a single urn containing balls with two colours (w white balls and b black balls). The replacement rule is modified so that s of the same coloured balls will be added after each discrete time step ($s = 1$ redueces to the basic Pólya model). After n time steps, the distribution of the number of black balls drawn is described by the following equation.

$$\mathbf{P}[k] = \binom{n}{k} \frac{b(b+s)...\{b+(k-1)s\}w(w+s)...\{w+(n-k-1)s\}}{(b+w)(b+w+s)...\{(b+w)+(n-1)s\}}, \tag{2.1}$$

where k specifies the number of black balls drawn. For the special case $s = 0$, it can be simplified to:

$$\mathbf{P}[k] = \binom{n}{k} \frac{w^k \; b^{n-k}}{(w+b)^n} \tag{2.2}$$

which is the standard binomial distribution.

The generalized Pólya-Eggenberger distribution is defined via the following replacement scheme in Table 2.1.

		Colour of the chosen ball	
		White	Black
Number of balls added to the urn	White	ω_w	ω_b
	Black	β_w	β_b

Table 2.1: Generalised Pólya-Eggenberger scheme [89].

According to Table 2.1, if we choose white at a particular time, there are ω_w white balls and β_w black balls being added. Otherwise, we will add ω_b white balls and β_b black balls. In both cases, the chosen ball will be returned to the urn as well. Suppose after n rounds we have b_n black balls and w_n white balls, then the

above reasoning can be written as:

$$b_{n+1} = b_n + T_n\beta_b + (1 - T_n)\beta_w, \tag{2.3}$$

where T_n is a random variable defined as:

$$\mathbf{P}[T_n = 0] = \frac{w_n}{b_n + w_n}, \tag{2.4}$$

$$\mathbf{P}[T_n = 1] = \frac{b_n}{b_n + w_n}. \tag{2.5}$$

Therefore, the expected value and variance can be found to be:

$$\mathbf{E}[b_{n+1}|b_n, w_n] = b_n + \frac{b_n\beta_b + w_n\beta_w}{b_n + w_n}, \tag{2.6}$$

$$\mathbf{var}[b_{n+1}|b_n, w_n] = \frac{(\beta_b - \beta_w)^2 b_n w_n}{(b_n + w_n)^2}. \tag{2.7}$$

Note $\beta_w = \omega_b = 0,\ \beta_b = \omega_w$ corresponds to the Pólya-Eggenberger model before generalisation.

2.2.2 Stagewise linkage model

Another interesting variant of the urn model is the 'stagewise linkage' model [105]. Only one urn is used, and it is filled with $n > 2$ balls, labelled 1 to n. In each round, a player picks out two balls. For example, in the first round, ball i and ball j are picked up say, they are then individually labelled with both labels i and j (so-called 'linkage'), before being returned to the urn. Now two balls are doubly labelled with both numbers i and j, and the remaining $(n - 2)$ balls are singly labelled. The game is played continuously, and all balls gain labels (links) until they are all labelled 1 to n eventually. What is the minimum number of rounds required to ensure all the balls have the same label? In other words, how long does it take to make all balls labelled 1, 2, ..., n? It can be shown that the expected

number of drawings C satisfies:

$$(1-\epsilon)n\ln n < \mathbf{E}[C] < (2+\epsilon)n(\ln n)^2 \quad \text{for all } n \geq N(\epsilon), \tag{2.8}$$

where $\epsilon \ll 1$, denotes any positive constant; and $N(\epsilon) \gg 1$, is an integer function of ϵ. The linkage model is equivalent to the telephone model [106], where n people each possessing a unique piece of news, and C random individual calls would be required before they all know the news.

2.2.3 Urn transfer model

The earliest urn transfer model was introduced by Bernoulli in 1713 [107]. There are two urns in this model, one of which contains k white balls and the other, k black balls. In each round, one ball is drawn from urn 1 and returned to urn 2. Then one ball is drawn from urn 2 and returned to urn 1. This is a repeated process. The general formula for the expected number of white balls in urn 1 is given by:

$$E_r = \frac{1}{2}k\left\{\left(\frac{k-1}{k+1}\right)^r + 1\right\}. \tag{2.9}$$

where k denotes the number of balls in each urn, and r represents the number of balls have been drawn.

2.2.4 Ehrenfest model

The Ehrenfest urn model involves two urns [108]. Urn 1 contains k' balls and urn 2 contains k'' balls. The Ehrenfest urn model is equivalent to a Pólya-Eggenberger urn model if we express the system as a single urn model which contains k' white balls and k'' black balls. We randomly select one ball in each round and replace it with one in the opposite colour. According to Table 2.1 , this is the case when $\omega_w = \beta_b = -1$, $\omega_b = \beta_w = 1$. The probability of having k white balls after n

rounds is defined as $P_n(k)$ which can be written as:

$$k_0 P_n(k) = (k+1)P_{n-1}(k+1) + (k_0 - k + 1)P_{n-1}(k-1), \tag{2.10}$$

where $k_0 = k' + k''$ (the total number of balls) with initial conditions $P_0(k') = 1$, and $P_0(k) = 0$ for all $(k \neq k')$. When $n \to \infty$, this distribution becomes a binomial distribution.

The Ehrenfest urn model can be generalised by adding a probability parameter p. Probability p describes the probability of changing the chosen ball with an opposite coloured ball. The remaining probability is $(1-p)$, which refers to the probability of returning the ball to the urn without changing its colour. The distribution of the number of white balls after n rounds becomes:

$$k_0 P_n(k) = (k+1)pP_{n-1}(k+1) + k_0 qP_{n-1}(k) + (k_0 - k + 1)pP_{n-1}(k-1), \tag{2.11}$$

where $q = 1 - p$. Note that the distribution does not depend on the probability p.

2.2.5 Application of the urn model to social science

In social science, issues such as analysing and interpreting social experiments can be viewed as allocation problems [97], which consist of categories and objects. Urns and balls can represent categories and objects respectively, thus the urn model has been used to understand the relationship between lottery winnings and political attitudes, the effect of voting costs on turnout [97]. Similarly, the urn model has been applied decision making, reinforcement learning, technology usage, and other statistics in our society [109].

Human populations can be divided according to geography (country, county, city, area, street, etc), and similarly to race or social class. When sampling, it is common to make a selection based on one criterion after another, a multistage sampling process. Suppose a large urn represents the whole population; it contains μ smaller urns each of which might contain even smaller urns, etc; eventually,

the lowest level urns contain balls representing people [89]. We could sample the population via simple random sampling, or we could perform a multistage sampling, but at each stage we have to weigh the probability of choosing an urn by the number of people it and its subsidiary urns contain, a process known as the probability proportional to size (PPS) sampling [110]. For simplicity, we consider only one intermediate stage, so that our μ smaller urns contain ν_1, ν_2,..., ν_μ people respectively. The selection rule is to choose m urns from the pool of μ urns and select n_i individuals from the ith urn if that urn has been chosen. The definition of a ith urn sampling fraction is n_i/ν_i. Let $x_{i1}, x_{i2}, ..., x_{i\nu_i}$ be the numbers on the ν_i balls in the i-th smaller urn, and these numbers represent the characteristics of interest. We can estimate the characteristics of the entire population via the following construction:

$$\xi = \sum_{i=1}^{\mu} \sum_{j=1}^{\nu_i} x_{ij} = \sum_{i=1}^{\mu} \nu_i \bar{x}_i, \tag{2.12}$$

where $\bar{x}_i = \nu_i^{-1} \sum_{j=1}^{\nu_i} x_{ij}$. The statistics of each stage of sampling can also be formulated following this construction.

2.2.6 Application of the urn model in genetics

In genetics, different generations may be represented by urns and their corresponding genes may be interpreted as balls, thus the urn model has been generalised to topics ranging from the spread of infectious diseases, population dynamics, to the biological evolutionary [111]. Limiting behaviour of Polya-like urn process has been applied to population genetics by Hoppe [112]. In particular, the process of coalescent, a retrospective trace back of genetic drift, is mapped to the urn model in reverse time [112]. In Trieb's work [113], a single urn model containing one black and various numbers of other coloured balls is used to analyse coalescent. The drawing of different coloured balls leads to the genetic variations of the next generation, with the black ball representing a genetic mutation [113]. Another notable example in population genetics is the Wright-Fisher model (may be viewed

as a variation of the urn model) [111], which analyses how specific allele frequencies in a finite population and their mating behaviour evolve over generations. It helps geneticists to understand different factors contributing to the evolutionary process.

In a simplified case, all balls in an urn represent the genes in a population. Each colour denotes one type of a gene. We pay attention to genetics in the language of urn models in two areas: the composition of the coloured balls in a sequence of urns in each time step and the colour compositions of lots of balls drawn from one urn. Suppose we have m genes in a generation of one population and each gene has two types, A_1 & A_2. A single population consists of i type A_1 and $(m-i)$ type A_2 genes. Assume the genetic composition from parents is binomially distributed. The probability of i genes of type A_1 in the next generation is:

$$p_{ij} = \binom{m}{j} \left(\frac{i}{m}\right)^j \left(1 - \frac{i}{m}\right)^{m-j}, \tag{2.13}$$

where j is the number of balls in the second urn.

This can be explained in the context of urn models. Suppose we have a sequence of urns. The first urn consists of m coloured balls. The colour can be either red or green. The second urn will be filled by the same coloured balls drawn from the first urn until it reaches the number of m. We then calculate the probability of j red balls in the second urn given that there are i red balls in the first urn. This rule is continuously applicable in the next urn. This can be extended to the concept of mutation if the next urn has a $(1-u)$ probability of being filled with the same coloured ball. And the remaining probability of u fills the next urn with an entirely new colour, where it indicates the appearance of a new property. In addition to the applications elaborated in this study, the urn models can also be applied to many other fields, such as the military, and in physiology and computer science.

2.3 The Hawk-Dove game

We seek to connect the urn model to evolutionary game models [114]. The Hawk-Dove game is first used to as a toy model to explore the implications. In the real world, some species behave aggressively and fight for their allocated resource maximisation. In contrast, the remaining groups possess a conservative attitude and opt to minimise their potential incurred costs, such as injuries. The Hawk-Dove game addresses this phenomenon mathematically. It was first introduced by Smith and Price in 1973 [115, 116]. This game model assumes that there are only two groups in the system. One group, namely 'H', representing 'hawk' players, fights for allocated resources until they win or lose. The other group, called 'D', denoting 'dove' players, avoids direct conflicts [117].

This simple game was initially used to explore the evolution of animal contest behaviour [118, 119]. For example, Pham and Feng, who studied Asian carp invasions, used a varied Hawk-Dove game model to establish simulations, aiming to provide an efficient and low-cost method to solve the problem [120]. The application of the Hawk-Dove game became popular not only in the field of biology, but also in the measurement of reciprocity and fairness [121]. Additionally, it has also been applied widely in modern economics and finance [122]. For instance, the financial crisis of 2008 was analysed by Hanauske et al. using the Hawk-Dove game in a quantum approach [122]. This study concluded that an evolutionary stable strategy (ESS) can emerge, which could help mitigate future economic and financial crises [122].

The basic Hawk-Dove game has been developed in a variety of forms for wider applications. In 2008, Carlsson and Johansson proposed a development of the Hawk-Dove game called the iterated Hawk-and-Dove game [123]. They noted that the evolutionary Hawk-Dove game is a repeated game throughout history. The iterated Hawk-and-Dove game was created to analyse the ESS [124]. The two-stage Hawk-Dove game was mathematically written by Cressman [125]. It emphasises the change of input in additional rounds in the game [125]. In social

science, the Hawk-Dove game can play a significant role in managing customer expectation, in that it helps firms achieve a better financial performance and create stronger values [126]. Moreover, the game itself can be used in political science to investigate international relations [127]. Finally, it has been applied to entrepreneurship in macro- and micro-economics [128].

2.3.1 Model definition

There are three situations in total: 1) hawk vs. hawk, 2) hawk vs. dove, and 3) dove vs. dove. In the first situation, each of the hawk strategy players has a 50% chance of winning the game. We assume there is V resource and the cost of a flight is C. Therefore, the payoff in this situation is $(V - C)/2$. In the hawk vs. dove situation, the payoff for the hawk is V and for the dove, 0. For the last situation, the payoff for each dove strategy player is $V/2$. The result is given in the following payoff matrix.

	Hawk (H)	Dove (D)
H	$(V - C)/2$	V
D	0	$V/2$

where $V > 0$ and $C > 0$.

Suppose that we have a group of players with the same initial fitness of W_0, and p denotes the probability of players choosing a hawk strategy. Therefore, the Hawk-and-Dove strategy players' fitness can be expressed respectively:

$$W(H) = W_0 + pE(H, H) + (1 - p)E(H, D), \tag{2.14}$$

$$W(D) = W_0 + pE(D, H) + (1 - p)E(D, D), \tag{2.15}$$

where $E(H, H)$ denotes the expected payoff when 'Hawk' strategy player plays against 'Hawk' strategy player, $E(H, D)$ demonstrates the expected payoff when 'Hawk' strategy player plays against 'Dove' strategy player, $E(D, D)$ shows the expected payoff when 'Dove' strategy player plays against 'Dove' strategy player.

Assume that the players reproduce their kind in proportion to their fitness. The probability of a hawk player being in the next generation is:

$$p' = pW(H)/\bar{W}, \tag{2.16}$$

where

$$\bar{W} = pW(H) + (1-p)W(D). \tag{2.17}$$

2.3.2 Evolutionary stable strategy

Now the dynamics of the game can be explored. Suppose we have a two-strategy (strategies: I and J) game [115], the evolutionary stable strategy I for a two-strategy game is satisfied by

$$W(I) = W_0 + pE(I,I) + (1-p)E(I,J), \tag{2.18}$$

$$W(J) = W_0 + pE(J,I) + (1-p)E(J,J). \tag{2.19}$$

If a population adopt evolutionary stable strategy I, this group cannot be invaded by any other strategies. In other words, strategy I does better than J in two-strategy game, i. e. $W(I) > W(J)$. As $J \neq I$, either

$$E(I,J) > E(J,I), \tag{2.20}$$

or

$$E(I,I) = E(J,I) \text{ and } E(I,J) > E(J,J). \tag{2.21}$$

In consideration of these conditions, the Hawk-Dove game's evolutionary stable strategy (ESS) can be found [129]. Because the payoff from dove against dove is less than the payoff from hawk against dove, the dove strategy cannot be ESS. If $V > C$, in other words, the cost of two hawks' flights is relatively small, the hawk strategy is pure ESS. Finally, the situation when $V < C$ is considered. In

this case, the cost of fights is higher than the rewards. Players will use a hawk strategy with probability p and a dove strategy with the probability $(1-p)$. This is known as the mixed ESS. The general form of probability p is calculated as:

$$p = \frac{(b-d)}{(b+c-a-d)}, \tag{2.22}$$

with a generalised payoff matrix

	I	J
I	a	b
J	c	d

2.3.3 Retaliator

When payoff values from the Hawk-Dove game are substituted, the probability of p is equal to V/C. Then the 'retaliator' strategy, R, is introduced to the model in order to demonstrate system behaviour with more than a two-strategy game. When the R strategy player meets the hawk strategy player, the R strategy player will use the hawk strategy. If a R strategy player meets the dove strategy player, they will behave like a dove. The following payoff matrix illustrates the ideas.

	H	D	R
H	-1	2	-1
D	0	1	0.9
R	-1	1.1	1

Strategy R is an ESS, since $E(R,R) > E(D,R)$ and $E(R,R) > E(H,R)$. The following calculations prove that the mixed strategy $I = H/2 + D/2$ is also an ESS.

$$E(H,I) = \frac{1}{2} \times (-1) + \frac{1}{2} \times 2 = \frac{1}{2}, \tag{2.23}$$

$$E(D,I) = \frac{1}{2} \times 0 + \frac{1}{2} \times 1 = \frac{1}{2}, \tag{2.24}$$

$$E(R, I) = \frac{1}{2} \times (-1) + \frac{1}{2} \times 1.1 = 0.05. \tag{2.25}$$

Therefore, the system has two ESSs, $I = H/2 + D/2$ and R. Smith has concluded that "a game with only two pure strategies always has at least one ESS; but if there are three or more strategies, there may be no ESS" [114].

The Hawk-Dove game can be applied to social science such as: negotiation skills, business strategy, management and cooperate social responsibility (CSR), etc. [130, 131, 132]. For example, García et al. provided an analysis based on the sequential Hawk-Dove game in order to improve the bargaining power [133]. Using the game, it can provide company throughout ideas to survive in the competition [134]. Additionally, the Hawk-Dove game is able to model the establishment of property rights and laws [135, 136]. Furthermore, the Hawk-and-Dove strategy has already been applied to the United Kingdom's grocery market, where the sacrifice of short-term profits can be defined as the 'hawk' strategy [137].

Chapter 3

The minority game and its extension

In order to establish a robust and thorough understanding of the MG, we include derivations and a series of generated graphs. The rules and logic of the MG are extended to create the new model to be developed in the following sections.

We follow Challet and Zhang's first formulation of the minority game of 1997 [65]. For simplicity, the number of participants is set to be odd; thus the minority side can be identified without ambiguity. During the decision-making process, each player has a finite set of strategies to engage with. Finally, each player's payoff is determined by the others' choices.

The rest of this chapter is structured as follows. In Section 3.1, the mathematical formulations of the MG are defined. In Section 3.2, major results from the MG are listed. In Section 3.3 and 3.4, the wealth distribution and bankruptcy rates are presented. The chapter ends with a brief conclusion.

3.1 Mathematical formulations

Suppose N players are engaged, where N is an odd number and each player has S strategies in a game (S is a finite number). These players can only choose one of two possible outcomes in each game, namely side 'A' or side 'B'. This game can be interpreted as the El Farol bar problem by setting side 'A' as 'going to the bar'. MG is played in discrete time, which equals number of times game is played.

$$a_i(t) = 1, \tag{3.1}$$

where $a_i(t)$ represents an individual participant's decision at time t, $i = 1, 2, ..., N$. Meanwhile, side 'B' represents 'staying at home'

$$a_i(t) = -1. \tag{3.2}$$

Consequently, when we collect the actions of all the players, the overall action can be expressed as

$$A(t) = \sum_{i=1}^{N} a_i(t). \tag{3.3}$$

Multiplying by individual decision with $A(t)$, each of them has the payoff in a mathematical form

$$\text{Payoff}_i = -a_i(t)g[A(t)], \tag{3.4}$$

where $g(x)$ is an odd function. Challet and Zhang initially chose $g(x) = \text{sign}(x)$ [65, 138]. However, this does not limit the choices of function $g(x)$, some other functions can also be applied to $g(x)$ (e.g. $g(x) = x/N$).

All of the players make their decisions using inductive reasoning [139]. In other words, players have finite limited memories for the record of past winning sides. The letter m stands for the value of memory to be taken into consideration, which means each player employs m historical records to make their decision in the next game round.

According to the information of the last m winning group, there are a total of $P = 2^m$ possible inputs for each strategy, which must predict an output (of 2 possible variations) for each of those inputs. Hence, the total number of possible strategies is 2^{2^m}. For example, when the value of memory is set to 3, the total number of strategies is 256. The following table shows one possible strategy in the case of $m = 3$.

Input			Output
-1	-1	-1	$+1$
-1	-1	$+1$	-1
-1	$+1$	-1	$+1$
-1	$+1$	$+1$	-1
$+1$	-1	-1	$+1$
$+1$	-1	$+1$	$+1$
$+1$	$+1$	-1	-1
$+1$	$+1$	$+1$	-1

Table 3.1: Example of a strategy for the case of $m = 3$.

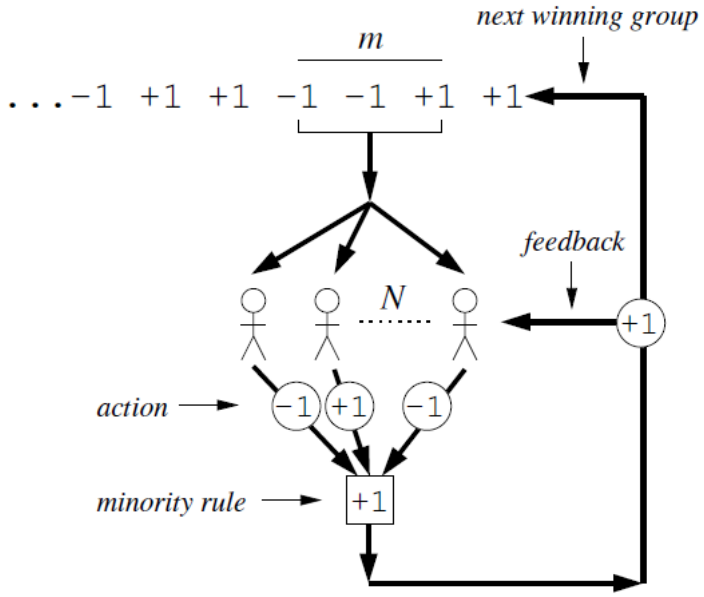

Figure 3.1: Demonstration of the MG [139].

Figure 3.1 illustrates the entire set-up of the classical minority game. The

logical flow starts from the top of the figure displaying a sequence of numbers with values of 1 or -1. The values represent the record of the full set of the historical winning group/side. Arrows below the historical data indicate that the records of previous m winning groups flow into each player's memory. According to their strategies, players will then perform their preferred actions. The winning group is established when all of the players have completed strategy selections, and the payoffs for each player will be calculated. Finally, the historical winning group is updated in a current time step.

We introduce the following vector formula

$$\vec{r_i}^a = (-1, -1, +1, -1, -1, +1, -1, +1) \tag{3.5}$$

to represent the a-th strategy belonging to the i-th player.

Then we use $\mu(t)$ to describe the set of possible strategies, where $\mu(t) \in \{1, .., 2^m\}$. Thus, each player's decision within one particular time step comes from one of its components. Recall that the entire set is expressed as $\{1, .., 2^m\}$. The changing of binary expressions of the historical winning group can be more efficient (i.e. $+1 \rightarrow 1$,$-1 \rightarrow 0$). Using updated notations, $\mu(t)$ can be expressed clearly. For instance, the original expressions for the historical data are given by set $\{+1, -1, -1\}$. Corresponding to the latest notation, the historical data is presented as $\{1, 0, 0\}$, where $\mu(t) = 5$.

Additionally, the new vector $\vec{I}(t)$ is introduced. This vector has all other zero components except the $\mu(t)$ component, which is 1. The product of $\vec{I}(t)$ and $\vec{r_i}^a$ provides the prediction of strategies. According to the example above, we obtain the $\mu(t) = 5$ and $\vec{I}(t) = (0, 0, 0, 0, 1, 0, 0)$. We assume that each player wants to maximise their payoffs. They track the virtual total payoffs of their available strategies:

$$p_i^a(t+1) = p_i^a(t) - \vec{r_i}^a \vec{I}(t) g[A(t)], \tag{3.6}$$

where t shows time step and p_i^a denotes the virtual total payoffs of the a-th strategy

of the i-th player, if it were used all the time. The minus sign arises from the payoffs equation (3.4). The virtual payoffs are then used to rank strategies in terms of their effectiveness, with the top ranking strategy being used for the next round. If two or more strategies are ranked joint top, then a random choice of those is made:

$$a_i = \vec{r_i}^{\beta_i(t)} \vec{I}(t), \tag{3.7}$$

where $\beta_i(t) \in \{1, ..., s\}$ represents the best performing of strategies, and it may vary with time steps.

In summary, we have described the basic formulation of the MG. In the following section, we reproduce some of the key results.

3.2 Results

3.2.1 Time evolution of attendance

Figure 3.2 shows some typical time evolution sequences of attendance for the standard MG. This is generated by program MATLAB [140].

The first curve has the property of periodicity, which indicates that the function has the relationship $f(x) = f(x + T)$, where T denotes the value of period. A player with a long memory (compared to T) could easily predict the outcome if pitched against a group of such players. Compared to the first curve, the second and third curves become less 'predictable', and the magnitudes of fluctuations also vary greatly amongst the three scenarios.

3.2.2 Volatility of the standard MG

The analyses of Figure 3.2 in previous section show the importance of the magnitude and periodicity of the fluctuations. The volatility/variance plot the minority game is key to characterising the behaviour of the system. The variance is defined

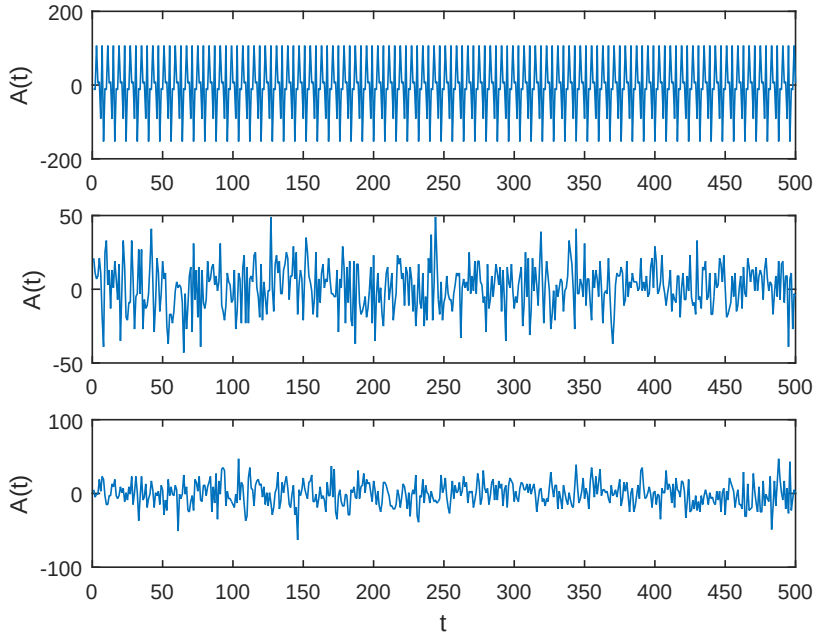

Figure 3.2: Time evolution of attendance for original MG. We assume the function $g(x) = x$, $N = 301$ and $s = 2$. From top to button, the memories are set to the values of $m = 2$, 7 and 15 respectively.

as:

$$\sigma^2 = \overline{\langle [A(t) - \langle A(t) \rangle]^2 \rangle}, \tag{3.8}$$

where $\langle ... \rangle$ devotes the time average, $\overline{\cdots}$ presents an average over possible realisations of $\vec{r_i^a}$.

Since the magnitude of $A(t)$ arises from the disparity of the winning and losing groups, the value of σ indicates the size of the winning and losing group. A larger σ implies that there is a smaller number of winners, and vice versa. Therefore, it is essential to analyse the behaviour of σ. Different parameters, such as length of memory of players' strategy, m, and number of players' accessible strategies, s, are used to characterise σ^2. Figure 3.3 plots the volatilities of the standard MG, where $N = 1001$, $t = 100000$, $s = 2$, repeats= 100.

In Figure 3.3, different shapes of symbols represent different numbers of players taking part in the MG (red circle: 51, green star: 101, blue plus: 201, black star: 301, up triangle: 501). It is interesting that the data generated from different number of players collapse into a single curve. The values of the memory parameter

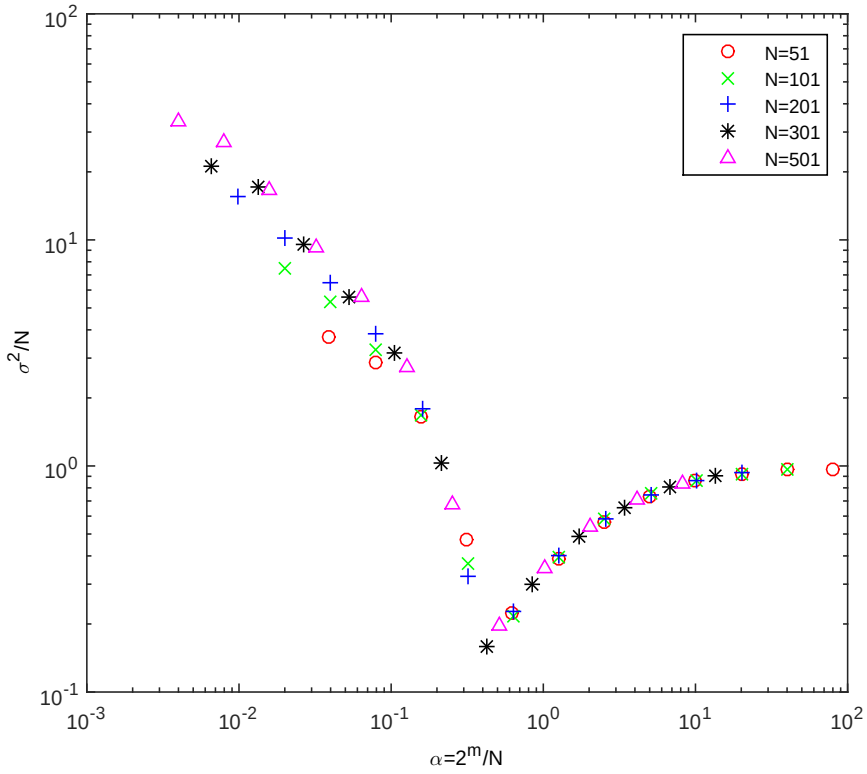

Figure 3.3: Volatility plot of standard MG.

are set from 1 to 12. Initially, the volatility decreases sharply with an increasing value of α. Volatility reaches its minimum value around $\alpha = 0.5$, it begins to increase and finally tends to 1 at larger values of α.

The random historical data does not affect the performance of variance as a function of α. The critical value, that is, the minimum value of volatility has practical implications. In the real world, if the volatility of the financial market stays at or around the critical value, the whole market would become desirably stabilised and create an investment environment with less risks. We assume that the simulated minority game is consistent with the efficient market hypothesis, which maintains that the resulting winning group (price) shown to each agent reflects all information [141, 142].

3.2.3 Information and frozen agents

Extensive studies on the MG model have shown that the optimal strategy can be determined [139]. The information is denoted by H, and the fraction of frozen agents is demonstrated by ϕ.

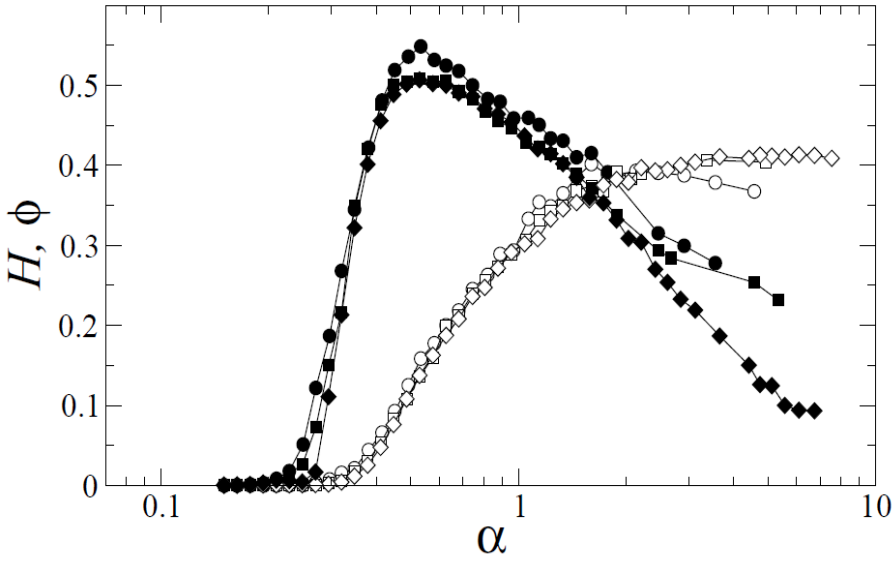

Figure 3.4: Information H (open symbols) and fraction of frozen agents ϕ (full symbols) as a function of the control parameter $\alpha = 2^m/N$ for $s = 2$ and $m = 5, 6, 7$ (circles, squares and diamonds respectively).

The figure above displays the information content of the distribution and the fraction of frozen agents [139]. These characteristics can be utilised to predict an optimal future strategy. The parameter α facilitates the prediction of future prices using past price records.

The data above show that a larger α is correlated with an increase in information content [143]. However, the agent's flexibility with strategies determines the probability of catching on this pattern. Identifying the pattern requires a large memory capability; therefore, few agents are able to identify these recurring patterns for exploitation. Furthermore, the market may retain its level of unpredictability if few agents are in play [143, 144, 145]. The recurrence of the pattern depends on the diversity of the strategies utilised by the agents [146].

On the other hand, a smaller α is likely to change the game. According to

Savit et al., the probability of landing into the winning pattern becomes low at this point [147]. With a large α, the pattern is bound to appear on several agents' plans, making identification likely. In this case, however, the pattern is likely to appear in one agent's range of strategies. However, the prediction of future prices is likely to be difficult in reality due to transaction costs.

3.3 Wealth distribution

3.3.1 Non-zero-sum case

The linkage between the MG and wealth distribution is explored in this section. The assumption of odd player numbers is retained. The initial total wealth of participants is set to a constant, and it could be any positive finite number (e.g. £100). This assumption can be relaxed in the later work using a number of methods, for instance, generating an initial wealth distribution for all players.

At the preliminary stage, the program simulates artificial data for the historical winning group. The players follow the rules in the standard MG to play the game in each round. For simplicity, the number of strategies, s, is set to the value of 2, and can be increased in the future. In the second step, the updated process for wealth will be added to the standard MG. The decision from each player at each round will be recorded.

Each participant chooses the most profitable strategy from the available strategies in order to maximise its own profits. We keep track of the change of wealth for all participants, which is described below. Each winning player gains 1 unit of wealth, and the rest lose 1 at each time step.

This method fundamentally assumes the equality of all players. This assumption can also be relaxed by adding payoff equations, organising the payoffs to each player after each round.

Figure 3.5 shows an example of artificial wealth distribution. In this figure, $N = 101$, $m = 3$ and $t = 1000$. The program generates a series of wealth distri-

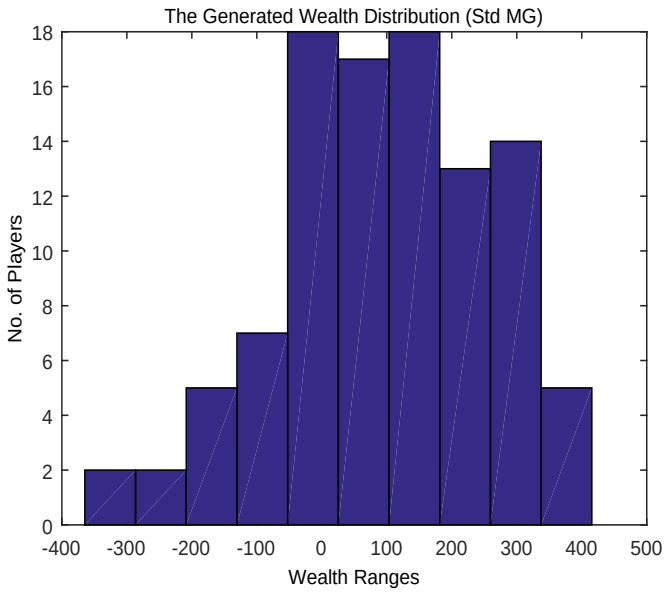

Figure 3.5: An example of generated wealth distribution.

butions using various values of time steps. However, the distribution generated in this fashion never truly stabilises. This is caused by the decrease in the sum of players' wealth: since only minority wins each time step, the total wealth of the group is not conserved. The distribution eventually contains increasing number of negative-value bins, indicating that the system allows players to continue playing the game even when their wealth is negative.

However, in the real world, investors must attract external resources to continue participating in the game when they are facing the risk of bankruptcy. Otherwise, they have to leave the market with losses. In order to make the statistical model more realistic, the study assumes that an equal number of new investors will come to the market with the same amount of initial wealth if any existing investors go bankruptcy.

The wealth distribution generated by the updated model no longer contains negative values, and the total number of players remains the same as the initial odd number throughout the game because the number of inflow players equals the number of outflow players. Thus, the system might be in a stable condition. The following figure shows the newly generated wealth distribution histograms.

Figure 3.6 is an example of non-negative wealth distribution ($T = 1000$). It

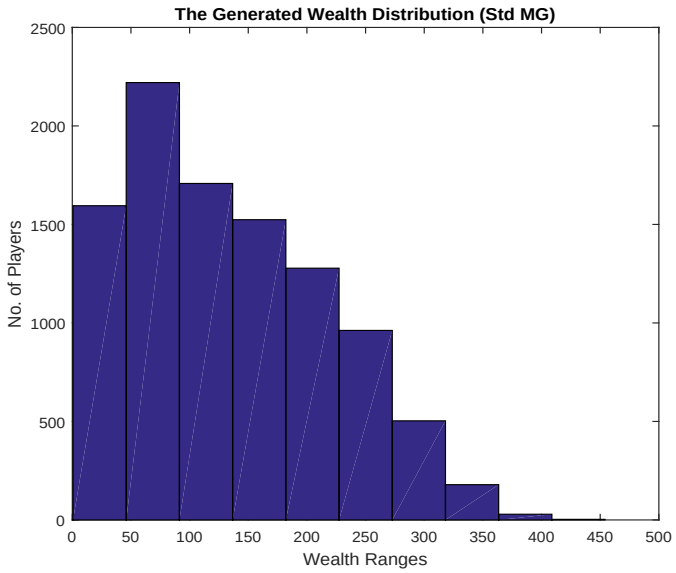

Figure 3.6: An example of generated wealth distribution without negative bins.

evidently contains no negative bins in the histograms, as we replace the bankruptcy players with fresh ones. However, the distributions from different program runs do not achieve a stationary state, continuing to evolve slowly with time. Figures 3.10 and 3.11 in the appendix demonstrate the cases that at very large time steps ($T = 2000$ and $T = 3000$ respectively), the distribution broadens with a sharp peak near the origin representing the fresh injection of players. Leaving aside the peak near the origin, we have been able to use the following equation to perform curve fitting on the generated wealth distributions.

$$f(x) = ax^{-b}, \tag{3.9}$$

where a, b are both non-zero constants.

The confidence bounds are set to 95% as default. Table 3.2 below shows the results from different runs.

N	m	T	The value of parameter b				
10001	3	2000	0.7559	0.7891	0.6694	0.5392	0.5263
10001	3	3000	0.8225	1.0390	0.7848	0.8448	0.8765
10001	3	4000	1.1150	0.9688	0.9983	1.0220	1.0110

Table 3.2: Example of the value of parameter b with different numbers of time steps.

According to Table 3.2, the value of power parameter, b, increases as the time step increases. Table 3.3 shows the average value of power from different runs with the same parameters' values.

N	m	T	b
10001	3	2000	0.6598 ± 0.1007
10001	3	3000	0.8543 ± 0.0870
10001	3	4000	1.0224 ± 0.0493

Table 3.3: The average value of parameter b with different numbers of time steps.

The standard deviation is relatively small compared to the value of power. However, the value of power still increases as time steps increase, indicating that the wealth distribution within the system continues to evolve. The following section suggests a method that potentially reduces this effect.

3.3.2 Zero-sum case

Recall that the wealth distribution from the standard MG is unstable due to the system's decreasing wealth. Increasing the system's wealth by introducing new players does not give rise to a stationary distribution either. Next, the system is adjusted to the zero-sum case.

A new option is added in order to achieve the zero-sum: the payoffs are scaled so that at each time step the gain made by the winners cancels exactly the loss made by the losers. In addition, if the wealth of any of the players decreases to zero, this(these) player(s) can borrow the initial wealth from other players repeatedly. The contributions from other players are proportional to their existing wealth. Then the modified model could be understood as a type of 'self-financing' system where there are either no external outflows or cash inflows [148].

As before, curve fitting is performed for the generated wealth distribution. Repeatedly, the system generates values of parameter b. The results are presented in Table 3.4.

N	m	T	The Value of Parameter b				
10001	3	2000	0.7135	0.8974	0.6696	0.5522	0.7559
10001	3	3000	0.8454	0.8717	0.8163	0.9425	0.9965
10001	3	4000	0.9316	1.0200	1.0610	1.0500	0.9842
10001	4	3000	0.6717	0.6604	0.5906	0.6688	0.6454
10001	4	4000	0.7342	0.7678	0.6851	0.8358	0.5758
10001	4	5000	1.0590	0.7585	0.9906	1.0040	0.8524

Table 3.4: Example of the value of parameter b with different values of memories and time steps (zero-sum case).

Table 3.5 lists the average values of power with different memories and time steps.

N	m	T	b
10001	3	2000	0.7177 ± 0.1260
10001	3	3000	0.8945 ± 0.0737
10001	3	4000	1.0094 ± 0.0527
10001	4	3000	0.6474 ± 0.0333
10001	4	3000	0.7197 ± 0.0973
10001	4	5000	0.9329 ± 0.1237

Table 3.5: The average value of parameter b with different values of time steps (zero-sum case).

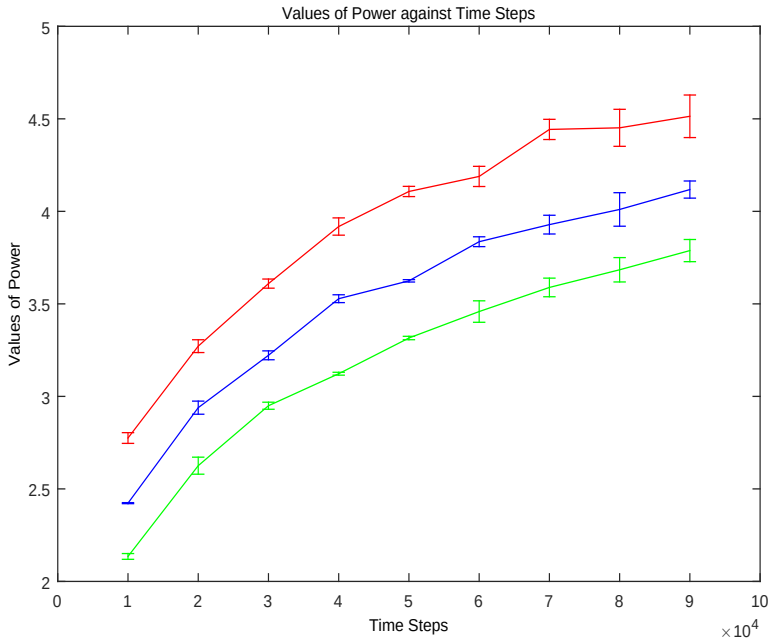

Figure 3.7: Values of calculated parameter b ($N = 1001$, repeats= 100).

Figure 3.7 represents the values of power from the fitting curves (red: $m = 3$, blue: $m = 4$, green: $m = 5$). As the figure illustrates, the appear to asymptote, but within the time and computational resources available, the system did not completely stabilise. The results obtained from zero-sum processes appear to improve on those from non-zero-sum processes, but the results are not deemed consistent enough for publication. This remains an area of possible future work.

3.4 Leverage effect

3.4.1 The leverage effect

Previously, the assumption was made that every player play had the same stake at each time step. With consideration of leverage products in the financial markets, we relax this assumption in this section. We introduce the double bet situation when a player loses the previous game. It offers the chance to potentially double their payoffs and win back losses. Table 3.6 presents the fitted values of power after this modification.

N	m	T	The Value of Parameter b				
10001	3	2000	1.427	1.252	1.267	1.393	1.606
10001	3	3000	2.103	3.594	2.308	2.148	2.345
10001	4	4000	2.206	1.265	2.033	1.548	2.210

Table 3.6: Example of the value of parameter b with leverage effect.

The values of parameter b range from 1.3 to 2.2. The following table shows the average value of power for each scenario when the leverage effect is introduced.

N	m	T	b
10001	3	2000	1.3890 ± 0.1434
10001	3	3000	2.4996 ± 0.6203
10001	4	4000	1.8522 ± 0.4250

Table 3.7: The average value of parameter b with leverage effect.

We see that changing the time step from 2000 to 3000 whilst keeping the memory as a constant, lead to a significant change of power. The leverage effect generally destabilises the system, which is confirmed by increased bankruptcy rates presented in the the next section. As risk theory states [149], the higher the risk is, the more profit one can gain. A leveraged product may create increased profits, but it may also lead to larger losses for investors.

3.4.2 The bankruptcy rate vs. memory

This section demonstrates the relationship between bankruptcy rate and memory. When the wealth of a player drops to zero, the player is considered bankruptcy. An example of a plot where $T = 500$ is given in Figure 3.8:

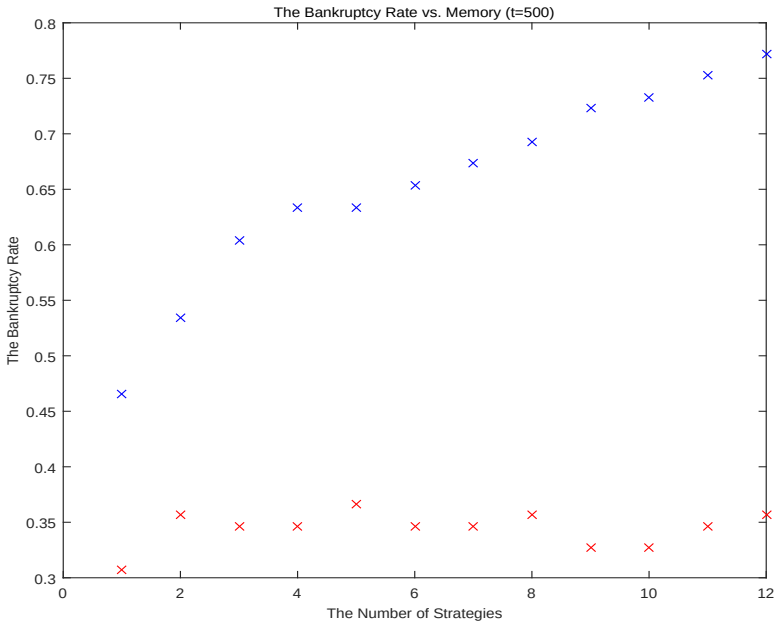

Figure 3.8: Bankruptcy rates vs. memory lengths when $t = 500$.

In Figure 3.8, the red crosses show cases without leverage effect, and the blue crosses shows cases with leverage effects. The bankruptcy rate climbs as the value of memory increases. In other words, the leverage effect increases the chance of going bankruptcy, which is in line with the financial theory that leverage products are highly risky [150]. Likewise, we have obtained plots from different time steps which are attached in this chapter's appendix (Figure 3.12 - Figure 3.15). According to the sets of figures, the leverage effect is found to affect instability in all cases. In the case where leverage is considered, the memory is also a factor for increasing the system's instability.

3.4.3 The bankruptcy rate vs. time steps

This section investigates the relationship between the bankruptcy rate and time steps. The memory is kept as a constant for each run of the program. An example is given in the following figure:

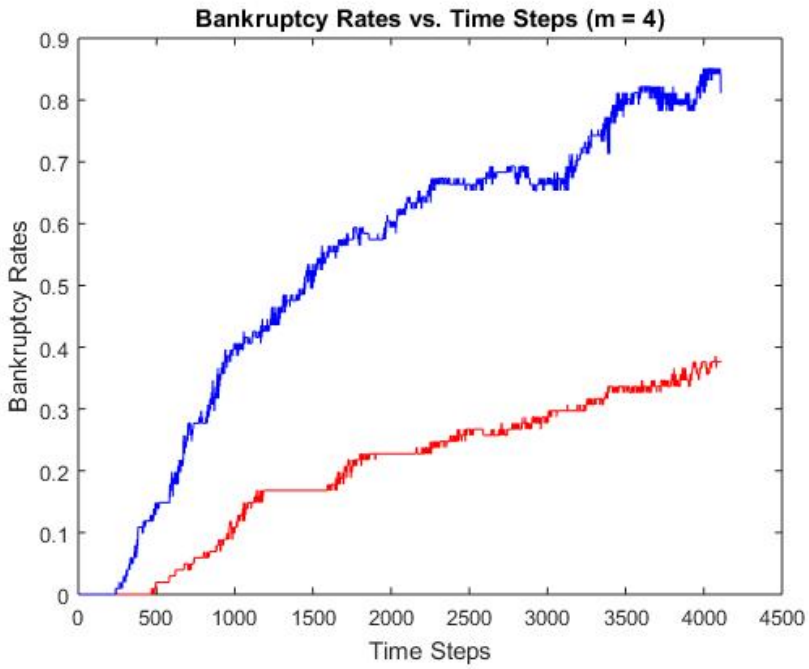

Figure 3.9: Bankruptcy rates vs. time steps when $m = 4$.

Figure 3.9 shows the relationship between bankruptcy rate and time steps ($m = 4$). The blue curve indicates cases with a leverage effect and the red curve indicates cases without a leverage effect. The leverage effect makes the player go bankruptcy quicker and also leads to more players going bankruptcy. The bankruptcy rate jumps when time increases, which refers to the 'cluster effect' [151]. As a result, one or some players' losses might affect other players.

Additional curves have been generated with different parameter values indicating similar patterns, which are attached in this chapter's appendix (Figure 3.16 - Figure 3.19). A proper risk analysis seems appropriate before investing in leveraged products.

The MG has drawn the attention of many researchers' attention and has been a popular research topic in recent years. In our study, we have extended the MG

to explore the wealth distribution and the leverage effect. We have found that leverage could dramatically increase the system's instability, which implies that in the real financial market, the risks of trading leveraged products should not be under-estimated. The statistics of our simulation did not reach the high standard for publication, but we believe our effort offers a basis for exploring broader issues of financial stability and market regulations. This area clearly merits further research work.

3.5 Appendix

The following section presents the figures generated from different parameter values. Firstly, the wealth distribution is generated by using two different time steps, $t = 2000$ and $t = 3000$.

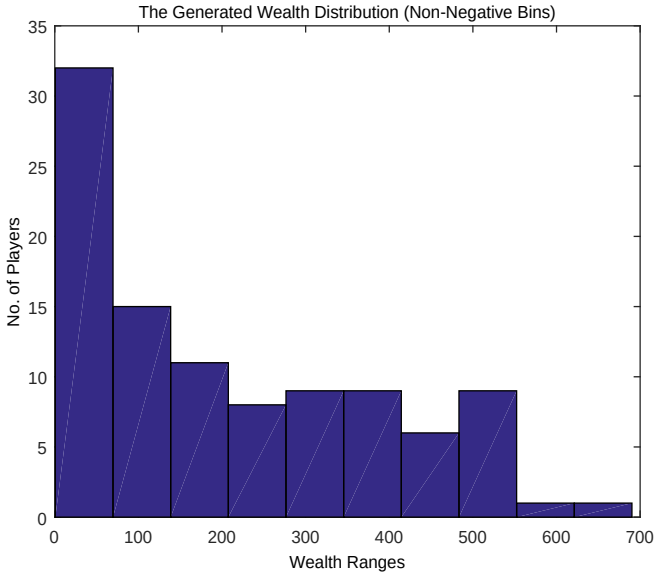

Figure 3.10: The generated wealth distribution without negative bins where $N = 10001$, $t = 2000$.

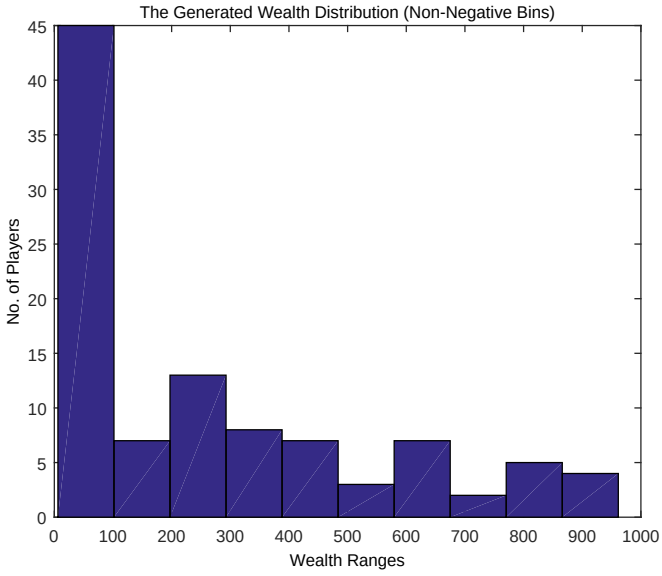

Figure 3.11: The generated wealth distribution without negative bins where $N = 10001$, $t = 3000$.

These generated wealth distributions indicate that they may be fitted by power

law distribution. Then the plots of bankruptcy rates against memory lengths are shown.

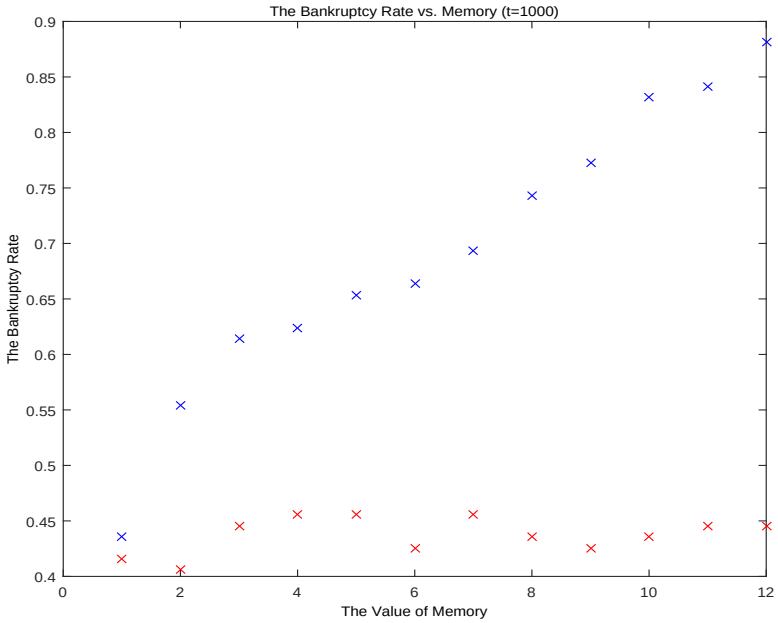

Figure 3.12: Bankruptcy rates vs. memory lengths when $t = 1000$.

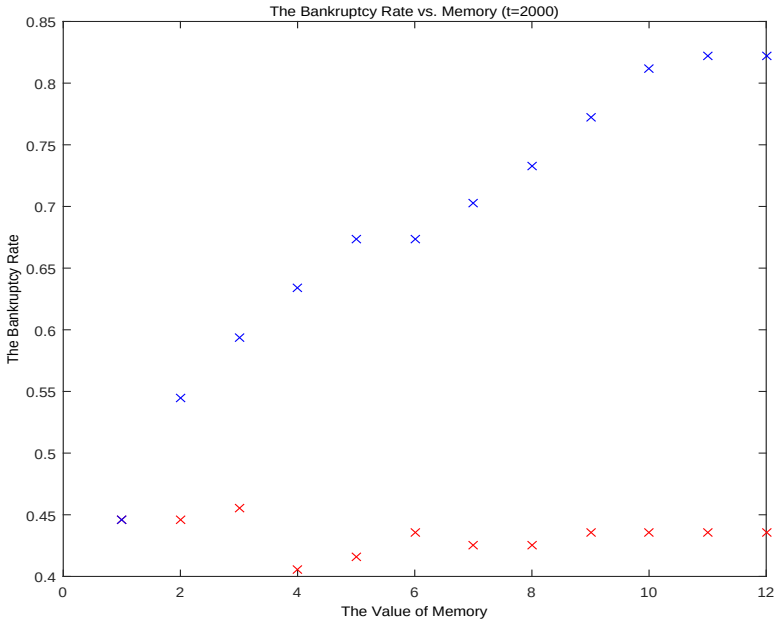

Figure 3.13: Bankruptcy rates vs. memory lengths when $t = 2000$.

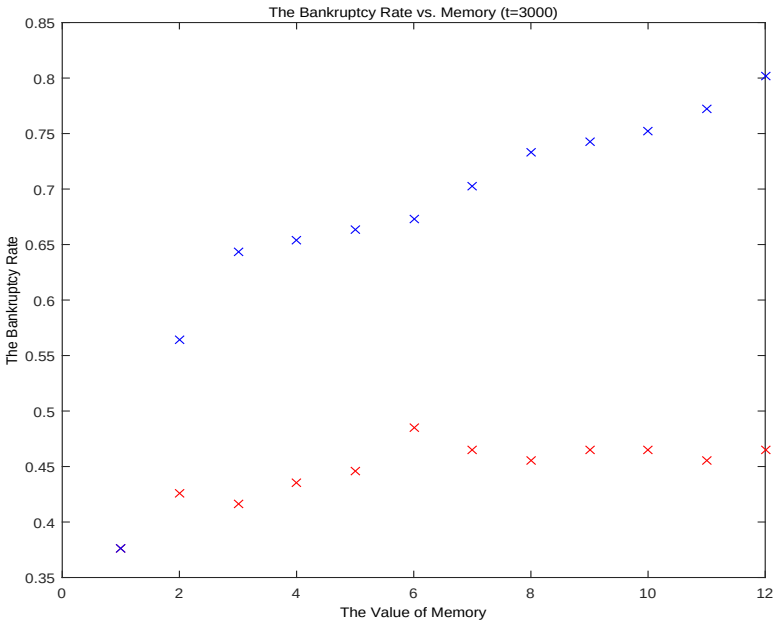

Figure 3.14: Bankruptcy rates vs. memory lengths when $t = 3000$.

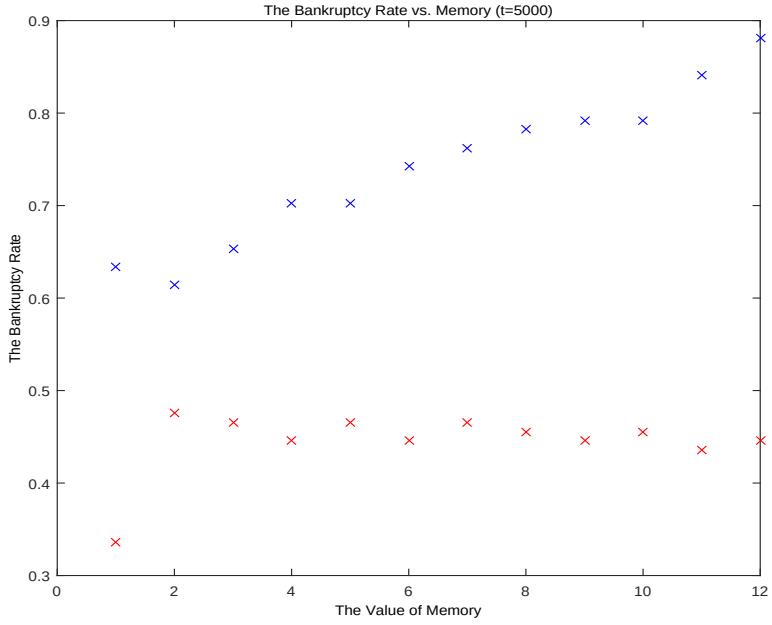

Figure 3.15: Bankruptcy rates vs. memory lengths when $t = 5000$.

These four generated figures follow similar patterns. It agrees that the leverage effect increases risk. Finally, we present the plots for bankruptcy rates against time steps using different agents' memory lengths.

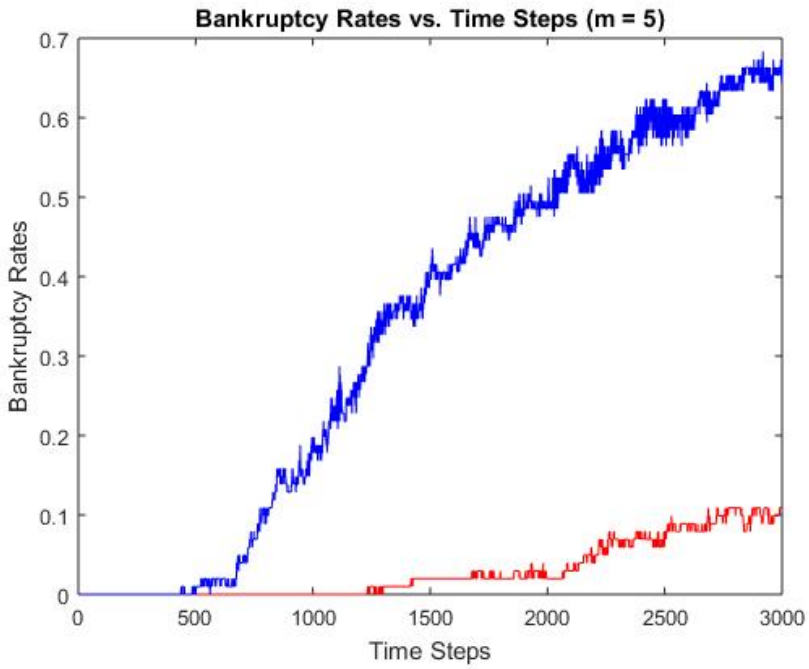

Figure 3.16: Bankruptcy rates vs. time steps when $m = 5$.

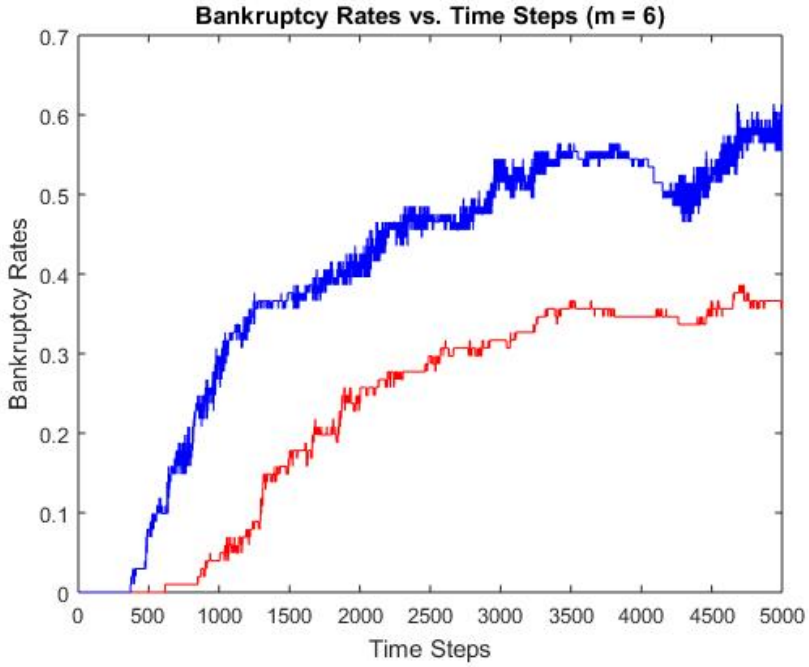

Figure 3.17: Bankruptcy rates vs. time steps when $m = 6$.

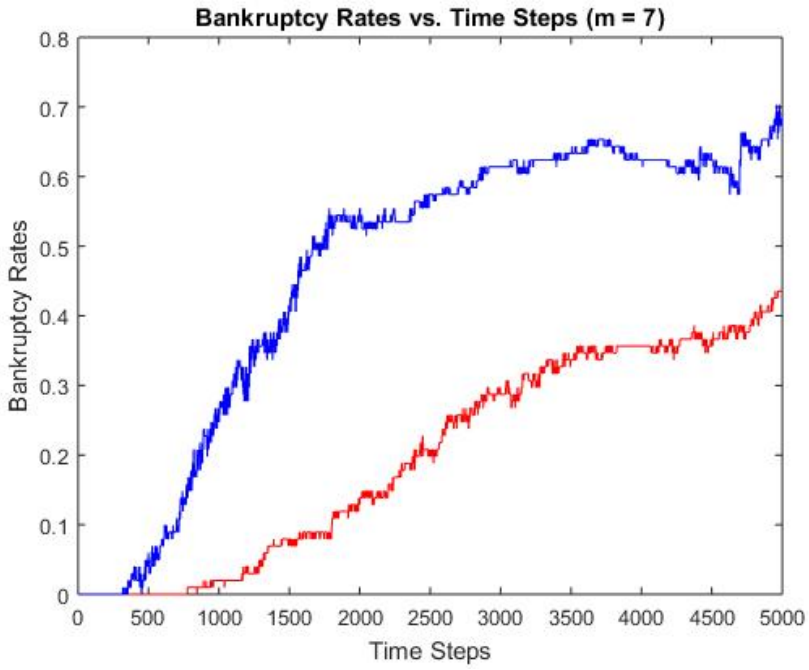

Figure 3.18: Bankruptcy rates vs. time steps when $m = 7$.

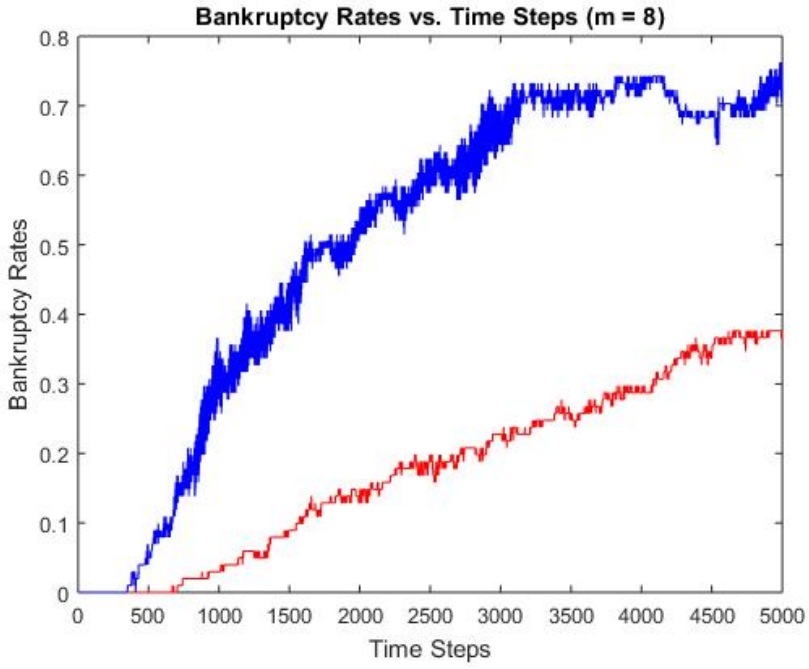

Figure 3.19: Bankruptcy rates vs. time steps when $m = 8$.

Chapter 4

New urn model

This chapter demonstrates how a model is built to illustrate the effectiveness of memory. Agents, in this model, have different memory lengths and compete for finite resources. Using analytical and numerical approaches, the research demonstrates that instability exists at a critical memory length; hence, players with different memory lengths are able to compete with each other and achieve a state of co-existence. The analytical solution is found to be connected to the urn models. Additionally, the findings also demonstrate that the temperature introduced in the urn model is mirrored by the agent's memory. This simple model could potentially be applied to a variety of other game models, where an example is investigated in the next chapter.

The rest of this chapter is structured as follows. In Section 4.1, the model is defined. In Section 4.2, simulation results are presented followed by theoretical analysis in Section 4.3. Finally, a conclusion is drawn, along with a brief discussion on the limitations of the study and potential future work.

4.1 Model definition

The case of two urns and a total of n agents is considered. The urns yield $U_1(t)$ and $U_2(t)$, where they are random variables uniformly distributed on $[0, \omega n]$ and $[0, n]$, at round t respectively. ω is a parameter we set, $\omega > 1$, so that urn 1 yields more on average than urn 2. This choice of yield distribution is motivated by simplicity-only one extra model parameter, ω, is required to describe it. The behaviour of the model is not tied to the particular choice of yield distribution; it requires only that the yields have finite variance, allowing the central limit theorem [152] to be applied to sums of payoffs. At time t, agents' access to the arithmetic mean of the last τ payoffs is allowed, however other forms of sampling could also be used. Letting ϕ_t be the fraction of agents in urn 1, then the difference in the average payoffs between urn 1 and urn 2 is

$$\Delta_t := \frac{1}{\tau} \sum_{s=0}^{\tau-1} \left[\frac{U_2(t-s)}{n(1-\phi_{t-s})} - \frac{U_1(t-s)}{n\phi_{t-s}} \right], \tag{4.1}$$

where τ is refereed as the "memory length" of the agents. Agent dynamics is encoded in transition probabilities between urns, which are deterministic functions of Δ_t. At each round, each agent will switch urns using the probabilities

$$W_{1\to 2}(\Delta) = \frac{\epsilon}{2}[1 + \tanh(\beta\Delta)], \tag{4.2}$$

$$W_{2\to 1}(\Delta) = \frac{\epsilon}{2}[1 - \tanh(\beta\Delta)]. \tag{4.3}$$

These transitions are used in evolutionary game models, where changes in strategy are made based upon perceived increases in payoff, but with some degree of noise or irrationality in the switching process. The level of this stochasticity in decision making, which has been experimentally measured in humans [153] is captured by the parameter β, the "inverse temperature". For finite β, agents may decide to switch strategies even though their estimate of the payoff difference is

unfavourable. In the limit $\beta \to \infty$, agents will only move if their estimate of the payoff difference indicates that the move is favourable. The parameter ϵ controls the rate at which strategy switching takes place compared to the rate at which yield information arrives, or equivalently the inertia in agent's decision making. It may also be seen as the frequency with which opportunities to switch strategy arise. In the limit $\epsilon \to 1$, at most one agent will move at each round. The effects which we uncover do not require that the transition probabilities take the particular forms of Equations (4.2) and (4.3). In Section 4.5.1, we show that the same qualitative behaviour is observed for transition probabilities that increase in proportion with the perceived payoff difference ($\pm\Delta$), provided the difference is positive and $|\Delta| < \epsilon^{-1}$.

4.2 Simulation results

4.2.1 Instability

The model for a series of values of τ when $n = 10^6$ is simulated. Two different values of ϵ are used; in Figure 4.1, we have $\epsilon^{-1} = 10^6 \gg \tau$ and in Figure 4.2, $\epsilon = 10^{-3}$ is set. For $\epsilon = 10^{-6}$, the expected number of moves at each step is < 1, and ϕ appears very stable. For larger ϵ, ϕ experiences much larger fluctuations about the steady-state value, driven by the yield process. For shorter memory values these fluctuations are random, but as τ approaches ϵ^{-1}, periodic oscillations appear and dominate. The appearance of these stable oscillations at critical memory, τ_c, calculated analytically in Section 4.3, is known as a Hopf bifurcation [47]. The bifurcation parameter is memory, which is a combination of ϵ and τ, whilst simulations are shown for different ϵ and same τ, analysis will be performed assuming varying τ with ϵ fixed. From Figures 4.1 and 4.2, the number of rounds taken for the system to evolve to steady state have been observed, in the probabilistic sense, starting from an equal distribution between the two urns, is $\approx \epsilon^{-1}$. By allowing agents to access only to the mean of their memory,

we implicitly assume that changes in the expected payoff over the course of their memory, brought about by oscillations, are too subtle for them to infer from noise.

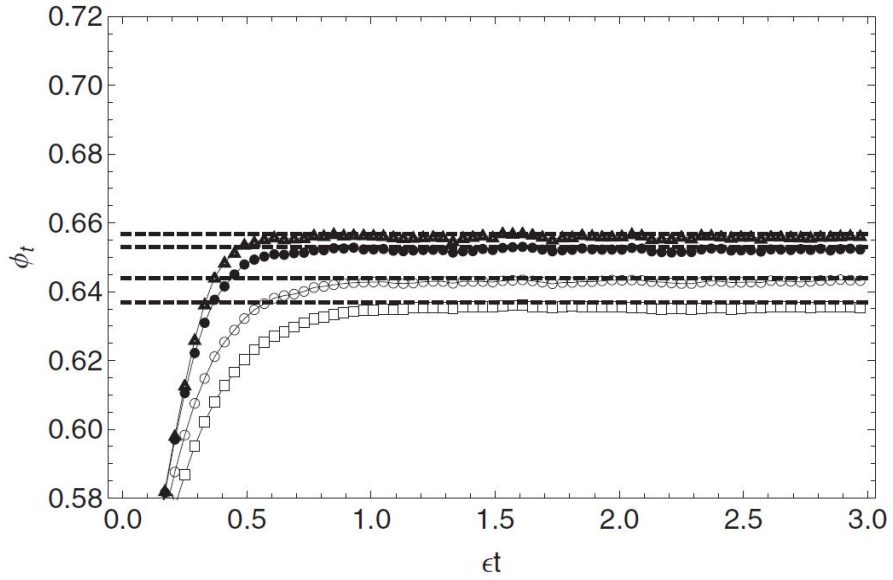

Figure 4.1: Evolution of ϕ_t when $n = 10^6$, $\omega = 2$, $\beta = 5$, $\epsilon = 10^{-6}$, and $\phi_0 = 0.5$. Memory values are $\tau \in \{5, 10, 50, 500\}$ (squares, circles, dots, triangles, respectively). Dashed lines are analytical equilibrium values [see Equation (4.12)]. Critical memory is $\tau_c = 1.8 \times 10^5$.

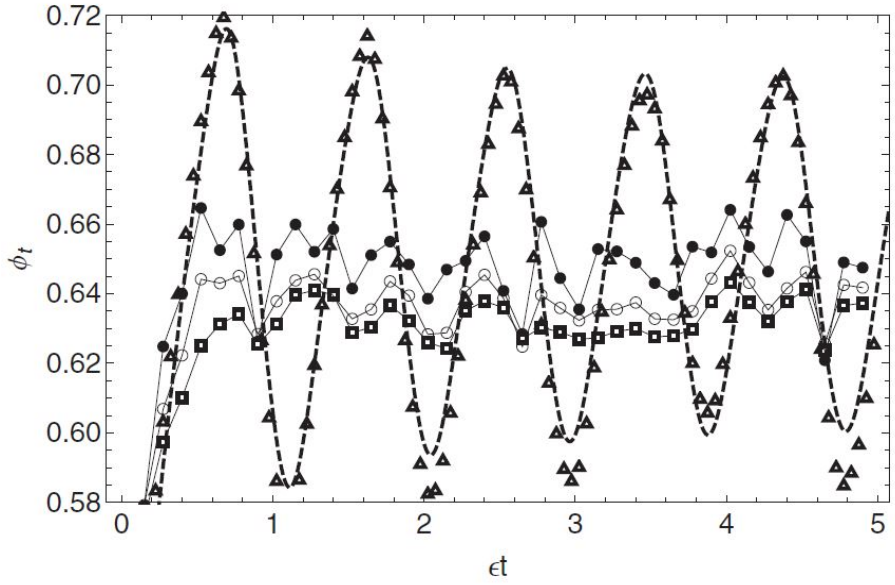

Figure 4.2: Evolution of ϕ_t when $n = 10^6$, $\omega = 2$, $\beta = 5$, $\epsilon = 10^{-3}$, and $\phi_0 = 0.5$. Memory values are $\tau \in \{5, 10, 50, 500\}$ (squares, circles, dots, triangles, respectively). Dashed lines is solution to Equation (4.16) when $\tau = 500$ and ω, β, ϵ are as above. Critical memory is $\tau_c \approx 390$.

4.2.2 Coexistence

We now investigate how agents switch two different memories, and compete against one another by interpreting the payoff as reproduction rate. The quantities δ and γ are defined as rates of death and reproduction per unit payoff, respectively. Reproduction is assumed to occur before death in each round, but in practice the probability of any one agent reproducing and dying in the same round is extremely small for the γ, δ values we choose. Letting $p_i^\tau(t)$ be the number of agents with memory τ in urn i at time t we set the probability of birth for each agent in urn i to be

$$\mathbf{P}(\text{birth}) = \frac{\gamma U_i(t)}{\sum_\tau p_i^\tau(t)}. \tag{4.4}$$

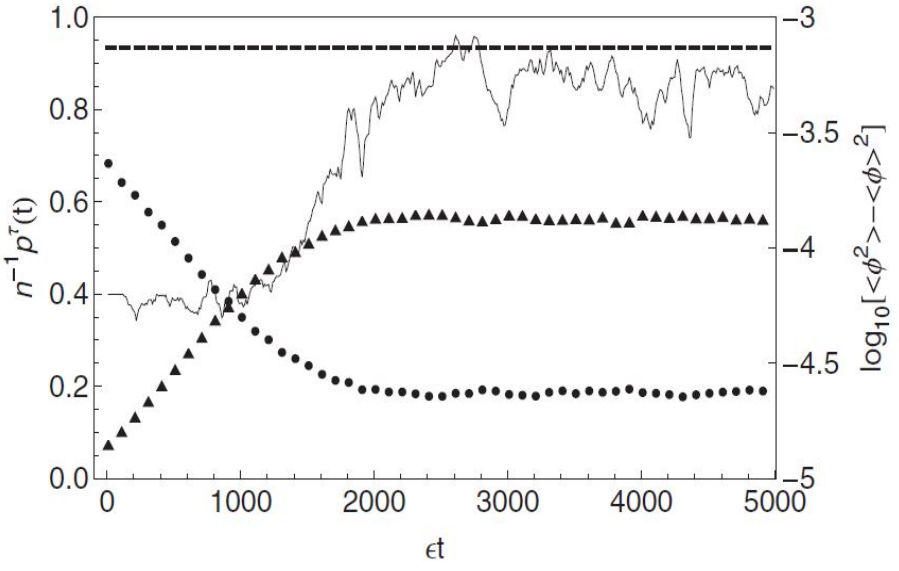

Figure 4.3: Scaled populations $p^\tau(t) := p_1^\tau(t) + p_2^\tau(t)$ for $\tau = 10$ (circles) and $\tau = 1000$ (triangles) when total initial populations is $n = 10^6$, $\epsilon = 10^{-3}$, $\beta = 5$ with $\gamma = 10^{-4}$ and $\delta = 2 \times 10^{-4}$. Also shown (thin black line) is evolution of variance of ϕ_t, over a moving time window of 105 steps, during population dynamics simulation. Straight dashed line shows variance of homogeneous population with the same ϵ, β, ω values at critical memory $\tau_c \approx 390$, where τ_c is calculated analytically using the theory of Hopf bifurcation. Note: rapid initial equilibration of population values (bringing birth and death into balance) is not visible on time scale of plot.

The denominator in this term is the total population in urn i, reflecting the fact that the yield $U_i(t)$ is shared between all agents in the urn. When a given agent reproduces, he produces a copy of himself in his current urn, having the

same memory length, τ. The death probability for each agent is set equal to δ. If populations are fixed in size and the system is not in an oscillatory state, the longer-memory agents will dominate the high yielding urn is expected. Their long memory allows them to perceive smaller statistical advantages that are obscured by noise for the short-memory agents. Using the thermodynamic analogy, the higher-temperature (shorter-memory) agents are more likely to make moves that leave them in an urn with a lower expected payoff, corresponding to a higher "energy" state. Above zero temperature, and in the absence of oscillations, the high yield urn will be under-exploited, placing long-memory agents at an advantage. This effect can be observed in Figure 4.3, where a mixed population of two memories $\tau \in \{10, 1000\}$ beginning with a ratio of 10 : 1 short-memory to long-memory agents has been simulated. We observe that initially the advantage afforded by the long-memory agents causes their population to grow, whereas the short-memory agents reduce in number. Were this advantage to be sustained indefinitely then we would expect the short-memory agents to eventually disappear, but in fact the populations stabilize. This effect appears because the long-memory agents cause oscillations to develop once they are in sufficiently high concentration. In the presence of oscillations the short-memory agents have an advantage because they can quickly observe opportunities offered by the oscillating payoffs. Therefore we expect the system to evolve to the point where oscillations are just beginning to form. We may observe this evolution by making use of the variance of ϕ_t as an order parameter that captures proximity to the Hopf bifurcation point. In Figure 4.3 we see that at a critical ratio of short- to long-memory agents, the variance climbs rapidly, stabilizing just below the value seen in a system where all agents have memory τ_c but all other parameters are equal. In this way the Hopf bifurcation may be viewed as a self-organized state.

4.3 Analysis

4.3.1 Equilibrium

The behaviour of our model is considered as $\epsilon \to 0$, allowing us to view it as an urn model in the Ehrenfest class [92], where agents independently make transitions using state (ϕ_t) dependent probabilities. Provided $\tau \ll \epsilon^{-1}$, the fraction ϕ_t may be approximated by a constant ϕ during the window over which payoff averaging takes place. In this case, by the central limit theorem, the marginal distributions of Δ_t for each t are approximately normal $N(\bar{\Delta}, \sigma^2/\tau)$, (the detailed derivations are produced in Section 4.5.2). Here we quote the expressions for $\bar{\Delta}(\phi, \omega)$ and $\sigma^2(\phi, \omega)/\tau$ as

$$\bar{\Delta}(\phi, \omega) := \frac{1}{2}\left(\frac{1}{1-\phi} - \frac{\omega}{\phi}\right), \tag{4.5}$$

$$\frac{\sigma^2(\phi, \omega)}{\tau} := \frac{1}{12\tau}\left[\frac{\omega^2}{\phi^2} + \frac{1}{(1-\phi)^2}\right], \tag{4.6}$$

respectively. Recall that Δ is the differential payoff of the 2 urns in an agent's memory (Equation (4.1)), and $\bar{\Delta}$ is its average over the urn payoff (characterised by ω) at any given ϕ; correspondingly, σ^2/τ is the standard deviation arising from this average. A intermediate time scale T is introduced which satisfies $\tau \ll T \ll \epsilon^{-1}$ and the time average $\langle ... \rangle$ is defined, over a window of length T,

$$\langle W_{i\to j}(\Delta)\rangle(t) := \frac{1}{T}\sum_{s=t-T+1}^{t} W_{i\to j}(\Delta_s). \tag{4.7}$$

This average is a random variable which, for constant ϕ, has expected value $\mathbf{E}[W_{i\to j}(\Delta)]$, where the expectation is taken over the marginal distribution of Δ. The condition $\tau \ll T \ll \epsilon^{-1}$ ensures that ϕ is approximately constant over the window and that the variance of $\langle W_{i\to j}(\Delta)\rangle$ is proportional to T^{-1} (because Δ_{t_1} and Δ_{t_2} are dependent only when $|t_2 - t_1| < \tau \ll T$). As $\epsilon \to 0$, then assuming T is sufficiently large, the probability that an agent will make a transition $i \to j$ during

interval T approaches $T\langle W_{i\to j}(\Delta)\rangle \approx T\mathbf{E}[W_{i\to j}(\Delta)]$, equivalent to a memoryless (Ehrenfest class) model, where transition probabilities, Equations (4.2) and (4.3), are replaced with their expectations $\mathbf{E}[W_{i\to j}(\Delta)]$. Averaging over the normally distributed difference Δ we find that

$$\langle W_{i\to j}(\Delta)\rangle \approx \mathbf{E}[W_{i\to j}(\Delta)] \approx \frac{\epsilon}{2}[1+\tanh(\alpha\bar{\Delta})], \tag{4.8}$$

where

$$\alpha = \sqrt{\frac{2\tau\beta^2}{2\tau+\pi\beta^2\sigma^2}}. \tag{4.9}$$

To obtain this result, the approximation $\tanh(\beta\Delta) \approx \mathrm{erf}(\sqrt{\pi}\beta\Delta/2)$ has been made, when $\beta\Delta$ is small, allowing us to make use of the exact relationship $\mathbf{E}[\mathrm{erf}(\sqrt{\pi}\beta\Delta/2)]$. The constant α acts as an effective inverse temperature and we see that increasing τ "cools" the system closer to the inverse temperature β, and in the limit $\beta\to\infty$, $\alpha\propto\sqrt{\tau}$. To complete our analogy to a thermal urn model we now write the probability of finding the agents in a particular arrangement, or microstate, i, such that a fraction ϕ are in urn 1, as $p_i(\phi)\propto e^{-\alpha E}$ where E is an "energy" function. Considering two microstates separated by a single transition, and defining $\delta\phi = 1/n$, then detailed balance requires that in equilibrium $2\alpha\bar{\Delta} = \partial_\phi(\alpha E)\delta\phi$. This condition allows $E(\phi)$ to be computed, in principle, by integration. A closed form approximation $E(\phi) \approx -n\ln[\phi^\omega(1-\phi)]$ is obtained by noting that α depends weakly on ϕ compared to E so that $\partial\phi(\alpha E) \approx \alpha\partial_\phi E$. Summing over all microstates corresponding to macrostate ϕ we have a Boltzmann probability distribution for ϕ,

$$\mathbf{P}(\phi) = \frac{n!}{(n\phi)![n(1-\phi)]!}\frac{e^{-\alpha(\phi)E(\phi)}}{Z}, \tag{4.10}$$

where Z is the partition function. Taking the thermodynamic limit $n\to\infty$, and making use of Stirling's approximation, we find that the most likely fraction, $\bar{\phi}$, satisfies (where detailed derivations can be found in Section 4.5.2)

$$\frac{1}{2n}\frac{\partial}{\partial\phi}\ln\mathbf{P}(\phi) = -\alpha\bar{\Delta} - 2\phi + 1 = 0. \tag{4.11}$$

As the memory increases and the system cools we expect the agents to arrange themselves so that yields are shared more fairly. Therefore Equation (4.11) is linearised about the perfectly fair state, $\phi = \omega/(1+\omega)$, where agents in both urns receive the same expected payoff, finding that

$$\bar{\phi} \approx \frac{f(\tau) + \frac{\beta(1+\omega)^2}{2}}{2f(\tau) + \frac{\beta(1+\omega)^3}{2\omega}}, \tag{4.12}$$

where

$$f(\tau) = \sqrt{1 + \pi\beta^2(1+\omega)^2/(12\tau)}. \tag{4.13}$$

The accuracy of this approximation is verified in Figure 4.1. For larger values of ϵ (Figure 4.2), agents move more quickly so the averaging effect Equation (4.8) damps fluctuations in transition rates less strongly, creating larger fluctuations in ϕ_t. For finite β the system cannot reach perfect fairness for any memory length, but in the limit $\beta \to \infty$ where the transition probabilities, Equations (4.2) and (4.3), become step functions, we have that

$$\bar{\phi} \approx \frac{\omega}{\omega+1}\left[1 - \frac{\sqrt{\pi}(\omega-1)}{\sqrt{3\pi}(\omega+1)^2} + \mathrm{O}\left(\tau^{-1}\right)\right]. \tag{4.14}$$

From this we see that the distance away from the fair state decreases as $\tau^{-1/2}$ as the memory of the agents becomes large.

We have shown that when the time-scales of switching and agent memory are sufficiently separated, our model behaves as a memoryless dynamical urn model [92, 108] with time-averaged transition rates. This averaging is equivalent to a rescaling of temperature, and we have given an approximate analytic expression for this new temperature, α, in terms of the underlying "selection temperature" of agents, β, and their memory length, τ. The study of the dynamics of particles in urns began with Ehrenfest's dog-flea model [108], where agents make random transitions between two urns at a fixed rate without reference to energy or temperature. Thermal models [92] include an energy, E, and have transition

probabilities that respect detailed balance with respect to the Boltzmann distribution. These probabilities are decreasing functions of $\beta\Delta E$, where ΔE is the energy change associated with the transition, and β is the inverse thermodynamic temperature, so that reducing temperature makes energy increasing transitions less likely. In our case, $\bar{\Delta}$ plays the role of an energy change and α is the inverse temperature. Increasing memory reduces α, making payoff reducing transitions less likely. However, if memory is increased to the extent that it becomes comparable to the timescale of switching between urns ($\approx \epsilon^{-1}$) then the model begins to behave quite differently to classical thermal urn models [92, 108]. It becomes important that the average payoff agents use to make decisions is calculated from the history of the system. This is because the populations in the urns are able to change significantly during the course of a single agent's memory, and so using delayed information for decision making can falsely identify the optimal urn. To understand mathematically why increasing τ too far, when ϵ is finite, destabilizes the system, we must make use of the theory of delay differential equations [47].

4.3.2 Instability

As τ increases, fluctuations in Δ_t due to the yield process are reduced but for finite ϵ we can no longer treat ϕ_t as a constant over the averaging window. It is instructive, therefore, to study the effect of variations in ϕ_t, neglecting the variations in yield. Promoting t to a continuous variable and replacing the urn yields with their mean values we have

$$\Delta_t \approx \frac{1}{2\tau}\int_{t-\tau}^{t}\left[\frac{1}{1-\phi_s}-\frac{\omega}{\phi_s}\right]ds. \tag{4.15}$$

Then the evolution of ϕ_t is approximated by using the following delay differential equation:

$$\dot{\phi}_t = (1-\phi_t)W_{2\to1}(\Delta_t) - \phi_t W_{1\to2}(\Delta_t). \tag{4.16}$$

A numerical solution to this equation is shown in Figure 4.2, along with simu-

lation results using the same parameter values. The oscillations in the simulation are accurately captured by Equation (4.16), but the stochastic yield disrupts their perfect periodicity. To discover the parameter values at which stable oscillations develop, Equation (4.15) is linearised by writing $\phi_t = \bar{\phi} + \psi_t$, where ψ_t are small fluctuations and $\bar{\phi}$ is the constant fixed point, not necessarily stable, of Equation (4.15). In terms of these new variables,

$$\Delta_t \approx \bar{\Delta}(\bar{\phi}, \omega) + 6\frac{\sigma^2(\bar{\phi}, \sqrt{\omega})}{\tau} \int_{t-\tau}^{t} \psi_s ds, \tag{4.17}$$

where the functions $\bar{\Delta}$ and σ^2 are defined in Equations (4.5) and (4.6). After expanding the tanh functions in the transition rates to first order about $\bar{\Delta}(\bar{\phi}, \omega)$, the following linear delay equation is obtained:

$$\dot{\psi}_t = -\epsilon \left[\psi_t + \frac{A}{\tau} \int_{t-\tau}^{t} \psi_s ds \right], \tag{4.18}$$

where

$$A = 3\beta \text{sech}^2[\beta \bar{\Delta}(\bar{\phi}, \omega)] \sigma^2(\bar{\phi}, \sqrt{\omega}). \tag{4.19}$$

To determine the stability of this equation, an exponential trial solution $\psi_t = e^{\lambda t}$ where $\lambda = x + iy$ is introduced. Substitution into Equation (4.18) yields a characteristic equation with real and imaginary parts given by

$$x^2 - y^2 + \epsilon x + \frac{\epsilon A}{\tau}(1 - e^{-\tau x} \cos \tau y) = 0, \tag{4.20}$$

$$2xy + \epsilon y + \frac{\epsilon A}{\tau} e^{-\tau x} \sin \tau y = 0. \tag{4.21}$$

For sufficiently small memory, τ, the real part, x, of the solutions to Equations (4.20) and (4.21) is negative so the fixed point $\bar{\phi}$ is stable. As τ is increased, λ crosses through the imaginary axis, destabilizing the fixed point and creating oscillations of exponentially increasing magnitude in the linearised version Equa-

tion (4.18) of the full delay Equation (4.16). Although the fixed point of the full Equation (4.16) shares this transition to instability, we find that the resulting oscillations are bounded. The appearance of these stable oscillations as τ passes through a critical value, which we denote τ_c, constitutes the Hopf Bifurcation [47]. To compute τ_c we set $x = 0$ in Equation (4.21) so that $\mathrm{sinc}(\tau y) = -A^{-1}$, where $\mathrm{sinc}(\tau y) = \sin(\tau y)/\tau y$. Expanding the sinc function to second order about its root at π/τ and solving the resulting quadratic, we find that

$$y \approx \frac{\pi}{2\tau}\left(3 - \sqrt{1 - 4A^{-1}}\right) := \frac{\kappa}{\tau}, \tag{4.22}$$

which defines a new constant κ. Substitution of this solution into Equation (4.20) yields the following expression for the critical memory length:

$$\tau_c = \frac{\kappa^2}{\epsilon A(1 - \cos\kappa)}. \tag{4.23}$$

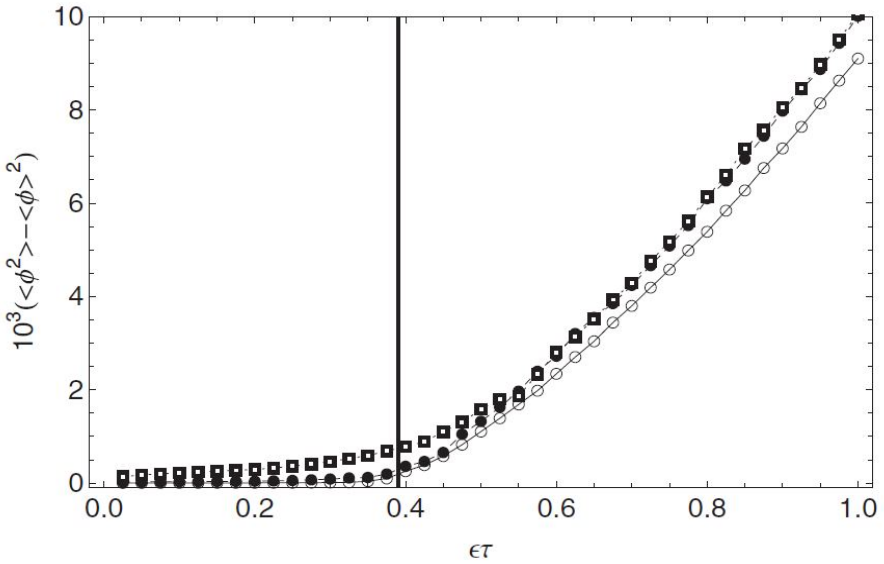

Figure 4.4: Estimated variance of ϕ_t in steady state, as a function of memory length τ, from simulations with $n = 10^6$, $\omega = 2$, $\beta = 5$ and $\epsilon = 10^{-3}$ (squares), 10^{-4} (dots), 10^{-5} (circles). Variance estimates computed using time average over 10^6 time steps for $\epsilon \in \{10^{-3}, 10^{-4}\}$ and 10^7 time steps for $\epsilon = 10^{-5}$. Vertical black line marks theoretical Hopf bifurcation point $\epsilon\tau_c = 0.39$, computed from Equation (4.16).

In order to test this analysis, in Figure 4.4 we have plotted estimates of the variance of ϕ_t in equilibrium as a function of memory length for three values of $\epsilon \in \{10^{-3}, 10^{-4}, 10^{-5}\}$. The transition from stable fixed point to limit cycles should, according to Equation (4.23), occur when the product $\epsilon\tau$ reaches a critical value, beyond which we expect the oscillations to increase the variance of ϕ_t. This behaviour is clearly observed in the Figure 4.4. For the largest ϵ value, the variance is significantly greater than zero for $\tau < \tau_c$ because the shorter memory length has a reduced damping effect on stochastic fluctuations in the yield process.

4.4 Conclusion

We have defined a simple thermal urn model of competition between agents with memory. Increasing memory allows agents to more accurately determine the most productive strategy and reduces the temperature of the model. However, a large number of long-memory agents can give rise to large collective fluctuations in the form of a limit cycle which reduces their competitiveness, whereas short-memory agents can exploit the fluctuations more effectively. By modelling payoffs as birthrate, we demonstrated a coexistence of different memories, and a self-organized Hopf bifurcation driven by population dynamics. The simplicity of our memory model, its connection to classical urn models, together with the fact that limit cycles arise naturally, suggest it might be fruitfully generalised and employed to study different games. For example, our approach may be applied to the Hawk-Dove game and the Rock-Paper-Scissors game [114], where agents, interacting pairwise, recall their last τ interactions [154]. Other natural extensions include the introduction of multiple urns to represent different sources of yield or game strategies, or heterogeneity in switching rates and a more general distribution of memory lengths. By introducing multiple urns we might expect to observe more complex patterns of oscillation [155] and regimes of behaviour [156]. Experimental research into the nature of human and animal memory [157, 158, 159, 160] places

emphasis on the "forgetting function", which describes how memories decay with time. Such a function, or greater powers of statistical inference, could be naturally incorporated into our analysis, and their effects on stability explored.

4.5 Appendix

4.5.1 Alternative transition probabilities

In this subsection, we address the following question: Is the (smoothed step) transition probability function essential to the effects we uncover? To motivate this question, we note that the step form,

$$W_{1\to 2}(\Delta) = \frac{\epsilon}{2}[1 + \tanh(\beta\Delta)], \tag{4.24}$$

produces transition rates that remain approximately constant for values of the payoff difference $\Delta \gg \beta^{-1}$. As β becomes large, agents become progressively less sensitive to the magnitude of the payoff difference, and in the limit $\beta \to \infty$ they react only to its sign. As an alternative we consider the following form of transition probability:

$$\tilde{W}_{1\to 2}(\Delta) = \begin{cases} \min(\epsilon\Delta, 1), & \text{if } \Delta \geq 0 \\ 0, & \text{if } \Delta < 0 \end{cases}, \tag{4.25}$$

with $\tilde{W}_{2\to 1} = \tilde{W}_{1\to 2}(-\Delta)$. Here we have no concept of irrationality in agent behaviour, and stochasticity in decision making is driven purely by noise inherent in the finite memory of agents. This corresponds to taking the limit $\beta \to \infty$ in the original rates. In contrast to the original form of Equation (4.24), here the transition probability is proportional to payoff difference provided that $\Delta < \epsilon^{-1}$. For the values of ϵ we consider, this condition is always met so, in contrast to the original rates, agents remain sensitive to the magnitude of Δ. With these new transition rates, the connection to thermal urn models is lost because they do not satisfy detailed balance with respect to a Boltzmann distribution for which Δ plays the role of an energy change.

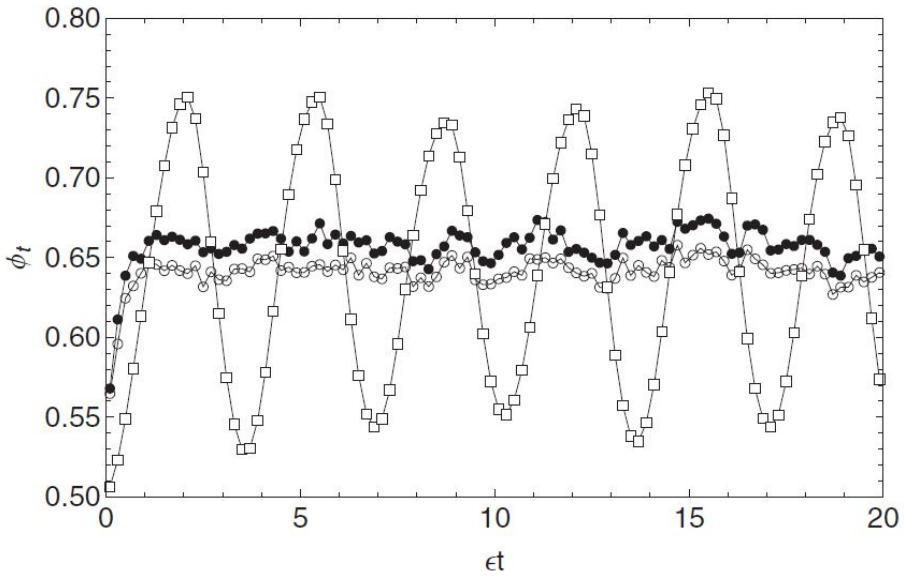

Figure 4.5: Evolution of ϕ_t (fraction of agents in urn 1) using alternative transition probabilities when $n = 10^6$, $\epsilon = 10^{-3}$, $\omega = 2$, and $\phi_0 = 0.5$. Memory values are $\tau \in \{5, 100, 1750\}$ (open circles, dots, squares).

We first explore the evolution of a system where all agents have identical memory. In Figure 4.5 we consider the case $\epsilon = 10^{-3}$ where we see that provided agents' memory is sufficiently short, the system remains stable. As with the original rates, increasing memory brings the system closer to the fair state $\phi = \omega/(1+\omega)$, but for long enough memory, high-amplitude regular oscillations appear. Qualitatively, therefore, the system behaves in the same way for both choices of rate. However, the critical memory length at which oscillations appear differs between the two choices.

We now consider the case of mixed memory with population dynamics. In Figure 4.6 we have simulated a population of two memory lengths $\tau \in \{100, 4000\}$ in the case $\epsilon = 10^{-3}$. From Figure 4.5 we see that these memory values lie below and above the critical length, respectively. We see that the behaviour of the system matches its behaviour in the case of smoothed step rates Equation (4.24): initially the population of short-memory agents declines. While the system possesses a stable fixed point (no oscillations) agents with a longer memory make more accurate estimates of the true payoff difference between the urns and are less

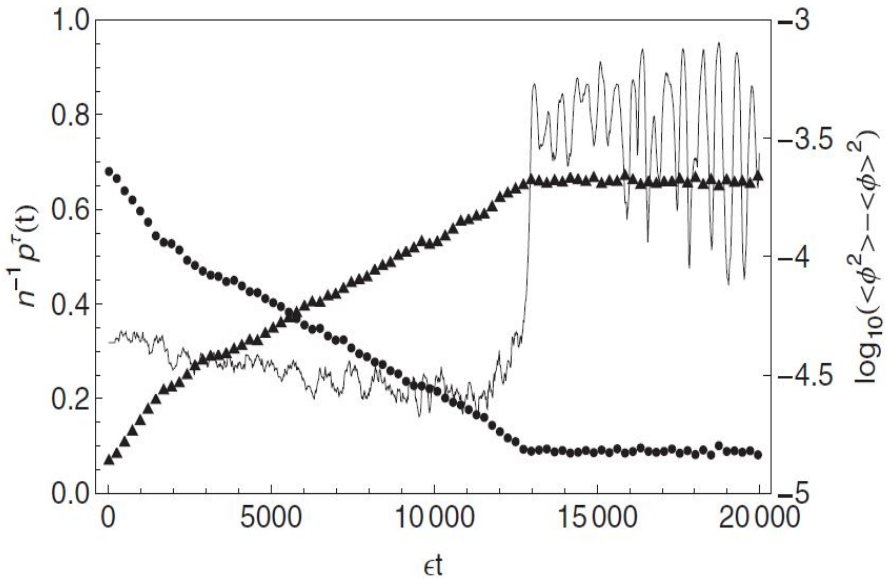

Figure 4.6: Scaled populations $p^{\tau}(t) := p_1^{\tau}(t) + p_2^{\tau}(t)$ for $\tau = 100$ (circles) and $\tau = 4000$ (triangles) when the initial populations is $n = 10^6$ with memory types in ratio short:long $= 10 : 1$. Parameters values are $\epsilon = 10^{-3}$, $\gamma = 10^{-4}$ and $\delta = 2 \times 10^{-4}$. Also shown (thin black line) is evolution of variance of ϕ_t, over a moving time window of 10^5 steps, during population dynamics simulation. Note: rapid initial equilibration of population values (bringing birth and death into balance) is not visible on time scale of plot.

likely to make detrimental moves. Once oscillations appear, short-memory agents have an advantage because they respond more quickly to opportunities created by oscillating payoffs. The onset of oscillations takes place once long-memory agents are in sufficient concentration and is marked by a dramatic jump in the window averaged variance ϕ_t. This jump coincides with a stabilization of the population dynamics, indicating that the advantage of long-memory players has disappeared. Figure 4.6 demonstrates that the phenomenon of a dynamical equilibrium between competing memory lengths appears both with "smoothed step" probabilities (W) and "proportional" probabilities ($\tilde{W}$).

To complete our analysis we perform a population dynamics simulation using the original transition probabilities (W) in the limit $\beta \to \infty$, obtaining a pure step functional form

$$\tilde{W}_{1\to 2}(\Delta) = \begin{cases} \epsilon, & \text{if } \Delta \geq 0 \\ 0, & \text{if } \Delta < 0 \end{cases}, \tag{4.26}$$

so that individual agents react only to the sign of the perceived payoff difference. In this way we are able to compare the two types of transition probability when agents have no intrinsic irrationality of behaviour. The simulation results are shown in Figure 4.7. We use the same ϵ value in both simulations, but agents make fewer moves with proportional rates because the payoff difference is typically small: $\Delta \ll 1 \Rightarrow \tilde{W}_{1\to 2}(\Delta) \ll \epsilon$. This delays the appearance of payoff differences between memory lengths that drive the population changes, so these changes take place on a longer time scale for proportional transition probabilities. This effect is evident in Figures 4.6 and 4.7.

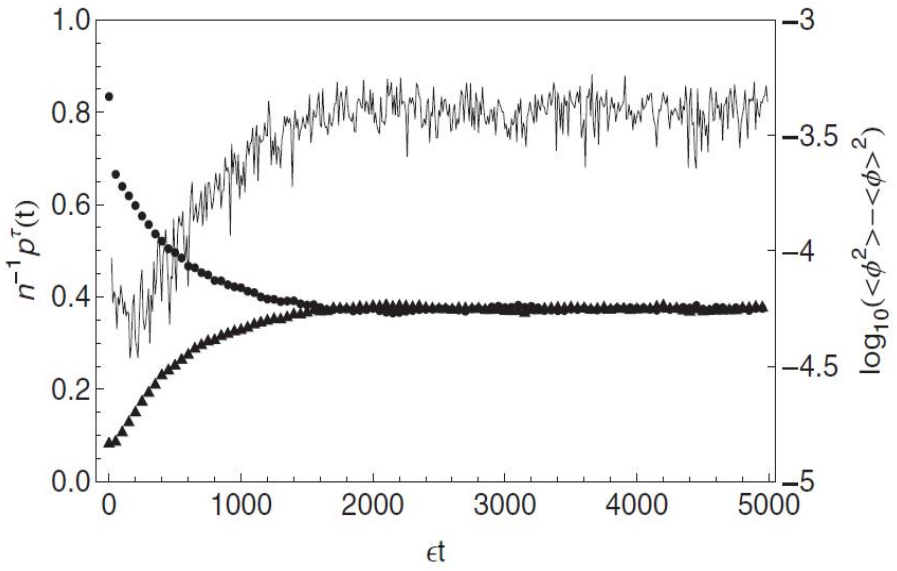

Figure 4.7: Scaled populations $p^{\tau}(t) := p_1^{\tau}(t) + p_2^{\tau}(t)$ in the original model with step rates when inverse temperature $\beta \to \infty$. Memory lengths are $\tau = 10$ (circles) and $\tau = 1000$ (triangles) and the initial populations is $n = 10^6$ with memory types in ratio short:long $= 10 : 1$. Parameters values are $\epsilon = 10^{-3}$, $\gamma = 10^{-4}$ and $\delta = 2 \times 10^{-4}$. Also shown (thin black line) is evolution of variance of ϕ_t, over a moving time window of 10^5 steps, during population dynamics simulation. Note: rapid initial equilibration of population values (bringing birth and death into balance) is not visible on time scale of plot.

In both Figures 4.6 and 4.7, we see that the population of short-memory agents initially declines, but eventually stabilises. This stabilisation occurs coincidentally with a jump in the variance of ϕ_t, indicating that Hopf Bifurcation is responsible for the dynamical equilibrium between memory lengths. It is interesting to note

that the jump in variance is more dramatic in the case of proportional probabilities (Figure 4.6). We suggest that this occurs because the proportional form of transition probability damps fluctuations more effectively than the step form, so that when oscillations do appear in ϕ_t they have a more significant effect on the behaviour of the system, and therefore on the relative competitiveness of agents with different memory lengths. Variance builds more gradually with step probabilities because fluctuations are damped less effectively, and prior to the fixed point losing stability, we see decaying oscillations (under damping) that increase variance when coupled with stochastic fluctuations. The relative equilibrium frequency of short- to long-memory agents depends, in a non-trivial way, on the functional form of switching probabilities, memory length, and population dynamics, and can vary quite considerably (Figures 4.6 and 4.7). A theoretical calculation of these equilibrium population sizes remains an open challenge.

We conclude by noting that the proportional transition probability we have considered in this appendix is a representative of a wider class of functional forms that are zero when $\Delta \ll 0$ and increase continuously with Δ for $\Delta > 0$. When Δ is small, the behaviour of such systems will depend on the first derivative of the transition probability at $\Delta = 0^+$, which in the case we have considered is equal to ϵ. We therefore expect to see similar behaviour for all such forms when fluctuations about the fixed point are small.

4.5.2 Derivation of analytical solutions

The derivation of Equation (4.5) and (4.6)

In this section of appendix we show the derivations in this chapter. Firstly, we show the derivation of Equations (4.5) and (4.6) from Equation (4.1). Assuming $\phi_t \approx \phi$, Δ_t becomes

$$\Delta_t \approx \frac{1}{\tau} \sum_{s=0}^{\tau-1} \left[\frac{U_2(t-s)}{n(1-\phi)} - \frac{U_1(t-s)}{n\phi} \right]. \tag{4.27}$$

Assuming ϕ to be constant and averaging over payoff, $\bar{\Delta}$ can be calculated as

$$\bar{\Delta}(\phi,\omega) \approx \frac{1}{n(1-\phi)} \int_0^n x \frac{1}{n} dx - \frac{1}{n\phi} \int_0^{\omega n} y \frac{1}{\omega n} dy. \tag{4.28}$$

Simplifying Equation (4.28), $\bar{\Delta}$ can be expressed as

$$\bar{\Delta}(\phi,\omega) \approx \frac{1}{2} \left(\frac{1}{1-\phi} - \frac{\omega}{\phi} \right). \tag{4.29}$$

Similarly, $\mathbf{E}[\Delta^2]$ can be calculated as

$$\mathbf{E}[\Delta^2(\phi,\omega]) \approx \frac{1}{n^2(1-\phi)^2} \int_0^n x^2 \frac{1}{n} dx - \frac{1}{n^2\phi^2} \int_0^{\omega n} y^2 \frac{1}{\omega n} dy. \tag{4.30}$$

Simplifying Equation (4.30), $\mathbf{E}[\Delta^2]$ can be expressed as

$$\mathbf{E}[\Delta^2(\phi,\omega)] \approx \frac{1}{3} \left[\frac{1}{(1-\phi)^2} + \frac{\omega^2}{\phi^2} \right]. \tag{4.31}$$

Combining Equations (4.29) and (4.31), we have

$$\frac{\sigma^2(\phi,\omega)}{\tau} \approx \frac{1}{\tau} \left[\mathbf{E}[\Delta^2] - \bar{\Delta}^2 \right], \tag{4.32}$$

Then, Equation (4.32) becomes

$$\frac{\sigma^2(\phi,\omega)}{\tau} \approx \frac{1}{3\tau} \left[\frac{1}{(1-\phi)^2} + \frac{\omega^2}{\phi^2} \right] - \frac{1}{4\tau} \left[\frac{1}{(1-\phi)^2} + \frac{\omega^2}{\phi^2} \right], \tag{4.33}$$

Finally, the variance, $\sigma^2(\phi,\omega)/\tau$ can be expressed as

$$\frac{\sigma^2(\phi,\omega)}{\tau} \approx \frac{1}{12\tau} \left[\frac{\omega^2}{\phi^2} + \frac{1}{(1-\phi)^2} \right]. \tag{4.34}$$

The verification of approximation of transition probability

The program Mathematica [161] is used to verify the approximation of transition probability. The equations below are defined in the program.

$$\text{WErf}[\text{x\_}, \beta\_] := \frac{1}{2}\left(1 + \text{Erf}\left[\frac{\pi^{1/2}}{2} x\beta\right]\right), \tag{4.35}$$

$$\phi[\text{x\_}, \mu\_, \sigma\_] := \frac{\text{Exp}\left[\frac{-(x-\mu)^2}{2\sigma^2}\right]}{(2\pi)^{1/2}\sigma}, \tag{4.36}$$

$$\alpha[\beta\_, \sigma\_] := \frac{\sqrt{2}\beta}{\sqrt{2 + \pi\beta^2\sigma^2}}, \tag{4.37}$$

$$\text{WErfBApx}[\mu\_, \beta\_, \sigma\_] := \text{WErf}[\mu, \alpha[\beta, \sigma]]. \tag{4.38}$$

Firstly, we set $\beta = 1$ and $\sigma = 1$. The plot is generated to show the difference between error function and the result from Gaussian averaging the error function. The code is as follows.

$$\text{Plot}[\{\text{WErfBApx}[\mu, 1, 1] - \text{NIntegrate}[\text{WErf}[x, 1]\phi[x, \mu, 1], \{x, -\infty, \infty\}]\}, \{\mu, 0, 20\}]. \tag{4.39}$$

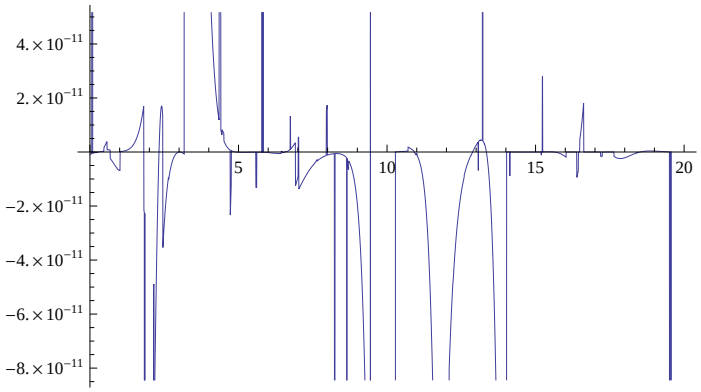

Figure 4.8: The difference plot when $\beta = 1$ and $\sigma = 1$.

Then, we set $\beta = 2$ and $\sigma = 3$.

$$\text{Plot}[\{\text{WErfBApx}[\mu, 2, 3] - \text{NIntegrate}[\text{WErf}[x, 2]\phi[x, \mu, 3], \{x, -\infty, \infty\}]\}, \{\mu, 0, 20\}]. \tag{4.40}$$

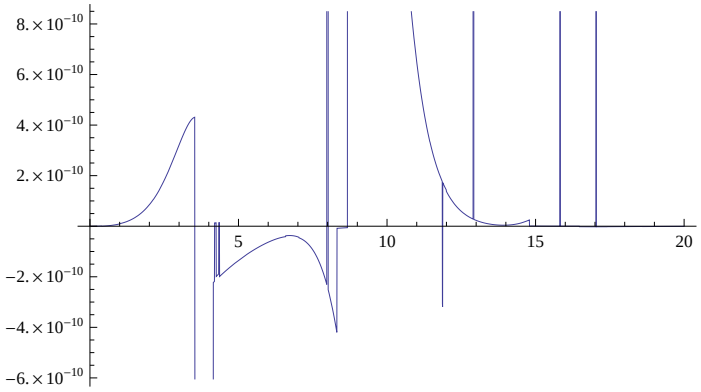

Figure 4.9: The difference plot when $\beta = 2$ and $\sigma = 3$.

From the two figures, the difference is in the range between 10^{-11} and 10^{-10}. Therefore, we conclude that Gaussian averaging the error function gives another error function.

The derivation of approximation for energy function

In equilibrium, the condition satisfies the relationship $2\alpha\bar{\Delta} = \partial_\phi(\alpha E)\delta\phi$. Rearranging this condition, we have

$$\alpha\left(\frac{1}{1-\phi} - \frac{\omega}{\phi}\right) = \frac{d(\alpha E)}{d\phi}. \tag{4.41}$$

Since α depends weakly on ϕ compared to E, the right hand side of Equation(4.41) is approximated to

$$\frac{d(\alpha E)}{d\phi} \approx \alpha\frac{dE}{d\phi}. \tag{4.42}$$

Substituting Equation (4.42) into Equation (4.41), we have

$$\left(\frac{1}{1-\phi} - \frac{\omega}{\phi}\right) = \frac{dE}{d\phi}. \tag{4.43}$$

Integrating both sides of Equation (4.43), we obtain

$$\int dE = \int \left(\frac{1}{1-\phi} - \frac{\omega}{\phi} \right) d\phi. \tag{4.44}$$

Then Equation (4.44) becomes

$$\int dE = \int \frac{1}{1-\phi} d\phi - \omega \int \frac{1}{\phi} d\phi. \tag{4.45}$$

So that, E is calculated as

$$E \approx -\ln(1-\phi) - \omega \ln \phi = -[\ln(1-\phi) + \ln \phi^{\omega}]. \tag{4.46}$$

Finally, E is approximated as

$$E \approx -\ln[\phi^{\omega}(1-\phi)]. \tag{4.47}$$

The derivation of equation (4.11)

The following part shows the derivation of Equation (4.11). Recall that Boltzmann probability distribution for ϕ,

$$\mathbf{P}(\phi) = \frac{n!}{(n\phi)![n(1-\phi)]!} \frac{e^{-\alpha(\phi)E(\phi)}}{Z}, \tag{4.48}$$

Recall that α depends weakly on ϕ compared to E in Equation (4.10). So that the partial derivative gives

$$\frac{1}{2n} \frac{\partial}{\partial \phi} \ln \mathbf{P}(\phi) = \frac{1}{2n} \left\{ \frac{\partial}{\partial \phi} [-\alpha E(\phi)] - \frac{\partial}{\partial \phi} \ln[(n\phi)!] - \frac{\partial}{\partial \phi} \ln ([n(1-\phi)]!) \right\}. \tag{4.49}$$

Since we use the Stirling approximation $\ln[z!] \approx z \ln z - z + \frac{1}{2} \log(2\pi z)$, the equation

becomes

$$\frac{1}{2n}\frac{\partial}{\partial\phi}\ln\mathbf{P}(\phi) \propto -\alpha\frac{\partial E(\phi)}{\partial\phi} - n\ln(n\phi) + n\ln[n(1-\phi)]. \tag{4.50}$$

Recall that $E(\phi) \approx -n\ln[\phi^{\omega}(1-\phi)]$ in Equation (4.10), we have

$$E(\phi) = -n\omega\ln\phi - n\ln(1-\phi), \tag{4.51}$$

so that

$$\frac{\partial E(\phi)}{\partial\phi} = n\left(\frac{1}{1-\phi} - \frac{\omega}{\phi}\right). \tag{4.52}$$

Therefore,

$$\frac{\partial E(\phi)}{\partial\phi} = 2n\bar{\Delta}. \tag{4.53}$$

The term $-n\ln(n\phi) + n\ln[n(1-\phi)]$ is approximated by Taylor series at $\phi = 1/2$ for simplicity, rather than $\omega/(1+\omega)$,

$$-n\ln(n\phi) + n\ln[n(1-\phi)] = n\ln\left(\frac{1-\phi}{\phi}\right) \approx 2n(1-2\phi). \tag{4.54}$$

Substituting Equation (4.53) and (4.54) into Equation (4.50), we obtain

$$\frac{1}{2n}\frac{\partial}{\partial\phi}\ln\mathbf{P}(\phi) = \frac{1}{2n}\left[-2n\alpha\bar{\Delta} + 2n(1-2\phi)\right], \tag{4.55}$$

$$= -\alpha\bar{\Delta} - 2\phi + 1. \tag{4.56}$$

The verification of approximations made in section 4.3.1

The following part demonstrates how the program Mathematica [161] is used to verify the approximation of $\bar{\phi}$. The definitions of α and σ are listed in Equations

(4.57) and(4.58)

$$\alpha[\beta\_, \sigma\_] := \frac{2\beta}{\sqrt{4 + 2\pi\beta^2\sigma^2}}, \tag{4.57}$$

$$\sigma[\omega\_, \phi\_, \tau\_] := \left(\frac{1}{12\tau}\left(\frac{\omega^2}{\phi^2} + \frac{1}{(1-\phi)^2}\right)\right)^{1/2}. \tag{4.58}$$

Substituting Equation (4.58) into Equation (4.57), we obtain

$$\alpha[\beta, \sigma[\omega, \phi, \tau]] = \frac{2\beta}{\sqrt{4 + \frac{\pi\beta^2\left(\frac{1}{(1-\phi)^2} + \frac{\omega^2}{\phi^2}\right)}{6\tau}}}. \tag{4.59}$$

Then α becomes a function of β, ω, ϕ and τ.

$$\alpha[\beta\_, \omega\_, \phi\_, \tau\_] := \alpha[\beta, \sigma[\omega, \phi, \tau]]. \tag{4.60}$$

Recall entropy derivative defined in Equation (4.11) and derived in Section 4.5.2 (Equation (4.48) - Equation (4.56)).

$$g[\phi\_, \omega\_, \alpha\_] := -2(-1 + 2\phi) - \alpha\left(-\frac{1}{1-\phi} + \frac{\omega}{\phi}\right). \tag{4.61}$$

Then, we linearise function $g[...]$ about $\omega/(1+\omega)$ using program Mathematica [161] language as below.

$$\text{Solve}\left[\text{Normal}\left[\text{Series}\left[g[\phi, \omega, \alpha[\beta, \omega, \phi, \tau]]/.\phi \to \frac{\omega}{1+\omega} - \delta, \{\delta, 0, 1\}\right]\right] == 0, \delta\right], \tag{4.62}$$

The result is displayed as

$$\left\{\delta \to \frac{2(-1+\omega)}{(1+\omega)\left(4 + \frac{2\beta\left(3 + \frac{1}{\omega} + 3\omega + \omega^2\right)}{\sqrt{4 + \frac{\pi\beta^2(1+2\omega+\omega^2)}{3\tau}}}\right)}\right\}. \tag{4.63}$$

Then, the definition of $\bar{\phi}_1$ is given as

$$\phi\text{Bar1}[\omega_-, \beta_-, \tau_-] := \frac{\omega}{1+\omega} - \frac{2(-1+\omega)}{(1+\omega)\left(4 + \frac{2\beta\left(3+\frac{1}{\omega}+3\omega+\omega^2\right)}{\sqrt{4+\frac{\pi\beta^2(1+2\omega+\omega^2)}{3\tau}}}\right)}. \tag{4.64}$$

Recall the definitions of function f and $\bar{\phi}_2$ in Equations (4.12) and (4.13).

$$f[\beta_-, \omega_-, \tau_-] := \left(1 + \frac{\pi\beta^2(1+\omega)^2}{12\tau}\right)^{1/2}, \tag{4.65}$$

$$\phi\text{Bar2}[\omega_-, \beta_-, \tau_-] := \left(\frac{f[\beta, \omega, \tau] + \beta\,(1+\omega)^2/\,2}{2f[\beta, \omega, \tau] + \beta\,(1+\omega)^3/\,(2\omega)}\right). \tag{4.66}$$

Comparing the difference between $\bar{\phi}_1$ in Equation (4.64) and $\bar{\phi}_2$ in Equation (4.66), we have

$$\text{Simplify}[\phi\text{Bar1}[\omega, \beta, \tau] - \phi\text{Bar2}[\omega, \beta, \tau]] = 0. \tag{4.67}$$

The results show that there is no difference between $\bar{\phi}_1$ and $\bar{\phi}_2$. Finally, we look at the simplification of $\bar{\phi}$ when $\beta \to \infty$ by using program Mathematica [161].

$$\text{Simplify}[\text{Series}[\text{Limit}[\phi\text{Bar2}[\omega, \beta, \tau], \beta \to \infty], \{\tau, \infty, 1\}], \text{Assumptions} \to \omega > 0]. \tag{4.68}$$

The program provides us the following result.

$$\frac{\omega}{1+\omega} - \frac{\sqrt{\frac{\pi}{3}}(-1+\omega)\omega\sqrt{\frac{1}{\tau}}}{(1+\omega)^3} + \frac{2\pi(-1+\omega)\omega^2}{3(1+\omega)^5\tau} + O\left[\frac{1}{\tau}\right]^{3/2}. \tag{4.69}$$

The derivation of equations in section 4.3.2

The following part shows the derivation from Equation (4.15) to Equation (4.17). Writing $\phi_t = \bar{\phi} + \psi_t$, we have

$$\Delta_t \approx \frac{1}{2\tau}\int_{t-\tau}^{\tau}\left[\frac{1}{1-(\bar{\phi}+\psi_s)} - \frac{\omega}{\bar{\phi}+\psi_s}\right]ds. \tag{4.70}$$

The variable $\bar{\phi}$ is being Taylor expanded in Equation (4.15), then the approximation becomes

$$\Delta_t \approx \frac{1}{2\tau}\int_{t-\tau}^{\tau}\left[\frac{1}{1-\bar{\phi}} + \frac{\psi_s}{(1-\bar{\phi})^2} - \frac{\omega}{\bar{\phi}} + \frac{\omega\psi_s}{\bar{\phi}^2}\right]ds, \tag{4.71}$$

$$\approx \frac{1}{2\tau}\int_{t-\tau}^{\tau}\left[\frac{1}{1-\bar{\phi}} - \frac{\omega}{\bar{\phi}}\right]ds + \frac{1}{2\tau}\int_{t-\tau}^{\tau}\left[\frac{(\sqrt{\omega})^2}{\bar{\phi}^2} + \frac{1}{(1-\bar{\phi})^2}\right]\psi_s ds. \tag{4.72}$$

According to the definition of $\bar{\Delta}(\bar{\phi},\omega)$ and $\sigma^2(\bar{\phi},\sqrt{\omega})$, finally we have

$$\Delta_t \approx \bar{\Delta}(\bar{\phi},\omega) + 6\frac{\sigma^2(\bar{\phi},\sqrt{\omega})}{\tau}\int_{t-\tau}^{t}\psi_s ds. \tag{4.73}$$

Since $\phi_t = \bar{\phi} + \psi_t$, we have $\dot{\phi}_t = \dot{\psi}_t$. Thus Equation (4.16) becomes

$$\dot{\psi}_t = (1-\phi_t)\frac{\epsilon}{2}\left[1-\tanh(\beta\Delta_t)\right] - \phi_t\frac{\epsilon}{2}\left[1+\tanh(\beta\Delta_t)\right]. \tag{4.74}$$

Simplifying Equation (4.60), we obtain

$$\dot{\psi}_t = \frac{\epsilon}{2} - \epsilon\bar{\phi} - \epsilon\psi_t - \frac{\epsilon}{2}\tanh(\beta\Delta_t). \tag{4.75}$$

Expanding tanh function at $\bar{\Delta}(\bar{\phi},\omega)$, we have

$$\tanh(\beta\Delta_t) \approx \tanh(\beta\bar{\Delta}) + \beta[1-\tanh^2(\beta\bar{\Delta})](\Delta_t - \bar{\Delta}). \tag{4.76}$$

Note the hyperbolic functions relation, $1 - \tanh^2(\beta\bar{\Delta}) = \text{sech}^2(\beta\bar{\Delta})$. Substituting Equation (4.17) into it, the tanh function becomes,

$$\tanh(\beta\Delta_t) \approx \tanh(\beta\bar{\Delta}) + \frac{6\beta\sigma^2\text{sech}^2(\beta\bar{\Delta})}{\tau}\int_{t-\tau}^{t}\psi_s ds. \tag{4.77}$$

Substituting Equation (4.77) into Equation (4.75), we obtain

$$\dot{\psi}_t = \frac{\epsilon}{2} - \epsilon\bar{\phi} - \frac{\epsilon}{2}\tanh(\beta\bar{\Delta}) - \epsilon\psi_t - \frac{\epsilon A}{\tau}\int_{t-\tau}^{t}\psi_s ds, \tag{4.78}$$

where $A = 3\beta\text{sech}^2[\beta\bar{\Delta}(\bar{\phi},\omega)]\sigma^2(\bar{\phi},\sqrt{\omega})$.

Since the first three terms give the value of zero, Equation (4.78) becomes

$$\dot{\psi}_t = -\epsilon\left[\psi_t + \frac{A}{\tau}\int_{t-\tau}^{t}\psi_s ds\right], \tag{4.79}$$

as required.

The derivation of characteristic equation

The following part demonstrates the derivations of Equations (4.20) and (4.21). Recall that the Equation (4.18).

$$\dot{\psi}_t = -\epsilon\left[\psi_t + \frac{A}{\tau}\int_{t-\tau}^{t}\psi_s ds\right], \tag{4.80}$$

and an exponential trial solution $\psi_t = e^{\lambda t}$ where $\lambda = x + iy$, we have

$$\dot{\psi}_t = \lambda e^{\lambda t}, \tag{4.81}$$

and

$$\int_{t-\tau}^{t}\psi_s ds = \int_{t-\tau}^{t}e^{\lambda s}ds, \tag{4.82}$$

$$= \frac{1}{\lambda}\left[e^{\lambda t} - e^{\lambda(t-\tau)}\right], \tag{4.83}$$

$$= \frac{e^{\lambda t}}{\lambda}\left(1 - e^{-\lambda\tau}\right). \tag{4.84}$$

Substituting above equations into Equation (4.18), we obtain

$$-\frac{\lambda e^{\lambda t}}{\epsilon} = e^{\lambda t} + \frac{A}{\tau}\frac{e^{\lambda t}}{\lambda}\left(1 - e^{-\lambda\tau}\right). \tag{4.85}$$

Simplifying equation above, we have

$$\lambda^2 + \epsilon\lambda + \frac{\epsilon A}{\tau}\left(1 - e^{-\lambda\tau}\right) = 0. \tag{4.86}$$

Recall that $\lambda = x + iy$, we have

$$\lambda^2 = x^2 - y^2 + 2xyi, \tag{4.87}$$

and

$$e^{-\lambda\tau} = e^{-\tau x}e^{-\tau yi}, \tag{4.88}$$

$$= e^{-\tau x}[\cos(\tau y) - i\sin(\tau y)]. \tag{4.89}$$

Substituting these equations above into Equation (4.86), we have

$$x^2 - y^2 + 2xyi + \epsilon x + \epsilon yi + \frac{\epsilon A}{\tau}[1 - e^{-\tau x}\cos(\tau y)] + \frac{\epsilon A}{\tau}\sin(\tau y)i = 0. \tag{4.90}$$

Since both real and imaginary parts equal zero, we obtain Equations (4.20) and (4.21)

$$x^2 - y^2 + \epsilon x + \frac{\epsilon A}{\tau}(1 - e^{-\tau x}\cos\tau y) = 0, \tag{4.91}$$

$$2xy + \epsilon y + \frac{\epsilon A}{\tau} e^{-\tau x} \sin \tau y = 0. \tag{4.92}$$

To compute τ_c we set $x = 0$ in Equation (4.21):

$$\epsilon y + \frac{\epsilon A}{\tau} \sin(\tau y) = 0. \tag{4.93}$$

Simplifying it, we have

$$\operatorname{sinc}(\tau y) = -A^{-1}, \tag{4.94}$$

as required.

Expanding the sinc function as Taylor series to the second order at π/τ, we have

$$-\frac{\tau(y - \pi/\tau)}{\pi} + \frac{\tau^2 (y - \pi/\tau)^2}{\pi^2} = -A^{-1}. \tag{4.95}$$

The solutions of above quadratic function are

$$y = \frac{\pi}{2\tau} \left(3 \pm \sqrt{1 - 4A^{-1}}\right). \tag{4.96}$$

The root which satisfies our system is

$$y = \frac{\pi}{2\tau} \left(3 - \sqrt{1 - 4A^{-1}}\right). \tag{4.97}$$

Chapter 5

Memory and limit cycles in the Hawk-Dove game

The Hawk-Dove game is an example of simple models from game theory. In this chapter, we extend the memory analysis from the previous chapter to this game, by introducing a finite but variable memory to each individual player. The analytical results obtained from this modified games are in agreement with the simulation results presented in Chapter 4. We draw special attention to the critical memory length affecting the instability of the system.

The rest of this chapter is structured as follows. In Section 5.1, the model of the Hawk-Dove game with memory parameter is defined. In Section 5.2, simulation results are presented followed by theoretical analyses in Section 5.3. Finally, we offer some concluding remarks.

5.1 Model definition

We adopt the standard Hawk-Dove game, with the following payoff matrix.

	H	D
H	$V/2 - C$	V
D	0	$V/2$

where $V > 0$ and $C > 0$.

A group of $L \geq 2$ agents play this Hawk-Dove game in discrete time. Interactions take places via random pairing between agents at a rate of $L/2$ per unit time, such that each agent has one interaction per unit time on average. When the interaction happens, each agent adopts either 'Hawk' or 'Dove', according to its specific probabilistic strategy, $\phi_i(t)$, defined as the probability of agent i adopting 'Hawk' at time t. Each interaction results in a payoff which is memorized by the pair. Each agent has a memory m of its previous interactions, which is used by the agent to adapt his/her strategy.

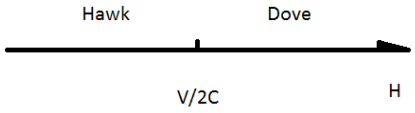

Figure 5.1: Domains in which either strategy is assessed to be optimal.

If h is the number of hawks encountered in an agent's memory of m interactions, then $\tilde{\phi} = h/m$ is its estimate of the average strategy of other agents. Given the payoff matrix, its optimal strategy is to adopt 'Hawk' if $\tilde{\phi} < V/2C$ and 'Dove' if $\tilde{\phi} > V/2C$, see Figure 5.1. The critical fraction, $V/2C$, is determined by equating the expected payoffs of the two strategies:

$$\left(\frac{V}{2} - C\right)\phi_c + V(1-\phi_c) = \frac{V}{2}(1-\phi_c), \tag{5.1}$$

which leads to

$$\phi_c = \frac{V}{2C}. \tag{5.2}$$

We denote the probability of $\tilde{\phi} < V/2C$ as $\tilde{p}_h$, which can be expressed in terms of the Heaviside function $\mathcal{H}$:

$$\tilde{p}_h(\tilde{\phi}) = \mathcal{H}\left(\frac{V}{2C} - \tilde{\phi}\right). \tag{5.3}$$

In a small time interval δt, an agent has a probability of $L\delta t$ interacting, and if so, it has a probability $\tilde{p}_h$ of evolving towards a pure 'Hawk' strategy $\phi = 1$, and a probability of $(1 - \tilde{p}_h)$ towards $\phi = 0$:

$$\phi_i(t+\delta t) = \begin{cases} \phi_i(t) & \text{w.p.} \quad (1 - L\delta t) \\ \phi_i(t) + \frac{\epsilon(1-\phi_i)}{L} & \text{w.p.} \quad \tilde{p}_h L\delta t \\ \phi_i(t) - \frac{\epsilon\phi_i}{L} & \text{w.p.} \quad (1-\tilde{p}_h)L\delta t \end{cases}, \tag{5.4}$$

where ϵ is the 'update' or 'learning' rate which regulates how fast agents adapt to change, and so should remain in the range of $[0, 1]$. The Equation (5.4) simplifies to

$$\frac{\delta\phi_i}{\delta t} = \epsilon\left[\tilde{p}_h(\tilde{\phi}) - \phi_i\right], \tag{5.5}$$

which shows the evolution of agent i's strategy evolution according to his/her memory $\tilde{\phi}$.

The overall probability weights associated with 'Hawk' is given by the average over the agents (denoted by i)

$$\phi(t) := \frac{1}{L}\sum_{i=1}^{L}\phi_i(t), \tag{5.6}$$

and the average probability of 'Dove' is $1 - \phi(t)$.

5.2 Simulation results

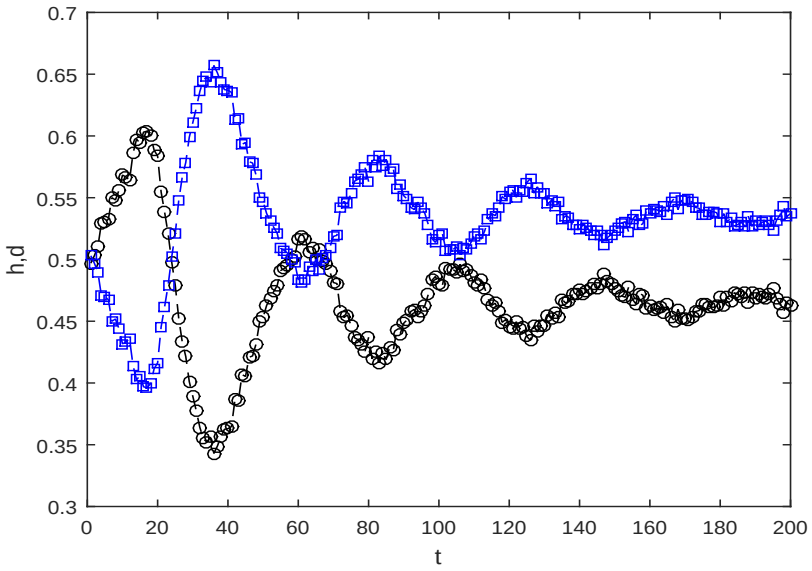

Figure 5.2: Probability weights of hawk (circle) and dove (square) agents in a group of size $L = 10000$ with $V = 1, C = 1$. All agents have memory $m = 100$ and update rate $\epsilon = 6 \times 10^{-3}$. Dashed lines show solutions to delay Equation (5.11) using the same parameter values.

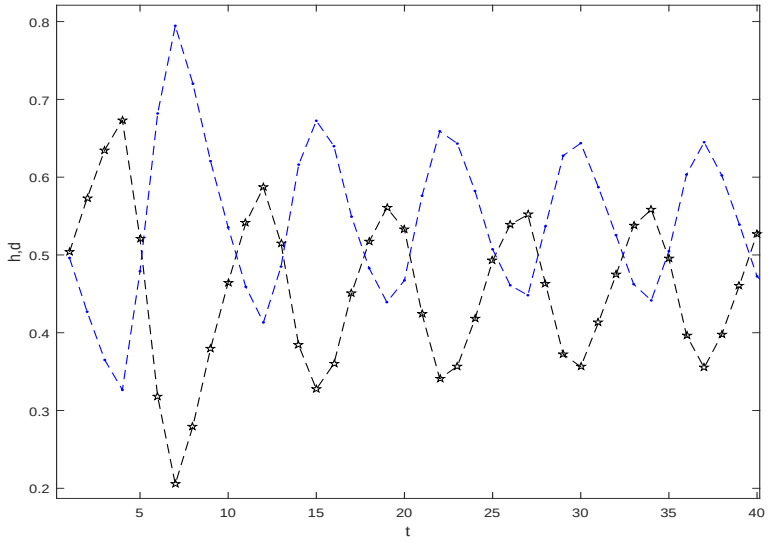

Figure 5.3: Probability weights of hawk (pentagram) and dove (dot) agents in a group of size $L = 10000$ with $V = 1, C = 1$ and $t \in [1, 40]$. All agents have memory $m = 100$ and update rate $\epsilon = 3 \times 10^{-3}$. Dashed lines show solutions to delay Equation (5.11) using the same parameter values.

A population of identical agents is simulated, with the same memory length

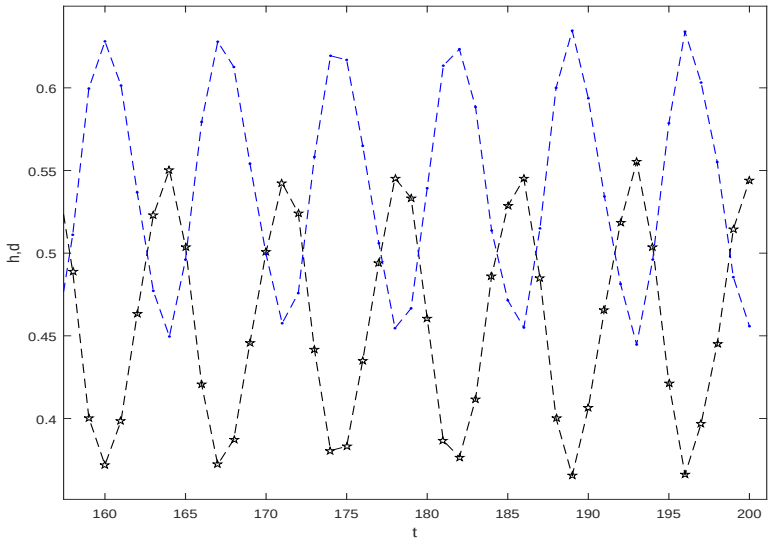

Figure 5.4: Probability weights of hawk (pentagram) and dove (dot) agents in a group of size $L = 10000$ with $V = 1, C = 1$ and $t \in [160, 200]$. All agents have memory $m = 100$ and update rate $\epsilon = 3 \times 10^{-3}$. Dashed lines show solutions to delay Equation (5.11) using the same parameter values.

and update rate. Figure 5.2 shows the evolution of probability weights. The values of update rate and memory are $\epsilon = 6 \times 10^{-3}$ and $m = 100$ respectively. We note that there is decaying oscillations associated with the probability weights. After all, the probability weight tends to be stable with minor volatilities. In Figures 5.3 and 5.4, the update rate is changed to $\epsilon = 3 \times 10^{-3}$, and the behaviour of the population dynamics has changed to stable oscillations. Since the update rate is large, this scenario occurs with fixed memory length for each player. It can also be achieved with large memory lengths for each player with the fixed updated rate. The relationship between the critical values of update rate for stable oscillations and agents' memory lengths analytically will be demonstrated later, which is in agreement with that of a Hopf Bifurcation.

5.3 Theory

In this section, an analysis of the system dynamics (exact in the limit of large m and L) is presented, and the mathematical expression for system stability is derived.

5.3.1 Strategy optimization

For large m and L, an individual agent encounters an average strategy over a memory of m, defined as:

$$\bar{\phi}_m := \frac{1}{m}\int_0^m \phi(t-s)ds. \tag{5.7}$$

Statistically, we expect its memory of m interactions to consist of h 'Hawk' strategies according to the binomial distribution associated with probability $\bar{\phi}_m$:

$$f(n,\bar{\phi}_m) = \frac{m!\ \bar{\phi}_m^n(1-\bar{\phi}_m)^{m-n}}{n!\ (m-n)!}. \tag{5.8}$$

In reality, this distribution is non-stationary over time and agents. However, we expect the approximation to be accurate for large memory, m, and agent number L, provided that the system reaches a steady state. This allows us to average over agents' memories, and thus the expectation value of $p(\bar{\phi}_m)$ can be defined as

$$p(\bar{\phi}_m) := \sum_{h=0}^{m} \tilde{p}_h(\frac{h}{m})\ f(h,\bar{\phi}_m), \tag{5.9}$$

and incorporating Equation (5.3), it simplifies to:

$$p(\bar{\phi}_m) = \sum_{h=0}^{\frac{mV}{2C}} f(h,\bar{\phi}_m), \tag{5.10}$$

which is the average probability of an agent evolving towards a pure 'Hawk' strategy, whilst in interaction with a population with an average strategy $\bar{\phi}_m$. The plots of Equations (5.7), (5.8) and (5.9) are presented in Section 5.5.1.

5.3.2 Delay equation

The strategy evolution Equation (5.5) can now be averaged over the population of agents and their memories. Taking the limit of δt to 0, we have

$$\frac{d\phi}{dt} = \epsilon \left[p(\bar{\phi}_m) - \phi \right], \text{where } p \text{ given by (5.9) and } \bar{\phi}_m \text{ by (5.7)}, \tag{5.11}$$

which is a delay equation for the evolution of $\phi(t)$ over time t, since $\bar{\phi}_m$ contains the memory m of the previous time. This delay equation can be solved numerically, and we have included the solutions in Figures 5.2, 5.3 and 5.4 for comparison. The agreement with the simulation results is excellent.

5.3.3 Linear stability analysis

In order to determine the critical condition for stability, we now seek to linearise the delay equation around its fixed point. The analysis can be carried out with general values of V and C. However, for simplicity, $V = C = 1$ is set, and therefore the fixed point is $\phi_0 = V/2C = 1/2$. Equations are introduced as follows.

$$\psi(t) := \phi(t) - \frac{1}{2}, \tag{5.12}$$

and

$$\bar{\psi}_m(t) := \frac{1}{m} \int_{t-m}^{t} \psi(\tau) d\tau. \tag{5.13}$$

To evaluate p, as given in Equation (5.10), the summation with a continuous integral is replaced, and the binomial distribution is approximated with a Gaussian distribution of the same mean, μ and variance, σ, where

$$\mu(\phi) = m\phi, \tag{5.14}$$

$$\sigma(\phi) = \sqrt{m\phi(1-\phi)}. \tag{5.15}$$

Then Equation (5.10) leads to the following approximate expression, of which detailed derivations are listed in the appendix:

$$p(\bar{\psi}_m) \approx \frac{1}{2} - \frac{\sqrt{2m}}{\sqrt{\pi}}\bar{\psi}_m. \tag{5.16}$$

The approximation is verified by comparing the expansion coefficients to the exact values of the derivatives of $p(\phi)$ evaluated at $\phi = 1/2$, as shown in Figure 5.5.

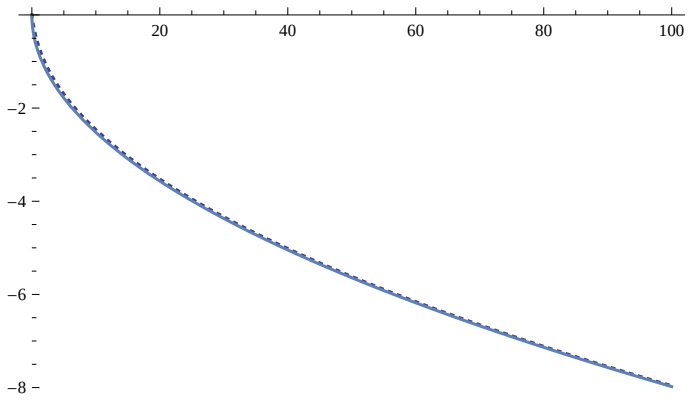

Figure 5.5: The derivative $\partial p/\partial\phi$ evaluated directly from Equation (5.10) at $\bar{\phi}_m = 1/2$. The derivative is plotted using black dot. The blue line shows corresponding expansion coefficients from Equation (5.16).

The delay Equation (5.11) is finally linearised to:

$$\frac{1}{\epsilon}\frac{d\psi}{dt} = -\frac{\sqrt{2m}}{\sqrt{\pi}}\bar{\psi}_m(t) - \psi(t). \tag{5.17}$$

The expression $\psi(t) = e^{\lambda t}$ is substituted as a trial solution to obtain the characteristic equation. Since $\psi(t) = e^{\lambda t}$, $d\psi(t)/dt = \lambda e^{\lambda t}$ is derived. Then the characteristic equation becomes:

$$\frac{\lambda e^{\lambda t}}{\epsilon} = -\frac{\sqrt{2}}{\sqrt{\pi m}}\frac{1}{\lambda}\left[e^{\lambda t} - e^{\lambda(t-m)}\right] - e^{\lambda t}. \tag{5.18}$$

By simplifying Equation (5.18), we obtain

$$\lambda^2 + \epsilon\lambda + \frac{\epsilon\sqrt{2}}{\sqrt{\pi m}}\left(1 - e^{-\lambda m}\right) = 0. \tag{5.19}$$

Substituting $\lambda = x+iy$, the real and imaginary parts of the characteristic equation are separated as:

$$x^2 - y^2 + \epsilon x + \frac{\epsilon\sqrt{2}}{\sqrt{\pi m}}\left(1 - e^{-mx}\cos(my)\right) = 0, \tag{5.20}$$

$$2xy + \epsilon y + \frac{\epsilon\sqrt{2}}{\sqrt{\pi m}}e^{-mx}\sin(my) = 0. \tag{5.21}$$

Numerical solution shows that the system is stable with fixed memory length m and small value of ϵ. As ϵ increases past a critical value, a stable limit cycle emerges, leading to instability. This is also known as a 'Hopf Bifurcation'. In order to calculate the critical value of the update rate ϵ_c, $x = 0$ is set in Equation (5.21) giving rise to:

$$\frac{\sin(my)}{my} = -\frac{\sqrt{\pi}}{\sqrt{2m}}. \tag{5.22}$$

Assuming m is large and choosing the root near $y = \pi/m$, we truncate the expansion for the limit $m \to \infty$:

$$y \approx \frac{\pi}{m} + \sqrt{\frac{\pi^3}{2m^3}}. \tag{5.23}$$

Setting $x = 0$ in Equation (5.20), we obtain

$$\epsilon = \frac{\sqrt{m\pi}}{\sqrt{2}}\frac{y^2}{1 - \cos(my)}. \tag{5.24}$$

Substituting our approximate expression for y into this equation where detailed derivations are produced in the appendix, we have

$$\epsilon_c \approx \frac{\pi^{5/2}\left(2\sqrt{m} + \sqrt{2\pi}\right)^2 \sec^2\left(\frac{\pi^{3/2}}{2\sqrt{2}\sqrt{m}}\right)}{8\sqrt{2}m^{5/2}}, \tag{5.25}$$

$$\approx \frac{\pi^{5/2}}{2\sqrt{2}m^{3/2}} + \frac{\pi^3}{2m^2} + \frac{\pi^{7/2}\left(4 + \pi^2\right)}{16\sqrt{2}m^{5/2}} + \frac{\pi^6}{16m^3}. \tag{5.26}$$

This analytical result has been verified using numerical solutions, see Figure 5.7.

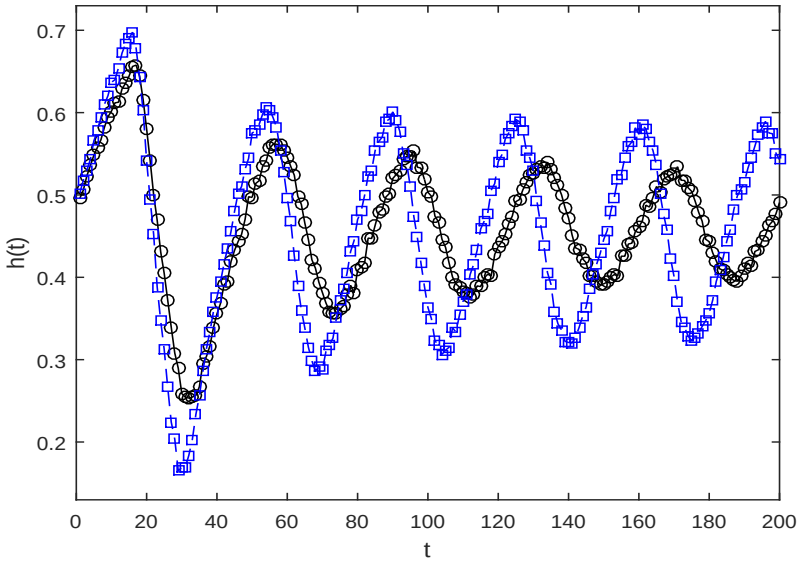

Figure 5.6: Black line shows $\phi(t)$ from the numerical solutions to Equation (5.11) in the symmetric case when $m = 100$ and $\epsilon = 5 \times 10^{-3}$. Blue dashed line shows corresponding solution when $\epsilon = 7 \times 10^{-3}$. Open black circles and open blue squares show corresponding simulation results in a system of size $L = 10000$.

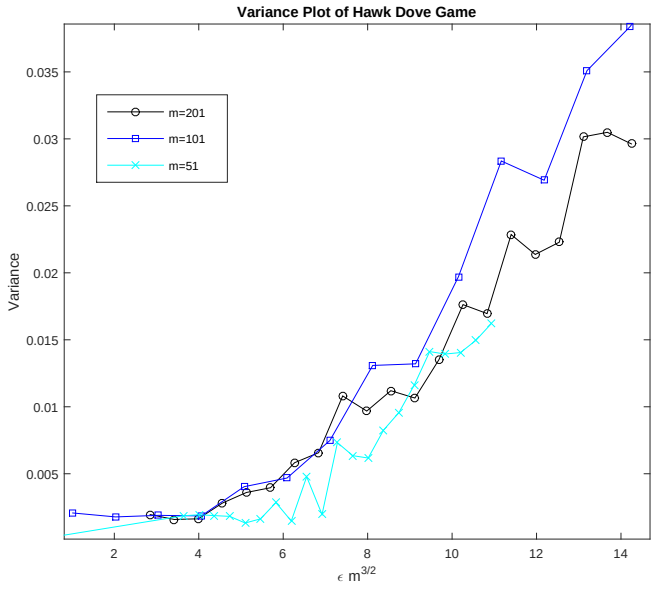

Figure 5.7: Dependence of the steady state amplitude of $\phi(t)$ on ϵ for $m = 51$ (light blue), $m = 101$ (blue) and $m = 201$ (black). $L = 100$ in all cases.

5.3.4 Numerical tests of stability

The delay Equation (5.11) can be numerically solved. The probability $p(\bar{\phi}_m)$ is obtained by summing over the binomial distribution. The critical point is calculated by our stability analysis, where the figure is generated. Plotting the result finally shows a set of stable oscillations, which is in line with the theoretical analysis.

The verification has numerically carried out to confirm the relationship between memory and the corresponding critical value of ϵ. We have obtained variance plot for three different values of memory. In Figure 5.7, x-axis indicates the increasing values of ϵ, and y-axis shows the corresponding values of variance. The results demonstrate that the simulated outcomes are in agreement of analytical solutions.

5.4 Conclusion

In this chapter, we have extended the traditional Hawk-Dove game to include memory effects. We have presented both numerical and analytical results which are in excellent agreements.

The system is found to have a stable fixed point. Initially players with longer memories are better at selecting an optimal strategy, as they are more accurate at assessing the true probability characteristics of the system. However, when the agent memory exceeds a certain value, large collective fluctuations can emerge in the form of limit cycles, and players with shorter memories can exploit the fluctuations more effectively than those with longer memories. In essence, for a population of players with different memories, a better memory does not always help with games.

5.5 Appendix

5.5.1 The plots of equations (5.7), (5.8) and (5.9)

We present the plots of Equations (5.7), (5.8) and (5.9).

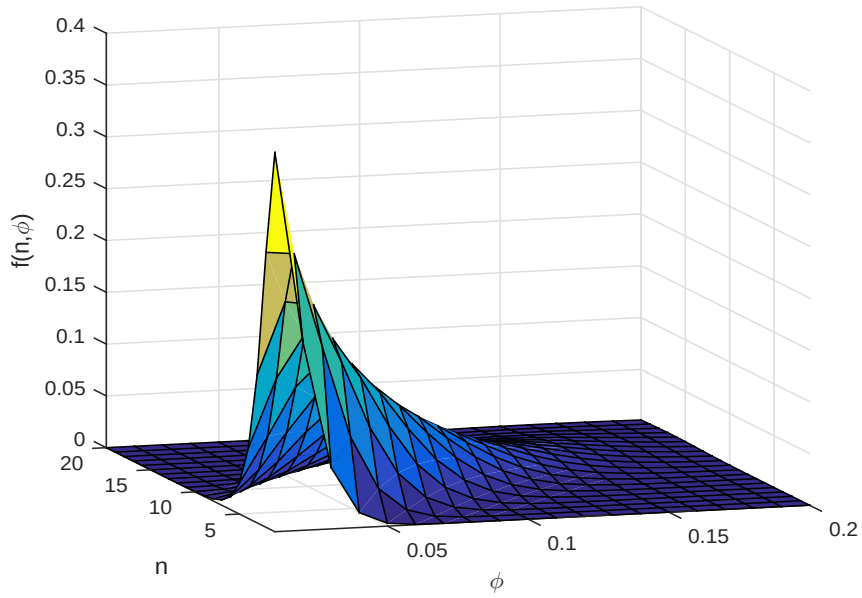

Figure 5.8: The plot for $f(n, \phi)$ in Equation (5.8) against n and ϕ.

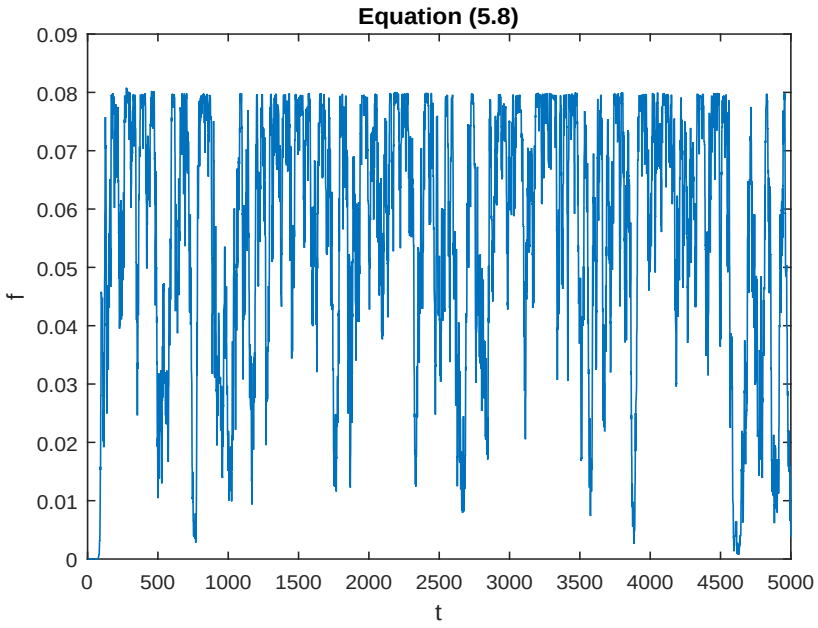

Figure 5.9: The plot for $f(h, \phi)$ in Equation (5.8) against time t for an individual agent where $m = 100$, $L = 10000$, $V = C = 1$, $\epsilon = 3 \times 10^{-3}$.

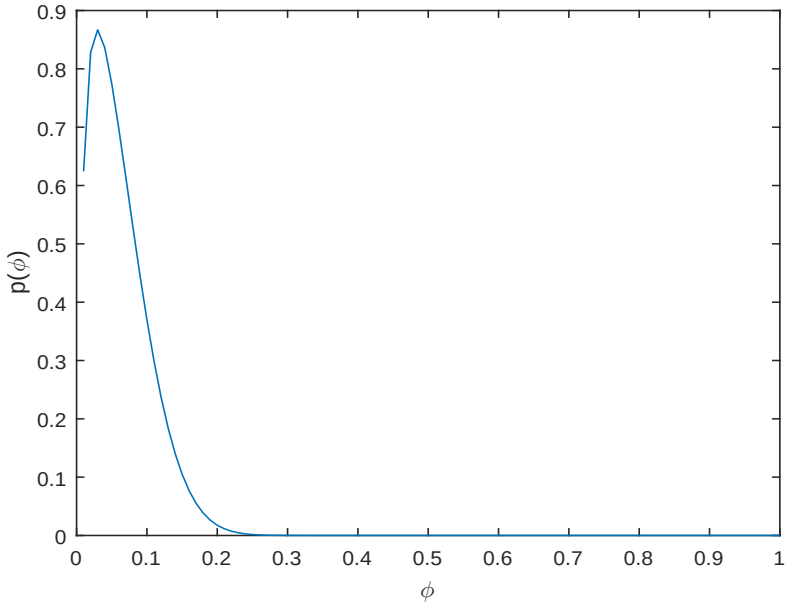

Figure 5.10: The plot for $p(\bar{\phi}_m)$ in Equation (5.9) against ϕ.

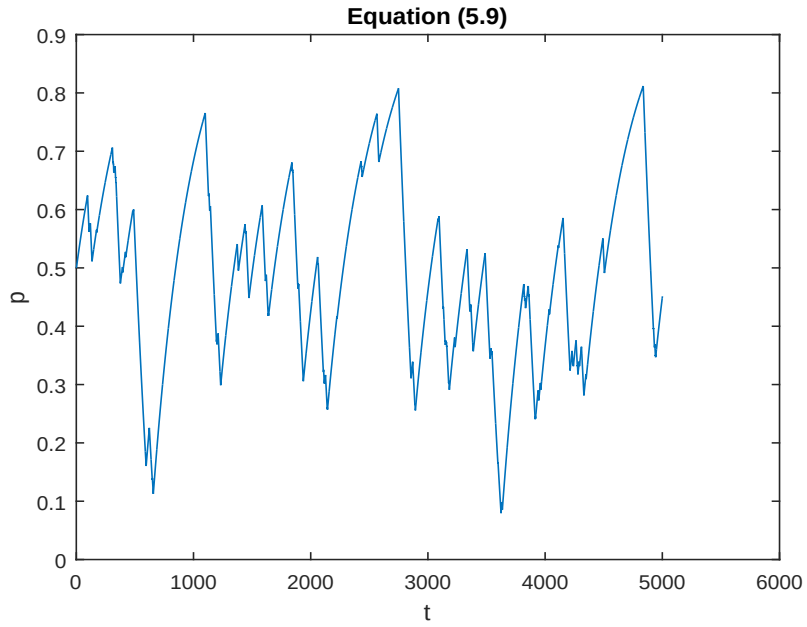

Figure 5.11: The plot for $p(\bar{\phi}_m)$ in Equation (5.9) against time t for an individual agent where $m = 100$, $L = 10000$, $V = C = 1$, $\epsilon = 3 \times 10^{-3}$.

As a reference, the term $\bar{\phi}_m$ in Equation (5.7) is plotted as well.

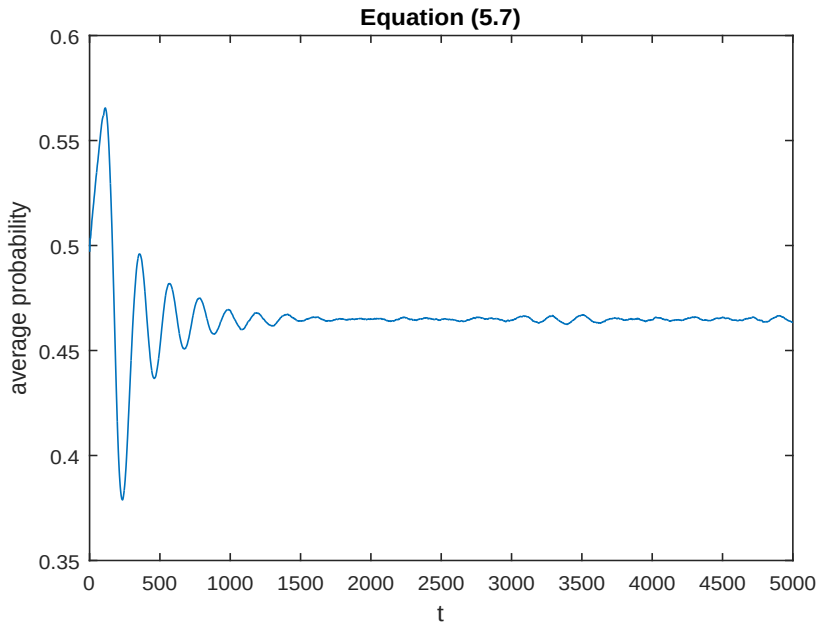

Figure 5.12: The plot for $\bar{\phi}_m$ in Equation (5.7) against time t for an individual agent where $m = 100$, $L = 10000$, $V = C = 1$, $\epsilon = 3 \times 10^{-3}$.

5.5.2 The derivation of equation (5.16)

We present the derivation for Equation (5.16). Recall Equation (5.10), and $V = C = 1$

$$p(\bar{\phi}_m) = \sum_{h=0}^{\frac{m}{2}} f\left(h, \bar{\phi}_m\right). \tag{5.27}$$

The summation can be approximated by integration, then Equation (5.27) becomes

$$p(\bar{\phi}_m) \approx \int_{h=0}^{m/2} f\left(h, \bar{\phi}_m\right). \tag{5.28}$$

The binomial distribution $f\left(h, \bar{\phi}_m\right)$ is approximated with a Gaussian distribution.

$$p(\bar{\psi}_m) \approx \frac{1}{\sigma\sqrt{2\pi}} \int_0^{m/2} \exp(-\frac{\left(h - \left(m\bar{\psi}_m + m/2\right)\right)^2}{2\sigma^2})dh. \tag{5.29}$$

Since the integrand is insignificant for $(-\infty, 0]$, the lower limit of the integration has been approximated to $-\infty$:

$$p(\bar{\psi}_m) \approx \frac{1}{\sigma\sqrt{2\pi}} \int_{-\infty}^{m/2} \exp(-\frac{\left(h - \left(m\bar{\psi}_m + m/2\right)\right)^2}{2\sigma^2})dh. \tag{5.30}$$

By expanding the exponential in Equation (5.30), we obtain

$$p(\bar{\psi}_m) = \frac{1}{\sigma\sqrt{2\pi}} \int_{-\infty}^{m/2} \exp(-\frac{(h-m/2)^2}{2\sigma^2}) \exp(\frac{m\bar{\psi}_m (h-m/2)}{\sigma^2})(1 + O\left(\bar{\psi}^2\right))dh. \tag{5.31}$$

The term $O\left(\bar{\psi}^2\right)$ is neglected due to its small value. The Equation (5.31) becomes

$$p(\bar{\psi}_m) \approx \frac{1}{\sigma\sqrt{2\pi}} \int_{-\infty}^{m/2} \exp(-\frac{(h-m/2)^2}{2\sigma^2}) \exp(\frac{m\bar{\psi}_m (h-m/2)}{\sigma^2})dh. \tag{5.32}$$

By changing of variable h, $x = h - m/2$, we have

$$p(\bar{\psi}_m) = \frac{1}{\sigma\sqrt{2\pi}} \int_{-\infty}^{0} \exp(-\frac{x^2}{2\sigma^2}) \exp(\frac{m\bar{\psi}_m x}{\sigma^2})dx. \tag{5.33}$$

The term $\exp(\frac{m\bar{\psi}_m x}{\sigma^2})$ has been approximated by Taylor series.

$$p(\bar{\psi}_m) = \frac{1}{\sigma\sqrt{2\pi}} \int_{-\infty}^{0} e^{-\frac{x^2}{2\sigma^2}} \left(1 + \frac{m\bar{\psi}_m x}{\sigma^2}\right) dx. \tag{5.34}$$

Rearranging the above equation, we have

$$p(\bar{\psi}_m) = \frac{1}{\sigma\sqrt{2\pi}} \int_{-\infty}^{0} e^{-\frac{x^2}{2\sigma^2}} dx + \frac{\bar{\psi}_m m}{\sigma^3\sqrt{2\pi}} \int_{-\infty}^{0} x e^{-\frac{x^2}{2\sigma^2}} dx. \tag{5.35}$$

The first term of Equation (5.35) is the Gaussian distribution with mean 0 and standard deviation σ.

$$\frac{1}{\sigma\sqrt{2\pi}} \int_{-\infty}^{0} e^{-\frac{x^2}{2\sigma^2}} dx = \frac{1}{2}. \tag{5.36}$$

The second term of Equation (5.35) can be calculated as

$$\frac{\bar{\psi}_m m}{\sigma^3\sqrt{2\pi}} \int_{-\infty}^{0} x e^{-\frac{x^2}{2\sigma^2}} dx = \frac{\bar{\psi}_m m}{\sigma\sqrt{2\pi}} \left[-e^{-\frac{x^2}{2\sigma^2}}\right]_{-\infty}^{0}, \tag{5.37}$$

$$= -\frac{m\bar{\psi}_m}{\sigma\sqrt{2\pi}}. \tag{5.38}$$

Recall that $\sigma = \sqrt{m}/2$. Finally, equation (5.35) becomes

$$p(\bar{\psi}_m) = \frac{1}{2} - \frac{\sqrt{2m}}{\sqrt{\pi}}\bar{\psi}_m. \tag{5.39}$$

5.5.3 The derivation of equation (5.25)

Recall Equation (5.22),

$$\mathrm{sinc}(my) = \frac{\sin(my)}{my} = -\frac{\sqrt{\pi}}{\sqrt{2m}}. \tag{5.40}$$

Expanding the sinc function as Taylor series to the second order at π/m, we have

$$-\frac{\tau(y-\pi/m)}{\pi} + \frac{\tau^2(y-\pi/m)^2}{\pi^2} = -\frac{\sqrt{\pi}}{\sqrt{2m}}. \tag{5.41}$$

The solutions of above quadratic function are

$$y = \frac{\pi}{2m}\left(3 \pm \sqrt{1 - 4\sqrt{\frac{\pi}{2m}}}\right). \tag{5.42}$$

The root which satisfies our system is

$$y = \frac{\pi}{2m}\left(3 - \sqrt{1 - 4\sqrt{\frac{\pi}{2m}}}\right). \tag{5.43}$$

Applying the Taylor expansion for $\sqrt{1-x} \approx 1 - x/2$, we have

$$y = \frac{\pi}{2m}\left(3 - \left(1 - 2\sqrt{\frac{\pi}{2m}}\right)\right). \tag{5.44}$$

Finally, we obtain the expression for Equation (5.23).

$$y \approx \frac{\pi}{m} + \sqrt{\frac{\pi^3}{2m^3}}. \tag{5.45}$$

Substituting Equation (5.23) into Equation (5.24), we obtain

$$\epsilon_c = \frac{\sqrt{m\pi}}{\sqrt{2}} \frac{\left(\frac{\pi}{m} + \sqrt{\frac{\pi^3}{2m^3}}\right)^2}{1 - \cos\left(m\left(\frac{\pi}{m} + \sqrt{\frac{\pi^3}{2m^3}}\right)\right)}. \tag{5.46}$$

The term of cos(.) can be simplified to

$$\cos\left(\pi + \frac{\pi^{3/2}}{\sqrt{2m}}\right) = -\cos\left(\frac{\pi^{3/2}}{\sqrt{2m}}\right). \tag{5.47}$$

Applying double angle formulas from trigonometric identities, $\cos(2x) = 2(\cos x)^2 - 1$, we obtain

$$\cos\left(\pi + \frac{\pi^{3/2}}{\sqrt{2m}}\right) = 2\left(\cos\left(\frac{\pi^{3/2}}{2\sqrt{2}\sqrt{m}}\right)\right). \tag{5.48}$$

Note that $\sec^2(.) = 1/\cos^2(.)$, then Equation (5.24) becomes

$$\epsilon_c \approx \frac{\pi^{5/2}\left(2\sqrt{m} + \sqrt{2\pi}\right)^2 \sec^2\left(\frac{\pi^{3/2}}{2\sqrt{2}\sqrt{m}}\right)}{8\sqrt{2}m^{5/2}}. \tag{5.49}$$

Chapter 6

Conclusion

I conducted research on the statistical modelling of a selection of three games, namely the minority games, the statistical urn models and the Hawk-Dove games.

In Chapter 3, the key characteristics of the minority game were explored. We extended the standard MG by allowing players to accumulate profits and losses in each game round. Bankruptcy and borrowing (leverage) were introduced, and the resulting game statistics were analysed numerically. Curve fitting was performed for wealth distributions, showing a weak evidence of power law behaviour. We explored a number of variations when curve fitting for wealth distributions, for example a zero-sum rule could be introduced. Due to the time limit of the research and possible variations in the system parameters, we did not obtain fitting of sufficient quality for publication. It is possible that with larger set of players simulated for longer time could lead to better statistics and higher quality curve fitting for wealth distributions. However, our results clearly demonstrated that leverage increases the instability of the system. This corresponds to the increased risks of trading leveraged financial products in the real market. Our model provides a possible testing ground for introducing new measures that might modify and control the risks arising from the leverage effects.

In Chapter 4, a new simple urn model was developed to investigate the effectiveness of memory. The model consists of a group of agents with different

memories competing against each other for finite resources. Our results showed that instability exists in the model at a critical memory length, which can be verified both numerically and analytically. Additionally, we showed that the temperature in the urn model is related by the agent's memory length, suggesting that this model may be applied to other game models with links to classical thermodynamics. Increasing memory lengths can allow agents to more accurately and reliably determine the optimal strategy, and in terms of thermodynamics, this is equivalent to less thermal noise and a lower temperature. However, if a sufficient number of agents with very long-memory lengths are present, instability in the form of a limit cycle occurs, resulting in reduced competitiveness, in which case agents with shorter memories can exploit the fluctuations more effectively. By modelling payoffs as birthrates, we demonstrated a coexistence of different memories, leading to a self-organised Hopf bifurcation driven by population dynamics. The simplicity of our memory model, its connection to classical urn models, together with the fact that limit cycles arise naturally, suggested that it might be fruitfully generalised to different games. Indeed Chapter 5 extended this approach to the Hawk-Dove game. However, other extensions might include using multiple urns to represent different sources of yield or game strategies, introducing heterogeneity in switching rates, and utilising a more general distribution of memory lengths and behaviour. Multiple urns might give rise to more complex patterns of oscillation and regimes of behaviour. Experimental research into the nature of human and animal memory puts an emphasis on the 'forgetting function', which describes how memories decay with time. Such a function, or greater powers of statistical inference, could be naturally incorporated into our analysis and their effects on stability explored.

In Chapter 5, the main findings from Chapter 4 were extended to the Hawk-Dove game. We generalised the standard HD game so that players possess finite memories and utilise them to optimise their strategies in each round. With each time step, agents use a form of online learning to amend their strategies. We

presented both analytical and numerical results for this generalised HD game, showing excellent agreement. In particular, we derived an analytical expression for the critical memory length where instability occurs, and this is confirmed by simulation. Our analysis is not only limited to HD game, it can also potentially be applied to, for example, all evolutionary games.

Our work on minority games and the two-urn model has shown a range of complex behaviours which offer possible future foci. A direct link between the game models and real financial markets still needs to be fully developed. Stock price movement may be related to minority game by assuming that one side in the game are the sellers and the other buyers. The prediction for markets needs to be verified by comparisons with historical stocks data. Similarly our urn model can be applied to real markets. It may also be used to analyse the effectiveness of financial resource allocation, by considering urn 1 to represent the cash holding, and urn 2 to be other financial instruments holdings, i.e. stocks, bonds, derivatives, etc. We can analyse the transition between these holdings under different investment environment. Furthermore, this urn model could be extended to multi-urn model, in order to capture the dynamics of different financial portfolios.

Bibliography

[1] Mantegna, R. N. and Stanley, H. E., 2000. *Introduction to Econophysics Correlations and Complexity in Finance*. Cambridge: Cambridge University Press.

[2] Savoiu, G., 2013. *Econophysics: Background and Applications in Economics, Finance, and Sociophysics*. Oxford Waltham, Mass: Academic Press.

[3] Grimmett, G. and Stirzaker, D., 2001. *Probability and random processes*. Third Edition. Oxford: Oxford University Press.

[4] Fry, J., 2015. Stochastic modelling for financial bubbles and policy. *Cogent Economics & Finance*, 3(1), 1002152.

[5] Cockshott, P., Cottrell, A. F., Michaelson, G. J., Wright, I. P. and Yakovenko, V. M., 2009. *Classical Econophysics*. London: Routledge.

[6] Slanina, F., 2014. *Essentials of Econophysics Modelling*. Oxford: Oxford University Press.

[7] Sinha, S., Chatterjee, A., Chakraborti, A., Chakrabarti, B. K., 2011. *Econophysics: An Introduction*. Weinheim: Wiley-VCH.

[8] Jovanovic, F. and Schinckus, C., 2013. The history of econophysics emergence: a new approach in modern financial theory. *History of Political Economy*, 45, pp. 443-474.

[9] Spânulescu, I. and Gheorghiu, A., 2013. A classification of the econophysics directions. *Hyperion International Journal of Econophysics & New Economy*, 6(2), pp. 175-198.

[10] Kutner, R. and Grech, D., 2008. Report on foundation and organization of econophysics graduate courses at faculty of physics of University of Warsaw and department of physics and astronomy of the Wroclaw University. *Acta Physica Polonica Series A*, 114(3), pp. 637-647.

[11] Namatame, A., Kaizouji, T., Aruka, Y., 2006. *The Complex Networks of Economic Interactions: Essays in Agent-Based Economics and Econophysics*. Berlin: Springer.

[12] Takayasu, H., 2004. *The Application of Econophysics proceedings of the Second Nikkei Econophysics Symposium*. Tokyo: Springer Japan.

[13] Roehner, B. M., 2005. *Patterns of Speculation: A Study in Observational Econophysics*. Cambridge: Cambridge University Press.

[14] Preis, T., 2011. Econophysics - complex correlations and trend switchings in financial time series. *The European Physical Journal Special Topics*, 194(1), pp. 5-86.

[15] Amaral, L. A. N., Cizeau, P., Gopikrishnan, P., Liu, Y., Meyer, M., Peng, C.-K. and Stanley, H. E., 1999. Econophysics: can statistical physics contribute to the science of economics? *Computer Physics Communications*, 121-122, pp. 145-152.

[16] Stanley, H. E., Amaral, L. A. N., Canning, D., Gopikrishnan, P., Lee, Y. and Liu, Y., 1999. Econophysics: can physicists contribute to the science of economics? *Physica A: Statistical Mechanics and its Applications*, 269, pp. 156-169.

[17] Garibaldi, U. and Scalas, E., 2010. *Finitary Probabilistic Methods in Econophysics*. Cambridge: Cambridge University Press.

[18] Silva, S. D., Matsushita, R., Gleria, I., Figueiredo, A., Rathie, P., 2005. International finance, Lévy distributions, and the econophysics of exchange rates. *Communications in Nonliner Science and Numerical Simulation*, 10(4), pp. 365-393.

[19] Figueiredo, A., Matsushita, R., Silva, S. D., Serva, M., Viswanathan, G. M., Nascimento, C. and Gleria, I., 2007. The Lévy sections theorem: an application to econophysics. *Munich Personal RePEc Archive Paper*, Paper No. 3810.

[20] Abergel, F., 2011. *Econophysics of Order-Driven Markets Proceedings of Econophys-Kolkata V*. New York: Springer.

[21] Gabaix, X., 1999. Zipf's law for cities: An explanation. *The Quarterly Journal of Economics*, 144, pp. 739-767.

[22] Sousa, T. and Domingos, T., 2006. Equilibrium econophysics: a unified formalism for neoclassical economics and equilibrium thermodynamics. *Physica A: Statistical Mechanics and its Applications*, 371(2), pp. 492-512.

[23] Aspromourgos, T., 1986. On the origins of the term 'neoclassical'. *Cambridge Journal of Economics*, 10(3), pp. 265-270.

[24] Scarfone, A. M., 2007. A mechanism to drive multi-power law functions: an application in the econophysics framework. *Physica A: Statistical Mechanics and its Applications*, 382 (1), pp. 271-277.

[25] Fan, Y., Li, M., Chen, J., Gao, L., Di, Z. and Wu, J., 2004. Network of econophysicists: a weighted network to investigate the development of econophysics. *International Journal of Modern Physics B*, 18(17-19), pp. 2505-2511.

[26] Bordley, R. F., 2005. Econophysics and individual choice. *Physica A: Statistical Mechanics and its Applications*, 354, pp. 479-495.

[27] Fry, J., 2011. Gaussian and non-Gaussian models for financial bubbles via econophysics. *Hyperion International Journal of Econophysics & New Economy*, 4(1), pp. 7-23.

[28] Fry, J., 2010. Bubbles and crashes in finance: a phase transition from random to deterministic behaviour in prices. *Journal of Applied Research in Finance Bi-Annually*, II(2), pp. 131-137.

[29] Fry, J. and Cheah, E-T., 2016. Negative bubbles and shocks in crytocurrency markets. *International Review of Financial Analysis*, (forthcoming).

[30] Hull, J. C., 2012. *Options, Futures, & Other Derivatives*. Boston: Prentice Hall.

[31] Etheridge, A., 2002. *A Course in Financial Calculus*. Cambridge: Cambridge University Press.

[32] Bodie, Z., Kane, A., Marcus, A. J., 2008. *Investments*. New York: McGraw-Hill/Irwin.

[33] Grima, S., 2012. The current financial crisis and derivative misuse. *Online Journal of Social Sciences Research*, 1(8), pp. 265-276.

[34] Reinhart, C. and Rogoff, K., 2009. *This time it's different: eight centuries of financial folly*. Princeton: Princeton University Press.

[35] McCauley, J. L., 2009. *Dynamics of Markets: The New Financial Economics*. Cambridge: Cambridge University Press.

[36] Huang, J. P., 2014. *Experimental Econophysics: Properties and Mechanisms of Laboratory Markets*. Heidelberg: Springer Verlag.

[37] Bouchaud, J. P. and Potters, M., 2003. *Theory of Financial Risk and Derivative Pricing : from statistical physics to risk management*. Cambridge: Cambridge University Press.

[38] Takayasu, H., Watanabe, T., 2010. *Econophysics Approaches to Large-Scale Business Data and Financial Crisis*. Tokyo: Springer Japan.

[39] Chai, H. and Song, D., 2010. Enterprise investment timing based on options game theory. *International Conference on Information Management, Innovation Management and Industrial Engineering (ICIII)*, 4, pp. 155-158.

[40] Ziegler, A. C., 2004. *A Game Theory Analysis of Options*. Heidelberg: Springer Verlag.

[41] Angelou, G. N. and Economides, A. A., 2009. A multi-criteria game theory and real-options model for irreversible ICT investment Decisions. *Telecommunications Policy*, 33(10-11), pp. 686-705.

[42] Challet, D. and Zhang, Y.-C., 1998. On the minority game: analytical and numerical studies. *Physica A: Statistical Mechanics and its Applications*, 256(3-4), pp. 514-532.

[43] Tanaka-Yamawaki, M., 2005. Minority Game and the wealth distribution in the artificial markets. *Knowledge-Based Intelligent Information and Engineering Systems*, 9th International Conference, KES 2005, Proceedings, Part I, pp. 15-20.

[44] Brzezinski, M., 2014. Do wealth distributions follow power laws? Evidence from 'rich lists'. *Physica A: Statistical Mechanics and its Applications*, 406, pp. 155-162.

[45] Newman, M. E. J., 2005. Power laws, Pareto distributions and Zipf's law. *Contemporary Physics*, 46(5), pp. 323-351.

[46] Sinha, S., 2006. Evidence for power-law tail of the wealth distribution in India. *Physica A: Statistical Mechanics and its Applications*, 359(1), pp. 555-562.

[47] Erneux, T., 2009. *Applied Delay Differential Equations*. London: Springer.

[48] Fisher, L., 2008. *Rock, Paper, Scissors: game theory in everyday life*. New York: Basic Books.

[49] Walker, D. and Walker, G., 2004. *The Official Rock Paper Scissors Strategy Guide*. London: Simon & Schuster.

[50] Shelton, R. B., 1997. *Gaming the Market: Applying Game Theory to Create Winning Trading Strategies*. Oxford: John Wiley & Sons.

[51] Greenwood, G. W. and Tymerski, R., 2008. A game-theoretical approach for designing market trading strategies. *IEEE Symposium on Computational Intelligence and Games*, pp. 316-322.

[52] Li, H., Wu, C. and Yuan, M., 2013. An evolutionary game model of financial markets with heterogeneous players. *Procedia Computer Science*, 17, pp. 958-964.

[53] Allen, F. and Morris, S., 2001. Chapter: Game theory and business applications, *Volume 35 of the series International Series in Operations Research & Management Science*, pp. 17-48.

[54] Zhou, W-X. and Sornette, D., 2007. Self-fulfilling Ising model of financial markets, *European Physical Journal B*, 55(2), pp. 175-181.

[55] Gonçalves, C. P. and Gonçalves, C., 2007. An evolutionary quantum game model of financial market dynamics - theory and evidence. [Online] available at Social Science Research Network: `http://ssrn.com/abstract=982086` [Accessed 16 March 2016].

[56] Wiszniewska-Matyszkiel, A., 2005. Stock market as a dynamic game with continuum of players. *Control and Cybernetics*, 37(3), pp. 617-647.

[57] Musolino, F., 2012. Game theory for speculative derivatives: a possible stabilizing regulatory model, *Atti della Accademia Peloritana dei Pericolanti*, 90(1), C1.

[58] Chen, F., Gou, C., Guo, X. and Gao, J., 2008. Prediction of stock markets by the evolutionary mix-game model. *Physica A*, 387, pp. 3594-3604.

[59] Chen, Y., Dimitrov, S., Sami, R., Reeves, D. M., Pennock, D. M., Hanson, R. D., Fortnow, L. and Gonen, R., 2009. Gaming prediction markets: equilibrium strategies with a market maker. *Algorithmica*, 58(4), pp. 930-969.

[60] Challet, D., Marsili, M. and Zhang, Y.-C., 2014. *Minority games: Interacting Agents In Financial Markets*. Oxford: Oxford University Press.

[61] Martino, A. D., Giardina, I. and Mosetti, G., 2003. Statistical mechanics of the mixed majority-minority game with random external information. *Journal of Physics A: Mathematical and General*, 36, pp. 8935-8954.

[62] Marsili, M., 2001. Market mechanism and expectations in minority and majority games. *Physica A*, 299, pp. 93-103.

[63] Alfi, V., Martino, A. D., Pietronero, L. and Tedeschi, A., 2007. Detecting the traders' strategies in minority-majority games and real stock-prices. *Physica A*, 382, pp. 1-8.

[64] Arthur, W., 1994. Inductive reasoning and bounded rationality (the El Farol problem). *The American Economic Review: Papers and Proceedings*, 84(2), pp. 406-411.

[65] Challet, D. and Zhang, Y.-C., 1997. Emergence of cooperation and organization in an evolutionary game. *Physica A: Statistical Mechanics and its Applications*, 246(3), pp. 407-418.

[66] Challet, D., Marsili, M. and Ottino, G., 2004. Shedding light on El Farol. *Physica A: Statistical Mechanics and its Applications*, 332, pp. 469-482.

[67] Jefferies, P., Hart, M. L., Hui, P. M. and Johnson, N. F., 2001. From market games to real-world markets. *The European Physical Journal B - Condensed Matter and Complex Systems*, 20(4), pp. 493-501.

[68] Challet, D., Marsili, M. and Zhang, Y.-C., 2001. Stylized facts of financial markets and market crashes in minority games. *Physica A: Statistical Mechanics and its Applications*, 294(3-4), pp. 514-524.

[69] Marsili, M., Challet, D. and Zecchina, R., 2000. Exact solution of a modified El Farol's bar problem: efficiency and the role of market impact. *Physica A: Statistical Mechanics and its Applications*, 280(3-4), pp. 522-553.

[70] Franke, R., 2003. Reinforcement learning in the El Farol model. *Journal of Economic Behavior & Organization*, 51(3), pp. 367-388.

[71] Luş, H., Aydın, C. O., Keten, S., Ünsal, H. İ. and Atılgan, A. R., 2005. El Farol revisited. *Physica A: Statistical Mechanics and its Applications*, 346(3-4), pp. 651-656.

[72] Lustosa, B. C. and Cajueiro, D. O., 2010. Constrained information minority game: how was the night at El Farol? *Physica A: Statistical Mechanics and its Applications*, 389(6), pp. 1230-1238.

[73] Valdez, S. and Molyneux, P., 2010. *An Introduction to Global Financial Markets*. Hampshire New York: Palgrave Macmillam.

[74] Benninga, S., 2014. *Financial Modelling*. Massachusetts: MIT Press.

[75] Boumans, M., 2005. *How Economists Model the World into Numbers*. London: Routledge.

[76] Challet, D. , Marsili, M. and Zhang, Y.-C., 2000. Modeling market mechanism with minority game. *Physica A: Statistical Mechanics and its Applications*, 276, pp. 284-315.

[77] D'hulst, R. and Rodgers, G. J., 2000. Strategy selection in the minority game. *Physica A: Statistical Mechanics and its Applications*, 278(3-4), pp. 579-587.

[78] Andersen, J. V. and Sornette, D., 2003. The $-game. *The European Physical Journal B*, 31, pp. 141-145.

[79] Challet, D. and Marsili, M., 2000. Relevance of memory in minority games. *Physical Review E*, 62, pp. 1862-1868.

[80] Huygens, C., 1655. *Tome XIV: Calcul des probabilités. Travaux de mathématiques pures 1655-1666 (1920)*, (In French). Den Haag: Nijhoff.

[81] Coolidge, J., 1925. *An Introduction to Mathematical Probability*. Oxford: Oxford University Press.

[82] Mahmoud, H., 2009. *Pólya Urn Models*. Boca Raton, FL: CRC Press.

[83] Chen, M. and Kuba, M., 2013. On generalized Pólya urn models. *Journal of Applied Probability*, 50(4), pp. 1169-1186.

[84] Chen, M. R., Hsiau, S.-R. and Yang, T.-H., 2014. A new two-urn model. *Journal of Applied Probability*, 51, pp. 590-597.

[85] Mahmoud, H. M., 2003. Pólya urn models and connections to random trees: a review. *Journal of Iranian Statistical Society*, 2(1), pp 53-114.

[86] Kac, M., 1976. *Probability and Related Topics in Physical Sciences*. Providence, R.I: American Mathematical Society.

[87] Metzler, R., Kinzel, W. and Kanter, I., 2000. On time's arrow in Ehrenfest models with reversible deterministic dynamics. *Journal of Physics A: Mathematical and General*, 34, pp. 317-326.

[88] Prestipino, S., 2005. The Ideal gas as an urn model: derivation of the entropy formula. *European Journal of Physics*, 26(1), pp. 137-153.

[89] Johnson, N. L. and Kotz, S., 1977. *Urn Models and Their Application: an approach to modern discrete probability theory*. New York: John Wiley & Sons Inc.

[90] Lexis, W., 1875. *Introduction to the Theory of Population Statistics*, (In German). Strassburg: Trübner.

[91] Lexis, W., 1903. *Treatises on Population and Social Statistics*, (In German). Jena: G. Fischer.

[92] Godrèche, C. and Luck, J. M., 2002. Nonequilibrium dynamics of urn models. *Journal of Physics: Condensed Matter*, 14(7), pp. 1601-1615.

[93] Buhot, A., Garrahan, J. P. and Sherrington, D., 2003. Simple strong glass forming models: mean-field solution with activation. *Journal of Physics A: Mathematical and General*, 36(2), pp. 307-328.

[94] Laruelle, S. and Pagès, G., 2013. Randomized urn models revisited using stochastic approximation. *The Annals of Applied Probability*, 23(4), pp. 1409-1436.

[95] Huillet, T. E., 2011. A Bose-Einstein approach to the random partitioning of an integer. *Journal of Statistical Mechanics: Theory and Experiment*, 2011(08), P08021.

[96] Inoue, J. and Ohkubo, J., 2008. Power-law behavior and condensation phenomena in disordered urn models. *Journal of Physics A: Mathematical and Theoretical*, 41(32), 324020.

[97] Dunning, T., 2012. *Natural Experiments in the Social Sciences - A Design-Based Approach*. Cambridge: Cambridge University Press.

[98] Levine, E., Mukamel, D. and Ziv, G., 2004. The condensation transition in zero-range processes with diffusion. *Journal of Statistical Mechanics: Theory and Experiment*, 2004(05), P05001.

[99] Cerqueti, R. and Ausloos, M., 2015. Cross ranking of cities and regions: population versus income. *Journal of Statistical Mechanics: Theory and Experiment*, 2015(7), P07002.

[100] Tong, Z. and Mahmoud, H. M., 2013. An urn model for population mixing and the phases within. *Methodology and Computing in Applied Probability*, 15, pp. 683-706.

[101] Lambersona, P. J. and Page, S. E., 2012. The effect of feedback consistency on success in markets with positive feedbacks. *Economics Letters*, 114, pp. 259-261.

[102] Zhang, L. X., Hu, F., Cheung, S. H. and Chan, W. S., 2011. Immigrated urn models - theoretical properties and applications. *The Annals of Statistics*, 39(1), pp. 643-671.

[103] Aletti, G., Ghiglietti, A. and Paganoni, A. M., 2013. Randomly reinforced urn designs with prespecified allocations. *Journal of Applied Probability*, 50, pp. 486-498.

[104] Eggenberger, F. and Pólya, G., 1923. Über die statistik verketteter vorgänge. *ZAMM - Journal of Applied Mathematics and Mechanics/Zeitschrift für Angewandte Mathematik und Mechanik*, 3(4), pp. 279-289.

[105] Moon, J. W., 1972. Random exchanges of information. *Nieuw Archief voor Wiskunde*, 20, pp. 246-249.

[106] Tijdeman, R., 1971. On a telephone problem, *Nieuw Arch. Wiskunde*, 19(3), pp. 188-192.

[107] Bernoulli, J., 1713. *Ars Conjectandi*, (In Latin). Basel: Impensis Thurnisiorum, fratrom.

[108] Ehrenfest, P., 1907. Über zwei bekannte Einwände gegen das Boltzmannsche H-theorem. *Physikalishce Zeitschrift*, 8, pp. 311-314.

[109] Alfred, B. M., 1987. *Elements of Statistics for the Life and Social Sciences*. New York: Springer New York.

[110] Thompson, M., 1997. *Theory of Sample Surveys*. London: Chapman and Hall/CRC.

[111] DasGupta, A., 2010. Urn Models in Physics and Genetics. *Chapter: Fundamentals of Probability: A First Course*, Part of the series Springer Texts in Statistics, pp. 379-407.

[112] Hoppe, F. M., 1987. The sampling theory of neutral alleles and an urn model in population genetics. *Journal of Mathematical Biology*, 25(2), pp. 123-159.

[113] Trieb, G., 1992. A Pólya urn model and the coalescent. *Journal of Applied Probability*, 29(1), pp. 1-10.

[114] Smith, J. M., 1982. *Evolution and the Theory of Games*. Cambridge: Cambridge University Press.

[115] Smith, J. M. and Price, G. R., 1973. The logic of animal conflict. *Nature*, 246, pp. 15-18.

[116] Smith, J. M., 1976. Evolution and the theory of games: in situations characterized by conflict of interest, the best strategy to adopt depends on what others are doing. *American Scientist*, 64(1), pp. 41-45.

[117] Smith, J. M., 1979. Game theory and the evolutionary of behaviour. *Proceedings of the Royal Society of London. Series B, Biological Sciences*, 205(1161), The Evolution of Adaptation by Nature Selection, pp. 475-488.

[118] Bernstein, A., 2014. Monte Carlo simulation of learning in the Hawk Dove game. *Spring 2014*, Paper 70. [Online] available from: `https://economics.wustl.edu/files/economics/imce/alex_bernstein_-_final.pdf` [Accessed 16 September 2015].

[119] McNamara, J. M. and Weissing, F. J., 2010. Evolutionary Game Theory, in: Székely, T., Moore, A. J., Komdeur, J. (eds), *Social Behaviour: Genes, Ecology and Evolution*. Cambridge: Cambridge University Press.

[120] Pham, K. and Feng, Y., 2013. Using the Hawk-Dove model and ordinary differential equation systems to study Asian carp invasion. [Online] available from: `http://www.math.uci.edu/icamp/summer/research/student_research/asian_carp.pdf` [Accessed 16 September 2015].

[121] Neugebnauer, T., Poulsen, A. and Schram, A., 2008. Fairness and reciprocity in the Hawk-Dove game. *Journal of Economic Behavior & Organization*, 66(2), pp. 243-250.

[122] Hanauske, M., Kunz, J., Bernius, S. and König, W., 2010. Doves and hawks in economics revisited: an evolutionary quantum game theory-

based analysis of financial crises. *Physica A: Statistical Mechanics and its Applications*, 389(21), pp. 5084-5102.

[123] Carlsson, B. and Johansson, S., 2006. An iterated Hawk-and-Dove game. *Chapter: Agents and multi-agent systems formalisms, methodologies, and applications*, Volume 1441 of the series Lecture Notes in Computer Science, pp. 179-192.

[124] Taylor, P. D. and Jonker L. B., 1978. Evolutionary stable strategies and game dynamics. *Mathematical Biosciences*, 40(1-2), pp. 145-156.

[125] Cressman, R., 1995. Evolutionary stability for two-stage Hawk-Dove games. *Rocky Mountain Journal of Mathematics*, 25(1), pp. 145-154.

[126] Hsieh, Y-H., Yuan, S-T. and Liu, H-C., 2014. Service interaction design: a Hawk-Dove game based approach to managing customer expectations for oligopoly service providers. *Information Systems Frontiers*, 16(4), pp. 697-713.

[127] Sartori, A. E., 2001. Hawks, doves, and diplomats; reputation and communication in a modified Hawk-Dove game. [Online] available from: `http://www.politics.as.nyu.edu/docs/IO/4760/Sartori4-13.pdf` [Accessed 16 September 2015].

[128] Friedman, D., 1998. On economic applications of evolutionary game theory. *Journal of Evolutionary Economics*, 8(1), pp. 15-43.

[129] Bishop, D. T. and Cannings, C., 1978. A generalized war of attrition. *Journal of Theoretical Biology*, 70, pp. 85-124.

[130] Crane, A., Matten, D., McWilliams, A., Moon, J. and Siegel, D. S., 2008. *The Oxford Handbook of Corporate Social Responsibility*. Oxford: Oxford University Press.

[131] Douma, S. W. and Schreuder, H., 2008. *Economic Approaches to Organizations*. Harlow: Pearson Education.

[132] Hatfield, M., 2012. *Game Theory in Management: Modelling Business Decisions and their Consequences*. Farnham: Gower Publishing Ltd.

[133] García, L. A. P., Aguilar, A. C. and Muñoz-Herrera, M., 2015. The bargaining power of commitment: an experiment of the effects of threats in the sequential Hawk-Dove game. *Rationality and Society*, 27(3), pp. 283-308.

[134] Erickson, K. H., 2014. *Game theory for business: a simple introduction*. CreateSpace.

[135] Ricketts, M., 2003. *The Economics of Business Enterprise: An Introduction to Economic Organisation and the Theory of the Firm*. Cheltenham: Edward Elgar Publishing.

[136] Polinsky, A. M. and Shavell, S., 2007. *Handbook of Law and Economics*. Amsterdam Boston: Elsevier.

[137] Parkin, M., Matthews, K., Powell, M., 2008. *Economics*. Harlow: Addison-Wesley.

[138] Challet, D. and Marsili, M., 1999. Phase transition and symmetry break in the minority game. *Physical Review E*, 60, R6271-R6274.

[139] Moro, E., 2004. The minority game: an introductory guide. In: Korutcheva, E. (ed.) *Advances in Condensed Matter and Statistical Physics*. New York: Nova Science Publishers, Inc.

[140] MATLAB and Statistics Toolbox Release 2015a, The MathWorks, Inc., Natick, Massachusetts, United States.

[141] Brenner, M., 1973. *The sensitivity of the efficient market hypothesis to alternative specifications of the market model*. New York: Cornell University.

[142] Malkiel, B. G., 2003. The efficient market hypothesis and its critics. *Journal of Economic Perspectives*, 17(1), pp. 5982.

[143] Johnson, N. F., Lamper, D., Jefferies, P., Hart, M. L. and Howison, S., 2001. Application of multi-agent games to the prediction of financial time series. [Online] available from: `http://arxiv.org/pdf/cond-mat/0105303.pdf` [Accessed 16 September 2015].

[144] Johnson, N. F., Jarvis, S., Jonson, R., Cheung, P., Kwong, Y. R. and Hui, P. M., 1998. Volatility and agent adaptability in a self organizing market. *Physica A: Statistical Mechanics and its Applications*, 258(1-2), pp. 230-236.

[145] Johnson, N. F., Hart, M., Hui, P. M., Zheng, D., 2000. Trader dynamics in a model market. *International Journal of Theoretical and Applied Finance*, 03(03), pp. 443-450.

[146] Ferreira, F. F., Francisco, G., Machado, B. S. and Muruganandam, P., 2003. Time series analysis for minority game simulations of financial markets. *Physica A: Statistical Mechanics and its Applications*, 321(3-4), pp. 619-632.

[147] Savit R., Manuca, R. and Riolo, R., 1999. Adaptive competition, market efficiency, phase transition. *Physical Review Letters*, 82(10), pp. 2203-2206.

[148] Fabozzi, F. and Nahlik, C., 2012. *Project Financing*. London: Euromoney Institutional Investor PLC.

[149] Vose, D., 2008. *Risk Analysis: a quantitative guide*. Chichester, England Hoboken, NJ: John Wiley & Sons.

[150] Maxwell, W. and Shenkman, M., 2010. *Leveraged Financial Markets: A Comprehensive Guide to Loans, Bonds, and Other High-Yield Instruments*. New York: McGraw-Hill Education.

[151] Porter, M. E., 1990. *The Competitive Advantage of Nations*. New York: Free Press.

[152] Grimmett, G. and Stirzaker, D., 2001. *Probability and Random Processses*. Oxford: Oxford University Press.

[153] Traulsen, A., Semmann, D., Sommerfeld, R. D., Krambeck, H-J. and Milinski, M., 2010. Human strategy updating in evolutionary games. *Proceedings of the National Academy of Sciences of the United States of America*, USA 107, 2962.

[154] Burridge, J., 2015. Limit cycles and the benefits of a short memory in Rock-Paper-Scissors games. *Physical Review E*, 92(4), 042111.

[155] Manfredi, P. and Fanti, L., 2004. Cycles in dynamics economic modelling. *Economic Modelling*, 21, pp. 573-594.

[156] Cavagna, A., 1999. Irrelevance of memory in the minority game. *Physical Review E*, 59(4), R3783.

[157] Estes, W. K., 1972. Research and theory on the learning of probabilities. *Journal of the American Statistical Association*, 67(337), 81.

[158] Killeen, P. R., 2001. Writing and overwriting short-term memory. *Psychonomic Bulletin and Review*, 8, pp. 18-43.

[159] Cook, R. G. and Blaisdell, A. P., 2006. Short-term item memory in successive same-different discriminations. *Behavioural Processes*, 72, pp. 255-264.

[160] Averell, L. and Heathcote, A., 2011. The form of the forgetting curve and the fate of memories. *Journal of Mathematical Psychology*, 55, pp. 25-35.

[161] Wolfram Research, 2012. Mathematica 9.0, *Wolfram Research Inc*, Champaign, Illinios.